

**INVESTIGATION ON THE EFFICIENCIES OF LOW
COST ADSORBENTS FOR THE TREATMENT OF
FLUORIDE CONTAMINATED WATER**

BY

MANISHA POUDYAL

**A THESIS SUBMITTED IN PARTIAL FULFILLMENT OF THE
REQUIREMENTS FOR THE DEGREE OF MASTER OF SCIENCE
(ENGINEERING AND TECHNOLOGY)
SIRINDHORN INTERNATIONAL INSTITUTE OF TECHNOLOGY
THAMMASAT UNIVERSITY
ACADEMIC YEAR 2015**

**INVESTIGATION ON THE EFFICIENCIES OF LOW
COST ADSORBENTS FOR THE TREATMENT OF
FLUORIDE CONTAMINATED WATER**

BY

MANISHA POUDYAL

**A THESIS SUBMITTED IN PARTIAL FULFILLMENT OF THE
REQUIREMENTS FOR THE DEGREE OF MASTER OF SCIENCE
(ENGINEERING AND TECHNOLOGY)**

SIRINDHORN INTERNATIONAL INSTITUTE OF TECH

THAMMASAT UNIVERSITY

ACADEMIC YEAR 2015



INVESTIGATION ON THE EFFICIENCIES OF LOW COST ADSORBENTS FOR
THE TREATMENT OF FLUORIDE CONTAMINATED WATER

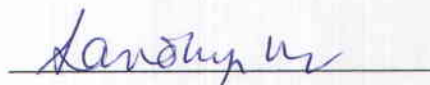
A Thesis presented

By
MANISHA POUDYAL

Submitted to
Sirindhorn International Institute of Technology
Thammasat University
In partial fulfillment of the requirements for the degree of
MASTER OF SCIENCE (ENGINEERING AND TECHNOLOGY)

Approved as to style and content by

Advisor and Chairperson of Thesis Committee



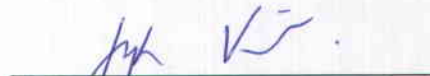
(Assoc. Prof. Sandhya Babel, D. Tech. Sc.)

Committee Member and
Chairperson of Examination Committee



(Assoc. Prof. Alice Sharp, Ph.D)

Committee Member



(Assoc. Prof. Soydo Vinitnantharat, D. Tech. Sc.)

NOVEMBER 2015

Abstract

INVESTIGATION ON THE EFFICIENCIES OF LOW COST ADSORBENTS FOR THE TREATMENT OF FLUORIDE CONTAMINATED WATER

by

MANISHA POU DYAL

Bachelor of Technology in Environmental Engineering, Kathmandu University, 2012

Clean and safe drinking water is fundamental right of human. The physical, biological and chemical parameters of water is very useful for evaluating its usefulness for intended purpose. One of such contaminants is fluoride, which occurs naturally or used as an additive to municipal water supplies. Fluoride in drinking water is gaining wide attention because of its unusual behavior as regards to its health impact in the living beings. The motivation for carrying out this study was to address the problems related to high fluoride levels in water by looking for an environmentally-friendly and cost-effective method for its treatment. This thesis embodies results of the laboratory-based studies on defluoridation of fluoride contaminated water. Agro-industrial wastes such as dewatered sewage sludge, sea shell, litchi peel and banana peel were selected for the fluoride adsorption experiments, and their performance was compared with the commercial granular activated carbon. An attempt was made to modify the litchi peel, both physically and chemically for the enhancement of adsorption efficiencies. The physicochemical characterization of the adsorbents was done by Brunauer–Emmett–Teller (BET) for surface area analysis, scanning electron microscopy (SEM) for surface morphological studies and Fourier transform infrared spectroscopy (FTIR) for functional group identification. The FTIR study highlighted the absorption bands pertaining to rich organic functional groups like hydroxyl, amine and carbonyl groups in the agro-based adsorbents like litchi peel and banana peel. The nature and morphology of the adsorbents were also clearly understood from the SEM images.

Moreover, the influence of operating parameters such as pH, adsorbent dose, agitation speed, contact time and initial fluoride concentration was studied by a series of batch experiments at $25\pm 3^\circ\text{C}$. The interference of co-existing ions (F^-/Cl^- and $\text{F}^-/\text{SO}_4^{2-}$) on the fluoride uptake was also tested for 10 mg/l fluoride solution using the banana peel (BP) adsorbent. For the studied adsorbents, the percentage removal of fluoride was found to increase with the increasing dose of adsorbents, agitation speed and time for a given fluoride concentration, while the removal followed decreasing trend for the rise in fluoride concentration. Further, solid addition method was employed to determine the point of zero charge (pH_{pzc}) of the adsorbents. The pH value for all the selected adsorbents was found to be lower than the pH_{pzc} values, making the surface positively charged in favor of negatively charged fluoride ions. Although remarkable removal efficiency was observed in acidic range for most of the adsorbents, removal at neutral pH is considered for all adsorbents from drinking water viewpoint. Sludge and BP rendered the maximum removal efficiency of 88% and ULP showed the least efficiency of 70% for 5 mg/l F^- solution at the optimum conditions. All the tested adsorbents showed good stability in lowering the fluoride level below the prescribed limit as specified by World Health Organization. The equilibrium was observed within 3 hours for most of the tested adsorbents. For BP there was no remarkable change in the fluoride removal in presence of monovalent chloride ions, while the presence of divalent sulfate at higher concentrations resulted in decrease of fluoride removal efficiency. The equilibrium adsorption data after the experiments were modeled with suitable isotherm and kinetic equations. The data fitted quite well with both Freundlich and Langmuir isotherms. Higher R^2 values for Freundlich isotherm confirms that adsorbents surface were highly heterogeneous and the sites having higher energy level were occupied first. Based on the experimental results, pseudo-second order kinetic model seems to be more compatible, with less fluctuations in calculated and experimental uptake capacities (q_e) for all the adsorbents. The adsorption process was found to be complex, with the involvement of more than one rate limiting mechanisms.

Keywords: Fluoride, Adsorption, Low-cost adsorbents, Isotherms, Kinetics

Acknowledgements

Foremost, my heartfelt thanks go to my advisor Assoc. Prof. Dr. Sandhya Babel for providing me with an excellent atmosphere for doing research, for her kind guidance, immense knowledge, unwavering support and motivation, and warm friendship throughout my research period. The numerous inspiring discussions with her have significantly shaped the present work and boosted my faith in myself as a researcher. I could not have certainly got a better supervisor for my graduate study.

I would like to convey my cordial gratitude and appreciation to my admirable thesis examination committees, Assoc. Prof. Dr. Alice Sharp and Assoc. Prof. Dr. Soydoa Vinitnantharat, for taking time out from their busy schedule to serve as examination committee. I am really indebted to them for their accommodative attitude, vigilant guidance, insightful comments and thought-provoking suggestions at all levels of this research study.

I wish to thank Mr. Prasitchai (P.Toey), our lab technician for the laboratory materials he offered me and the discussions he made on some analytical laboratory procedures. I am deeply and strongly obliged to all faculty members at University of Tokyo for their research consultancy and practical lab tips that have made my long lab hours fly by with ease.

Last but not the least, I really acknowledge and offer my heartiest gratitude to all my family members for supporting me spiritually throughout my life. I am grateful to the God for my good health and wellbeing that were necessary to complete this study. During the period of two years, I am indebted to all the friends that I met in SIIT, who provided me with interesting interdisciplinary and intercultural experiences.

Finally, I wish to acknowledge the Department of Biochemical Engineering and Technology, Sirindhorn International Institute of Technology, Thammasat University for supporting the financial budget and laboratory for this research work.

Table of Contents

Chapter	Title	Page
	Signature Page	i
	Abstract	ii
	Acknowledgements	iv
	List of Tables	ix
	List of Figures	xi
1	Introduction	1
	1.1 General Background	1
	1.2 Problem Statement	1
	1.3 Objectives of the Study	3
	1.4 Scope of the Study	3
2	Literature Review	5
	2.1 Fluoride	5
	2.1.1 Sources and Environmental Levels	6
	2.1.2 Health Impacts of Fluoride	8
	2.1.3 Worldwide distribution of Fluoride	11
	2.2 Technologies for Defluoridation of water	18
	2.2.1 Chemical Additive Methods	18
	2.2.2 Filtration	19
	2.2.3 Dialysis and Electrodialysis	21
	2.2.4 Ion Exchange Method	22
	2.2.5 Adsorption	23
	2.3 Adsorption Isotherms	38

2.3.1	Langmuir Adsorption Isotherm	38
2.3.2	Freundlich Adsorption Isotherm	39
2.4	Adsorption Kinetics	41
2.4.1	Weber and Morris Intraparticle Diffusion Model	41
2.4.2	Pseudo First-Order Kinetic Model or Lagergren's equation	43
2.4.3	Pseudo Second-Order Kinetic Model	44
2.4.4	Elovich Equation	46
3	Methodology	48
3.1	Materials	48
3.1.1	Raw materials to prepare adsorbents	49
3.1.2	Reagents and Chemicals	50
3.2	Preparation of Adsorbate Solution	51
3.3	Preparation of Buffer Solution	51
3.4	Experimental Methodology for Adsorbents Preparation	51
3.4.1	Preparation of powdered sewage sludge	51
3.4.2	Preparation of clams shell powder	52
3.4.3	Preparation of untreated litchi peel powder (ULP)	52
3.4.4	Preparation of carbonized litchi peel powder (CLP)	52
3.4.5	Preparation of acid treated litchi peel powder (ALP)	53
3.4.6	Preparation of banana peel powder (BP)	53
3.5	Characterization of adsorbents	54
3.5.1	Nitrogen Adsorption Desorption Isotherms	54
3.5.2	Scanning Electron Microscopy	54
3.5.3	Fourier Transform Infrared Spectroscopy (FTIR)	55
3.6	Experimental set up for Batch Adsorption Studies	55
3.6.1	Effect of Adsorbent Dose	56
3.6.2	Effect of pH	57
3.6.3	Effect of Agitation Speed	57
3.6.4	Effect of Contact Time	57

3.6.5	Effect of Initial fluoride concentration	58
3.6.6	Effect of co-existing ions	58
3.7	Adsorption Isotherms	58
3.7.1	Langmuir Adsorption Isotherm	59
3.7.2	Freundlich Adsorption Isotherm	59
3.8	Batch Kinetic Studies	60
3.8.1	Weber and Morris intraparticle diffusion model	60
3.8.2	Pseudo First-Order Kinetic Model or Lagergren's equation	61
3.8.3	Pseudo Second-Order Kinetic Model	61
3.8.4	Elovich Equation	61
3.9	Analysis of samples	62
4	Results and Discussion	63
4.1	Characterization of adsorbents	63
4.1.1	Surface area and Pore Characteristics	63
4.1.2	Surface Morphology	65
4.1.3	FTIR spectra of adsorbents	68
4.2	Batch Adsorption Studies	73
4.2.1	Effect of Adsorbent dose	73
4.2.2	Effect of pH	75
4.2.3	Effect of Agitation Speed	80
4.2.4	Effect of Contact Time	82
4.2.5	Effect of Initial Fluoride Concentration	84
4.2.6	Effect of co-existing ions	86
4.3	Batch Adsorption Isotherms	87
4.3.1	Langmuir Isotherm Model	87
4.3.2	Freundlich Isotherm Model	90
4.4	Batch Kinetic Studies	92
4.4.1	Weber and Morris intraparticle diffusion model	93
4.4.2	Pseudo-First Order Kinetic Model	95
4.4.3	Pseudo-Second Order Kinetic Model	96

4.5 Fluoride removal efficiencies of various low-cost adsorbents	100
5 Conclusions and Recommendations	103
5.1 Conclusions	103
5.2 Recommendations for Future Work	105
References	106
APPENEDICES	117
Appendix A	118
Appendix B	120
Appendix C	123

List of Tables

Tables	Page
2.1 Fluoride containing minerals	6
2.2 Health impacts related to the levels of fluoride in drinking water	11
2.3 Fluoride concentration in Northern China basins	14
2.4 Fluoride concentration in groundwater of India	15
2.5 Fluoride adsorption capacity of Alumina/Aluminum based adsorbents	25
2.6 Fluoride removal efficiency of Calcium based adsorbents	26
2.7 Fluoride removal efficiency of Iron based adsorbents	27
2.8 Fluoride adsorption capacity of metal oxides/hydroxides	28
2.9 Fluoride removal efficiency of Carbon based adsorbents	29
2.10 Fluoride removal efficiency of Natural materials based adsorbents	30
2.11 Fluoride adsorption capacity of nano-sorbents	31
2.12 Fluoride removal efficiency of Building materials based adsorbents	32
2.13 Fluoride adsorption capacity of apatite and hydroxyapatite	33
2.14 Fluoride adsorption capacity of Industrial wastes	34
2.15 Major binding groups responsible for the biosorption process	35
2.16 Adsorption capacities of various plant parts and agricultural wastes	37
2.17 Linear forms of Langmuir isotherm model	39
2.18 Isotherm Constants and Correlation Coefficients for the adsorption of fluoride using different adsorbents at 298 K	40
2.19 Weber and Morris model parameters of various adsorbents for 5 mg/l F ⁻	42
2.20 Pseudo-first-order kinetic model parameters of various adsorbents for 5mg/l F ⁻	44
2.21 Pseudo-second-order kinetic model linearized forms	45
2.22 Parameters of Pseudo-second-order kinetic model of various adsorbents for 5 mg/l F ⁻	46
2.23 Elovich model parameters of adsorbents for 5 mg/l F ⁻	47
3.1 List of Reagents and Chemicals	50
3.2 Variation of adsorbent doses at constant operating parameters	56

4.1 Surface area and pore characteristics of prepared adsorbents	64
4.2 Wavenumber (cm^{-1}) for dominant peaks from FTIR study of sewage sludge	69
4.3 Wavenumber (cm^{-1}) for dominant peaks from FTIR study of shell powder	70
4.4 Wavenumber (cm^{-1}) for dominant peaks from FTIR study of ULP, ALP and CLP	71
4.5 Wavenumber (cm^{-1}) for dominant peaks from FTIR study of BP powder	72
4.6 Zero Point Charge (pH_{PZC}) values of prepared adsorbents	77
4.7 Calculated parameters of Langmuir isotherm for the selected adsorbents	89
4.8 Separation factor (R_L) for the selected adsorbents	89
4.9 Calculated parameters of Freundlich isotherm for the selected adsorbents	92
4.10 Calculated parameters of Intraparticle diffusion model for selected adsorbents	94
4.11 Calculated parameters of Pseudo first order kinetic model for selected adsorbents	96
4.12 Calculated parameters of Pseudo second order kinetic model for selected adsorbents	98
4.13 Calculated parameters of Elovich model for the selected adsorbents	99
4.14 Optimum reaction conditions for adsorbents to treat 5 mg/l fluoridated water	100
4.15 Comparison of F^- removal with other adsorbents (5 mg/l F^- solution at neutral pH)	102

List of Figures

Figures	Page
2.1 Prevalent sources of fluoride in the environment	8
2.2 Dental caries due to fluoride deficiency	9
2.3 Cases of Dental fluorosis	9
2.4 Cases of Skeletal fluorosis	10
2.5 Countries with elevated fluoride concentration across the world	12
2.6 Fluorosis affected provinces in China	13
2.7 Fluorosis affected provinces in India	16
2.8 Map of Thailand showing dotted provinces as endemic fluorosis zones	17
3.1 Research Framework	48
3.2 Agro-industrial Residues for preparing the adsorbents	50
3.3 Preparation of powdered activated sludge adsorbent	51
3.4 Preparation of clams shell powder adsorbent	52
3.5 Preparation of untreated litchi peel powder adsorbent	52
3.6 Preparation of carbonized litchi peel powder adsorbent	53
3.7 Preparation of acid treated litchi peel powder adsorbent	53
3.8 Preparation of banana peel powder adsorbent	54
3.9 Steps for analyzing residual fluoride solution in the sample using Fluoride Ion- selective electrode	62
4.1 SEM images of sludge before (left) and after (right) defluoridation (4000x)	65
4.2 SEM images of shell before (left) and after (right) defluoridation (500 x)	66
4.3 SEM images of ULP before (left) and after (right) defluoridation (500 x)	66
4.4 SEM images of ALP (left) and after (right) defluoridation (500 x)	67
4.5 SEM images of CLP (a) before and (b) after defluoridation (500x)	68
4.6 SEM images of BP before (left) and after (right) defluoridation	68
4.7 Effect of adsorbent dose on the removal of fluoride by (a) GAC, Sludge and Shell (b) ULP, CLP and ALP (c) BP	74

4.8 Zero point of (a) GAC, Sludge and Shell (b) ULP, CLP and ALP (c) BP; Effect of solution pH on the removal of fluoride by (d) GAC, Sludge and Shell (e) ULP, CLP and ALP (f) BP	76
4.9 Effect of agitation speed on the removal of fluoride by (a) GAC, Sludge and Shell (b) ULP, CLP and ALP (c) BP	81
4.10 Effect of contact time on the removal of fluoride by (a) GAC, Sludge and Shell (b) ULP, CLP and ALP (c) BP	83
4.11 Effect of initial fluoride concentration on the removal of fluoride by (a) GAC, Sludge and Shell (b) ULP, CLP and ALP (c) BP at neutral pH	85
4.12 Effect of anions on fluoride adsorption onto BP	86
4.13 Langmuir adsorption isotherm for (a) GAC, Sludge and Shell (b) ULP, CLP and ALP (c) BP at neutral pH and 298 K	88
4.14 Separation factor R_L values verses initial fluoride concentration (C_i)	90
4.15 Freundlich adsorption isotherm for (a) GAC, Sludge and Shell (b) ULP, CLP and ALP (c) BP at pH 7 and 298 K	91
4.16 Intraparticle diffusion model for (a) GAC, Sludge and Shell at 5 mg/l F^- (b) ULP, CLP and ALP at 5 mg/l F^- (c) BP for 10 mg/l F^- at pH 7	93
4.17 Pseudo first-order kinetic model for (a) GAC, Sludge and Shell at 5mg/l F^- (b) ULP, CLP and ALP at 5 mg/l F^- (c) BP for 10 mg/l F^- at pH 7	95
4.18 Pseudo second-order kinetic model for (a)GAC, Sludge and Shell at 5mg/l F^- (b) ULP, CLP and ALP at 5 mg/l F^- (c) BP for 10 mg/l F^- at pH 7	97
4.19 Elovich model for (a) GAC, Sludge and Shell at 5 mg/l F^- (b) ULP, CLP and ALP at 5 mg/l F^- (c) BP for 10 mg/l F^- at pH 7	99
4.20 Order of effectiveness of adsorbents at their optimum conditions and initial fluoride concentration of 5 mg/l	101

Chapter 1

Introduction

1.1 General Background

Inaccessibility to potable drinking water is the main problem the world population is facing today and this situation is expected to worsen in the near future. Polluted water is not only devastating to environment, but also can pose a severe impact on the human health. All water sources in general are subjected to potential contamination by the substances like microbes, inorganic/organic chemicals and radioactive substances. Particularly, the dissolved inorganic contaminants and impurities exist as ions in solution and certain inorganic ions can be toxic even though they are found rarely and in much smaller quantities. These contaminants does not bear any health risks unless they exceed the Maximum Contaminant Level (MCL).

Fluoride is formed when the element fluorine combines with minerals in soil or rocks. It is released into environment from the geological strata and, to a varying extent through the anthropogenic activities like mining, industry or agriculture. Calcite and fluorite are two major solubility-control minerals influencing geochemistry of high fluoride content water. In soil, fluoride is mainly combined with calcium or aluminum, while in atmosphere it is released via aluminum and steel smelters, coal-fired plants and phosphate processing industries. Fluoride is also a component of the cigarette smoke (WHO). The emitted fluoride can exist as hydrogen fluoride and silicon tetrafluoride or in the form of particles attached to aerosols.

Fluoride containing compounds are commonly present in the basic household appliances like toothpaste and insecticides. The most common route of fluoride intake is through the consumption of foodstuffs and drinking water containing fluoride. Although all foodstuffs contain trace amounts of fluoride, its concentration can rise if highly fluoridated water is used for its preparation.

1.2 Problem Statement

In recent years, there is a growing concern over the water quality problem because clean and safe water is the foundation of life and prosperous communities. The change in water quality parameters directly affect the living organisms residing in water

and one who consumes the infected water. Fluoride ion occurs most frequently in groundwater and is considered as the major toxicological hazard. Besides, water fluoridation is practiced in most of the communities. The promoters of water fluoridation offer proclaimed belief of strong and healthy teeth, while this idea has given rise to fear and suspicion. According to the Centers for Disease Control and Prevention (CDC), about 90% of fluoride added for fluoridation comes from silicofluorides, a chemical obtained mainly as by-products from processing of phosphate fertilizers [1]. The implications of this SiF-induced mechanism for human health can be extremely serious in some instances.

The primary concern of fluoride toxicity is related to the high levels of fluoride present in water than in any other medium like air or soil because water is the easiest medium to reach the human body via consumption. Ingestion of fluoride below the prescribed limit can cause dental carries. On the contrary, presence of fluoride beyond the permissible limit (>1.5 ppm) is harmful and not suitable for the proper functioning of bones and teeth. Excess intake of fluoride results in various infirmities varying from skeletal deformities to the soft tissue problems, and may also affect the mental health. It is estimated that around 80% of the diseases is attributed to poor drinking water quality, of which uptake of fluoridated water accounts for 65% of fluorosis [2].

The groundwater in most countries is reported to have exceedingly high fluoride concentration, mainly because of the lacking treatment infrastructures. Alternative water sources including surface water, less-fluoridated groundwater and rainwater can be one option to prevent fluorosis. Yet, periodic monitoring is required to avoid the mixing of high fluoride containing water from different aquifers. The conventional rural defluoridation techniques like Nalgonda technique and activated alumina generates a large amount of fluoride sludge. Despite having high fluoride removal efficiencies, the charcoals are manufactured from energy-intensive processes and work well only at extremely acidic pH ranges. Moreover, better removal technologies like reverse osmosis, ion exchange, dialysis and electrodialysis and adsorption by commercial carbons are invariably more costly and not feasible just for that purpose in a small scale.

Because the exceeding fluoride contents in drinking water is a severe issue associated with public health, this problem should be taken into consideration urgently. Also, in order to completely remove fluoride from the water sources, suitable

defluoridation technology is undoubtedly needed. The main prerequisites for water purification is the low cost technology accepted by the end users. An inexpensive adsorbent capable of treating fluoridated water at high efficiencies could therefore be a preferred alternative.

1.3 Objectives of the Study

In this study, low-cost adsorbents are selected for removing fluoride from water. There are four main specific objectives as follows:

- To explore adsorbents of biogenic origin for the removal of fluoride from aqueous medium under predefined reaction conditions, and to find adsorption capacities of the respective adsorbents.
- To compare the performance of selected adsorbents with the commercially available granular activated carbon.
- To study the effect of various experimental parameters on the fluoride adsorption process.
- To fit the experimental results with suitable isotherm models and investigate the adsorption mechanisms using appropriate kinetic models.

1.4 Scope of the Study

The adsorption characteristics of granular activated carbon, dewatered sludge, untreated and modified litchi peel, sea shell powder, and banana peel are studied with respect to fluoride removal from the prepared synthetic water. The scope of this study is briefly summarized under the following points.

- Characterize the adsorbents in detail using the techniques like BET for surface area analysis, Fourier transform infrared spectroscopy (FTIR) analysis for functional groups identification, and Scanning Electron Microscopy (SEM) to find textural properties of the selected adsorbents before and after adsorption.
- Perform batch adsorption experiments under the influence of parameters like adsorbent dose, pH, speed, time, varying fluoride concentrations, and co-existing ions (for BP only).

- Test the Langmuir and Freundlich isotherm models to ascertain feasibility of adsorption process, and to calculate adsorption capacities of the respective adsorbents.
- Evaluate the adsorption kinetic process of adsorbents using pseudo-first order, pseudo-second order reaction models, intraparticle diffusion model and Elovich equation.

Chapter 2

Literature Review

The given chapter provides the complete review on the general background of fluoride, its prevalent sources, environmental levels, and the health issues related to the ingestion of fluoride. The global scenario of fluoride occurrence is well documented, with the emphasis on three main fluoride affected countries in Asia, particularly, China, India and Thailand. A critical assessment of various defluoridation technologies is discussed with the main focus on adsorption process. The list of adsorbents are compiled and their adsorption capacities are reported under favorable conditions. The different isotherms and kinetic models applicable to fluoride adsorption process are described in detail.

2.1 Fluoride

The element fluorine is the lightest member of halogen family isolated by Nobel laureate Henri Moissan in 1886. It has an atomic no. 9 and the electronic configuration of $[\text{He}] 2s^2 2p^5$. At STP, fluorine occurs as diatomic gas molecule F_2 , with pale yellow-green color and pungent odor. Its density is 1.51 g/cm^3 , and the melting and boiling point occurs -220°C and -188°C , respectively. The element fluorine is most abundantly found on earth with an estimated crustal abundance of 0.32 g/kg [3]. It has the highest electronegativity of all elements, thus is the most reactive non-metal existing in combined form. It forms compounds by accepting an electron from another atom, and its compounds have oxidation state of -1 characterized by high bond strength. Fluorine-19 is the only naturally occurring stable isotope of fluorine. The pure fluorine find its application as oxidizer in rocket fuels.

Fluoride (F^-) is the simplest ion of fluorine and its salts are used as precursor to form hydrogen fluoride and fluorocarbons. Anthropogenic organofluorine compounds are used as refrigerants, propellants, high octane gasoline, agrochemicals, herbicides, pharmaceuticals surfactants and lubricants. Due to chemical inertness of C-F bond, the organofluorine compounds have high resistance to degradation, and can persist in the environment for longer time. Fluoride ion structurally resembles hydroxide ions

because of their similar geochemistry. The ionic radius of fluoride is strongly hydrated (0.352 nm) than other monovalent anions (0.332 nm for Cl^- and 0.335 for NO_3^-).

2.1.1 Sources and Environmental Levels

Fluoride is ubiquitous in all environmental components like air, water, soil and rocks. Its concentration is dependent on the proximity to the sources of emission.

Fluoride in Atmosphere

The natural sources of atmospheric fluoride emission are volcanic eruptions, wind-blown soil and marine aerosols. The anthropogenic sources include aluminum and steel smelters, brick, pottery and cement works, ceramic industries, plastic factories, coal-fired power plants, glass manufacture, electrical utilities, and indoor combustion of low grade coals containing high fluoride [4]. Its fate is highly influenced by vaporisation, aerosol formation, wet/dry deposition, turbulence and hydrolysis. Natural background concentration of fluoride in atmosphere is in the order 0.5 ng/m^3 , while the worldwide concentration is 3 ng/m^3 including anthropogenic emissions [5]. Airborne fluoride like HF or SiF_4 , are among the important air pollutants.

Fluoride in Soil

Soil is naturally rich in fluoride as its formation is favored by physical disintegration and chemical decay of solid bedrocks containing high fluoride. Fluoride occurs in the rock forming minerals like fluorite (CaF_2) in igneous and sedimentary rocks, apatite $\text{Ca}_5[\text{PO}_4]_3(\text{Cl}, \text{F}, \text{OH})$ in igneous rocks and marine sediments, pegmatites like topaz $\text{Al}_2\text{F}_2[\text{SiO}_4]$, halides, clay minerals like kaolinite and montmorillonite, mica minerals like mica phlohopite $\text{KMg}_3(\text{OH}, \text{F})_2[\text{AlSi}_3\text{O}_{10}]$, and amphiboles [6].

Table 2.1 Fluoride containing minerals

Mineral	Chemical Formula	% Fluorine
Sellaite	MgF_2	61%
Villianmite	NaF	55%
Fluorite (Fluorspar)	CaF_2	49%
Cryolite	Na_3AlF_6	45%
Bastnaesite	$(\text{Ce}, \text{La})\text{CO}_3\text{F}$	9%
Fluorapatite	$\text{Ca}_3(\text{PO}_4)_3\text{F}$	3-4%

Source: Retrieved from Nagendra Rao (2003) [7]

Fluorite is common in granites, gneiss and pegmatite veins, while fluorapatite is more common in metamorphic and igneous rocks. Fluoride concentration in soil and rocks vary widely depending on the soil depth. Fluorine precipitate in marine sediments and returns to continental landmasses over geologic time. Agricultural use of phosphate fertilizers also result in addition of fluoride in soil.

Fluoride in Water

All water sources contain trace amount of fluoride released dominantly from the natural processes. Fluoride act as strong ligand in water and readily form complexes with Al, B, Be, V, U, Fe³⁺ and Si. The [AlF]²⁺ and [AlF₂]⁺ complexes contain from few tenths milligram per liter to a few milligrams per liter of fluoride. Basically, fluoride is released into the water bodies due to runoff from disintegrated fluoride bearing minerals, or leaching from soil into groundwater under favorable hydrolysis conditions and percolating water pressure. In addition, atmospheric deposition, percolation of chemicals from the farmland, and industrial discharge of fluoridated water also account for high fluoride content in water. In groundwater with high fluoride concentration, there exists a negative and positive correlation of fluoride with calcium and bicarbonate concentration. Rock-water interaction, hydrogeological conditions, and prevailing climate all contribute to fluoride mobility in groundwater.

Surface water and shallow groundwater have recently infiltrated rainwater and thus contain lesser fluoride. The fluoride concentrations can range from 1 to more than 35 mg/l in shallow aquifers found near active volcanic premises. In natural water containing total dissolved solids below 1,000 mg/l, fluoride concentration is below 1 mg/l. The occurrence of fluoride in freshwater ranges from 0.01 to 0.3 mg/l, while in sea water it is mainly associated with magnesium (MgF⁺ ions) with average concentration of 1.3 mg/l. Elevated inorganic fluoride levels upto 25–50 mg/l has been reported in hot springs, and ~ 2800 mg/l in certain East African Rift Valley lakes [8].

Besides, community water fluoridation is practiced by adding industrial-grade fluoride chemicals (sodium hexa-fluorosilicate or hexa-fluorosilicic acid) to drinking water supplies, so that the fluoride concentration reaches optimal level (~ 0.7 mg/l) for preventing tooth decay. But in some areas, the concentration may rise up to ~2mg/l even though the WHO recommended value for artificial fluoridation is 0.5 to 1 mg/l. A brief summary of the various fluoride sources in environment is shown below.

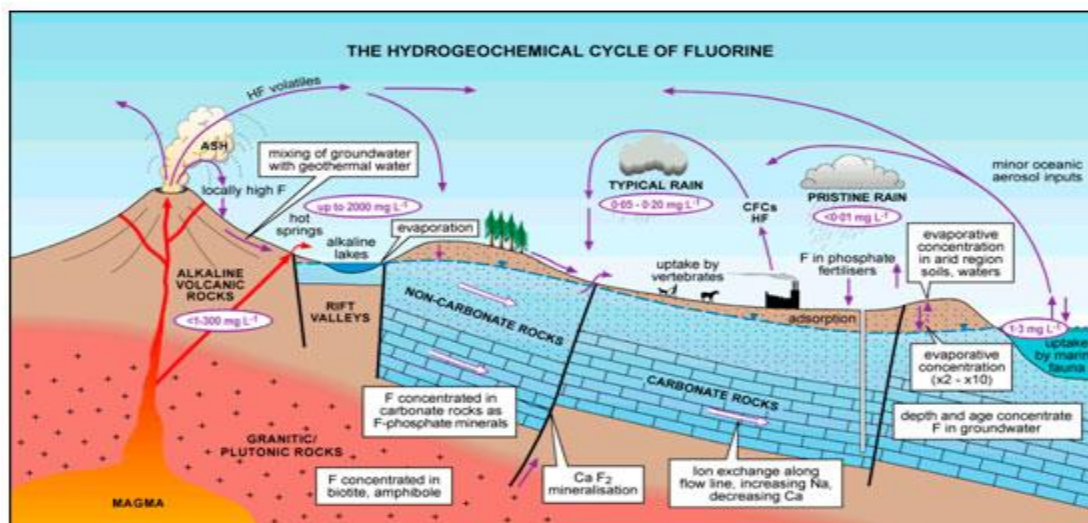


Figure 2.1 Prevalent sources of fluoride in the environment

Source: Water & Development Information for Arid Lands [9]

Dietary and non-dietary sources

Major dietary sources of fluoride includes water and fluoridated water-based beverages, tea, poultry products, eggs, marine fish, and fluoridated salt. The unprocessed foods contains 0.1-2.5 mg/kg fluoride. Vegetables and fruits contain 0.02 to 0.2 mg/kg fluoride per fresh weight, cereals comprises 0.1-0.29 mg/kg fluoride, while milk products have 0.05-0.15 mg/kg fluoride. Diets rich in Ca, Mg, vitamin C and D, and protein rich food also help in abrogating adverse effects of fluoride.

In addition to this, the major non-dietary sources are toothpastes, mouth rinses, fluorinated pharmaceuticals, topical gels and fluoride supplements. Toothpaste contain significant fluoride up to 1000-1500 mg/kg, and the total ingestion is estimated to be 0.36-0.72 mg/day. This can increase the risk of drug induced dental fluorosis in children. Mouth rinses for regular use contains 230 to 500 mg/l fluoride, and mouthwash products meant for weekly use contain 900–1000 mg/l fluoride [10]. The estimated range of safe intake of fluoride for adult is 1.5 to 4 mg/day.

2.1.2 Health Impacts of Fluoride

Fluorine is one of the 14 essential elements for human life. Its inclusion in diet can prevent dental decay and helps in the formation of dental enamel. According to American Dietetic Association, 0.5 to 1 mg/l fluoride is beneficial for mineralization

of skeletal structures and tissues. Below this limit, a carious lesion occurs in interproximal areas and teeth edge resulting in the pits and fissures. Children living below the poverty level with poor nutritional status are most vulnerable.



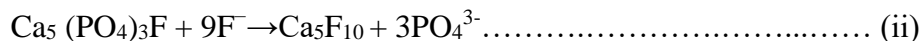
Figure 2.2 Dental caries due to fluoride deficiency

Source: G.V. Black's Classification of Carious Lesions [11]

Toxicity of fluoride depends mainly on four factors: total uptake, duration of exposure, nutritional status and body's response. Fluoride has highest affinity for calcium phosphate, so approximately 99% fluoride is localized in calcified tissues. The hypothesis behind useful and detrimental effects of fluoride on skeletal structure is based on ion exchange between OH and F⁻ in calcium hydroxy-phosphate [12].



When hydroxide is replaced by fluoride ions, fluoroapatite is formed due to recrystallization of hydroxyapatite. It protects tooth enamel from acid attacks and inhibit bacterial acid release. But excess fluoride results in the formation of calcium decafluoride, which causes a problem in functioning of the skeletal structures.



Dental fluorosis is related to the dullness of teeth due to loss of luster in dental enamel. The appearance of white and yellow spots gradually changes to brown and black streaks. Other associated symptoms of dental fluorosis are enamel hypoplasia, surface irregularities and highly noticeable pits. Although dental fluorosis is not a life-threatening disease, it is related to cosmetic condition of teeth.



A mild case of dental fluorosis

A severe case of dental fluorosis

Figure 2.3 Cases of Dental fluorosis

Source: Dental Fluorosis [13]

The skeletal fluorosis is identified by periosteal thickening, hyperostosis, bone histopathological alterations, osteoporosis and osteophytes in muscle attachments [14]. The stiffness increases steadily until the whole spine becomes continuous column of bone manifesting, referred as ‘poker back’. In case of crippling fluorosis, extremities become weak and the vertebrae partially fuse together. Pediatric groups, young adults and females are mostly affected by osteoclerosis. Long term fluoride exposure seems to be cancerous (osteosarcoma), where the cells in growth plate tends to develop faster.



Figure 2.4 Cases of Skeletal fluorosis

Source: Wikispaces, CC licence

Moreover, cumulative exposure of fluoride causes non-skeletal diseases like muscle fibre degeneration, fatigue, abdominal pains, tingling fingers, nervousness and depression, anemia, deformities of red blood cells, polyurea and polydipsia, reduced immunity, brain damage, and neurological manifestations similar to pathological changes in Alzheimer’s disease patients [15, 16]. A positive correlation between increased fluoride concentration and low IQ levels in children of India and China was recorded from several epidemiological studies. Excessive oral ingestion of fluoride affects soft tissue organs like aorta, thyroid, gastrointestinal tract, lungs, kidneys, pancreas, brain and spleen. It can also have genotoxic effects related to alteration of gene expression. The health effects associated with fluoride concentrations is shown in the Table 2.2.

Table 2.2 Health impacts related to the levels of fluoride in drinking water

Fluoride Concentration (mg/l)	Chronic Health Effects
Nil	Limited growth and fertility
0-0.5	Dental Caries
0.5-1.5	Promotes dental health and prevents decay
1.5-4	Dental fluorosis (Mottled teeth)
4-10	Dental fluorosis, Skeletal fluorosis
>10	Crippling fluorosis

Retrieved from Dissanayake, 1991 [17]

People relying on drinking water > 4 mg/l F^- and consuming less nutritious foods are more prone to skeletal and dental fluorosis. Since the diseases related to high fluoride levels is incurable, the only option is to maintain the fluoride uptake within permissible limits. World Health Organization (WHO) and ISO: 10500 has recommended 1-1.5 mg/l F^- concentration in drinking water, but target of 0.8–1.2 mg/l is set to maximize the benefits and offset the harmful effects.

2.1.3 Worldwide distribution of Fluoride

Many countries in the world have extensive geographical fluoride belts: marine sedimentary basins in semiarid regions and mountainous footage, volcanic and geothermal domains, and igneous and metamorphic terrains comprising granitic rocks. The well-known fluoride belts in the Great Rift Valley system stretches from northern Syria through North Africa and Sub-Saharan countries (Libya, Sudan, Tunisia, Somalia, Algeria, Morocco and Mauritania), West Africa (Ghana, Ivory Coast and Senegal), Republic of South Africa and East African Rift Valley (Ethiopia, Uganda, Kenya, Rwanda, and Tanzania to Mozambique). Pacific volcanic belt is the largest volcanic belt and The East African Rift valley have tectonic depression extending from Eritrea to Malawi. An additional belt extends from Turkey to eastern Mediterranean countries (Egypt, Iraq, Iran, Jordan, Afghanistan), and middle-east and south Asia. Similar belt is found in Sierra, Nevada, USA Rocky Mountain, Central America, Columbia, Peru, Bolivia, Andel Mountains, Japan (Kitakami Mountains), Phillipines and Indonesia. Moreover, igneous and metamorphic terrain encompasses large parts of

India, Sri Lanka, northern Thailand, Senegal, Ghana, Cameroon, South Africa, the Pampean ranges in South America, and Scandinavia [12, 18].

High fluoride in water need not have an exclusively natural origin, as water fluoridation is commonly practiced in Australia, Brazil, USA, Hong Kong, South Korea, Singapore, Malaysia and Vietnam. There are more than 25 developed and developing countries, where ~ 200 million population depend on fluoride contaminated water sources [19]. A total of 14 countries in Africa, 8 in Asia and the Middle East and 6 in Americas have water sources exceeding 1.5 mg/l F⁻ concentration. Fluoride build-up has become significantly apparent in basement aquifers of Asia due to prevailing arid and semi-arid climate. The presence of faults in most Asian deltas provide channel for mixing of high fluoride water from neighboring aquifers with shallow groundwater.

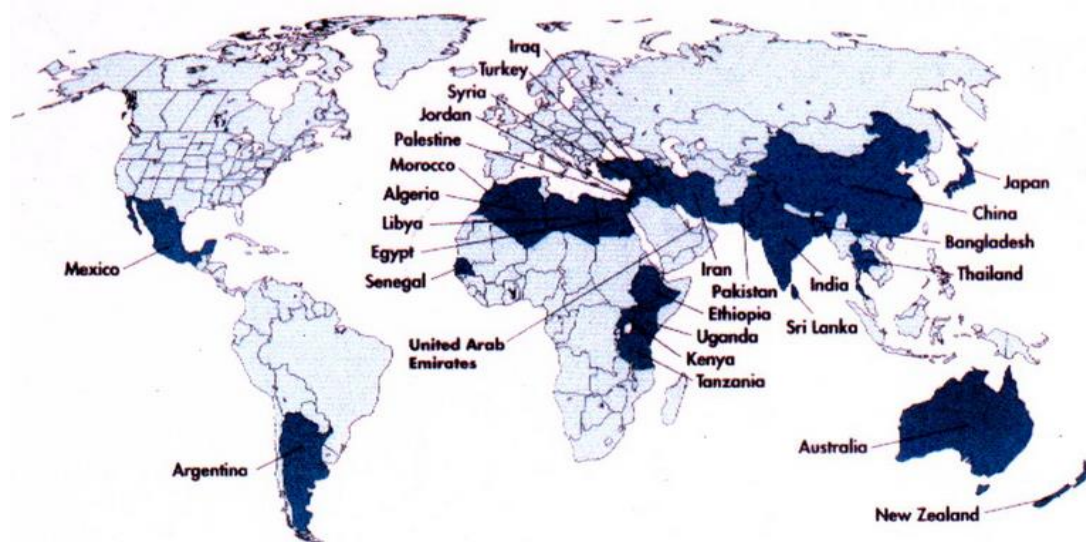


Figure 2.5 Countries with elevated fluoride concentration across the world

Source: Fluoride and fluorosis [20]

Occurrence of Fluoride in China

In China, problem related to fluoride is because of its high concentration in groundwater and contamination from the use of fluoride-laden coal. Drinking water with high fluoride level is recorded in all the 29 provinces, autonomous areas and municipalities except Shanghai [21]. It has been estimated that around 45 million population is suffering from dental fluorosis, of which 26 million cases is because of consuming high fluoridated water and remaining cases account for coal smoke pollution. Likewise, over 2 million cases of skeletal fluorosis is attributed to the

consumption of fluoride contaminated water and the excessive uptake from air or foods dried over burning briquettes made from coals and clay [22]. Coal-burning endemic fluorosis is common in mountainous areas of southwest China, where the local coal contains up to 3106 mg/kg fluoride. Brick tea-type fluorosis is discovered in China caused by habitual consumption of brick tea. Its manifestations can be more severe than water-type and coal combustion-type fluorosis.

Fluoride distribution of is of regional scale (about 1000 km²) in North China, while in south, it is local type (<100 km²). The regions with high fluoride levels is classified based on geochemical environments pertaining to sodium rich groundwater in inland basins of north and northwestern part, brackish groundwater in coastal aquifers of northern part, and soil rich in iron in southern China [23].



Figure 2.6 Fluorosis affected provinces in China

Source: China Health Statistical Yearbook, 2009 [24]

The fluorosis related to water is common in North-Eastern region including Yellow River flooding delta, and Hunan province is most acutely affected. Although Ministry of Health in PRC has set 1 ppm as maximum fluoride limit in drinking water, the concentration exceeds more than 3 mg/l in most of the northern inland basins. Table 2.3 shows general characteristics of aquifers bearing high fluoride in northern China.

Table 2.3 Fluoride concentration in Northern China basins

Inland Basins	Groundwater [F⁻] (mg/l)	Characteristics of aquifers
Zhangye Basin	0.2-3.1	Quaternary, unconsolidated and lacustrine sediment
Hetao Plain, Inner Mongolia	0.3-6	Quaternary, alluvial–pluvial sand, lacustrine and fluvial sandy silt, clay, highly organic
Huhhot Basin	0.1 to 8	Quaternary (largely Holocene) lacustrine & fluvial sediment in a fault-bounded Cenozoic rift
Datong Basin, Shanxi Province	0.1–22	Quaternary, alluvial–pluvial aquifers, organic-rich reducing lacustrine sediment interlayered with alluvial sands deposited in fault-bounded Cenozoic basin of Shanxi rift system
Taiyuan Basin	0.1–6.2	Quaternary alluvial–pluvial, lacustrine aquifers with Tianzhuang Fault separating the flow regime; Interaction between recharge areas and fluoride containing minerals; Evaporation and mixing of karst water in discharge areas
Yuncheng Basin	0.1–6.6	Quaternary aquifer of interlayered sediments including a shallow, intermediate and deep unit
Songnen Plain, Jilin & Heilongjiang Province	0.5–10	Meso–Cenozoic fault basin, neo-tectonic depression filled by alluvial lacustrine deposits. Quaternary unconfined aquifer with silt & sand, and confined aquifer. Deposited in Pleistocene and Pliocene

Retrieved from Wen, 2013 [25]

Occurrence of Fluoride in India

India is known to have very high levels of fluoride in groundwater. Total fluoride deposits on the earth crust is 85 million tons, of which 12 million tons is found in India. India lies geographically in the fluoride belt extending from Turkey to Afghanistan. According to Indian Government, ~ 25 million people from 9000 villages

are affected by fluorosis with another 66 million people at risk of its development [26].

Table 2.4 shows the prominent sources of groundwater fluoride in India.

Table 2.4 Fluoride concentration in groundwater of India

State/District	Groundwater [F] ranges (mg/l)	Sources
Andhra Pradesh, Kurmapalli	Up to 21	Fluoride rich rocks
Andhra Pradesh, Nalgonda	0.4 – 20	Fluoride rich granitic rocks
Andhra Pradesh, Vamsadhara River Basin	Up to 3.4	Pyroxene amphibolites and pegmatites
Andhra Pradesh, Wailapally watershed	0.5 – 7.6	Hornblende, biotite, apatite, fluorite and calcretes
Andhra Pradesh and Jharkhand	0.1 - > 4	Coal ash
Assam, Guwahati	0.18 – 6.88	Granite
Delhi	0.1 – 16.5	Irrigation and brick industries
Gujarat, Mehasana	0.94 – 2.81	Granite, gneiss and pegamite
Haryana, Bhiwani	0.14 – 86	Fluoride rich rocks
Karnataka, Bellary	0.33 – 7.8	Apatite, Hornblende and biotite
Kerala, Palghat	0.2 – 5.75	Hornblende and biotite gneiss
Maharastra, Yavatmal	0.3 – 13.41	Amphibole, biotite, fluorapatite
Rajsthan, Hanumangarh	1.01 – 4.42	Fluoride rich host rocks
Tamil Nadu, Erode	0.5 – 8.2	Host rocks and weathering of fluorite
Orissa	0.1-10.1	Groundwater
Agra, Uttar Pradesh	0.1–17.5	Shallow–deep Groundwater

Retrieved from Brindha et al, 2011[27]

The fertilizers containing leachable fluoride and fluoride containing coal have polluted the groundwater in east Punjab. Nutritional deficiencies and hot climates make the Indian population more susceptible to fluoride toxicity.

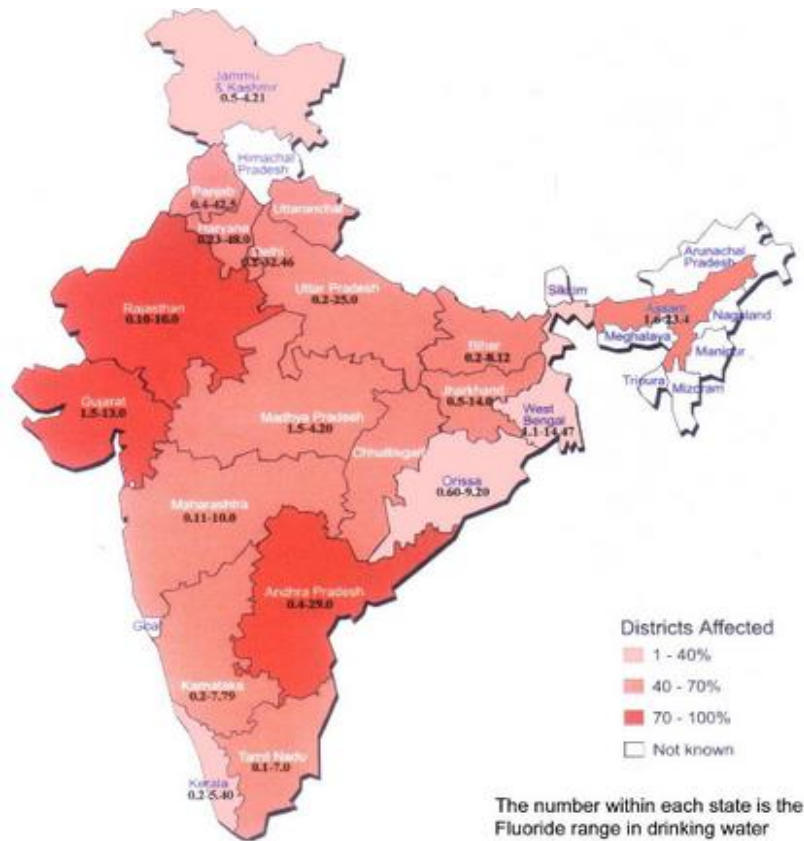


Figure 2.7 Fluorosis affected provinces in India

Source: Fluoride and fluorosis [20]

Occurrence of Fluoride in Thailand

The arc passing through Indian subcontinent and northern Thailand is among the well-known fluoride belts. Fluoride is found naturally in the northern and southern regions of Thailand due to the geological features of these areas cf. Figure 2.8. High fluoride levels with increased water hardness is reported in Ratchaburi and Saraburi provinces. The volcanic rocks comprising rhyolite, andesite, tuff, pebble and breccia release fluoride under favorable conditions. On top of that, more than 40 hot springs are associated with fluorite deposits in northern Thailand. In the hotspots of high-fluoride regions, concentrations as high as 12.8 ppm and 14.12 ppm are reported in surface and sub-surface water due to intrusion of fluoride-rich thermal waters.

An excess of naturally occurring fluoride in groundwater systems in Chiang Mai and Lamphun provinces has become a severe problem, posing health risks to around 8,500 communities. People consume both surface and groundwater and Chiang Mai Basin, the Buak-kang, Poo-kha and Chae-chang sub-districts has average fluoride concentrations of 0.75–7.46, 0.76–6.54 and 0.75–2.18 mg/l [28]. The presence of fault line within the deep aquifers facilitates upward intrusion of fluoride-rich thermal waters, possibly derived from dissolution of biotite in the underlying granitic bedrock.

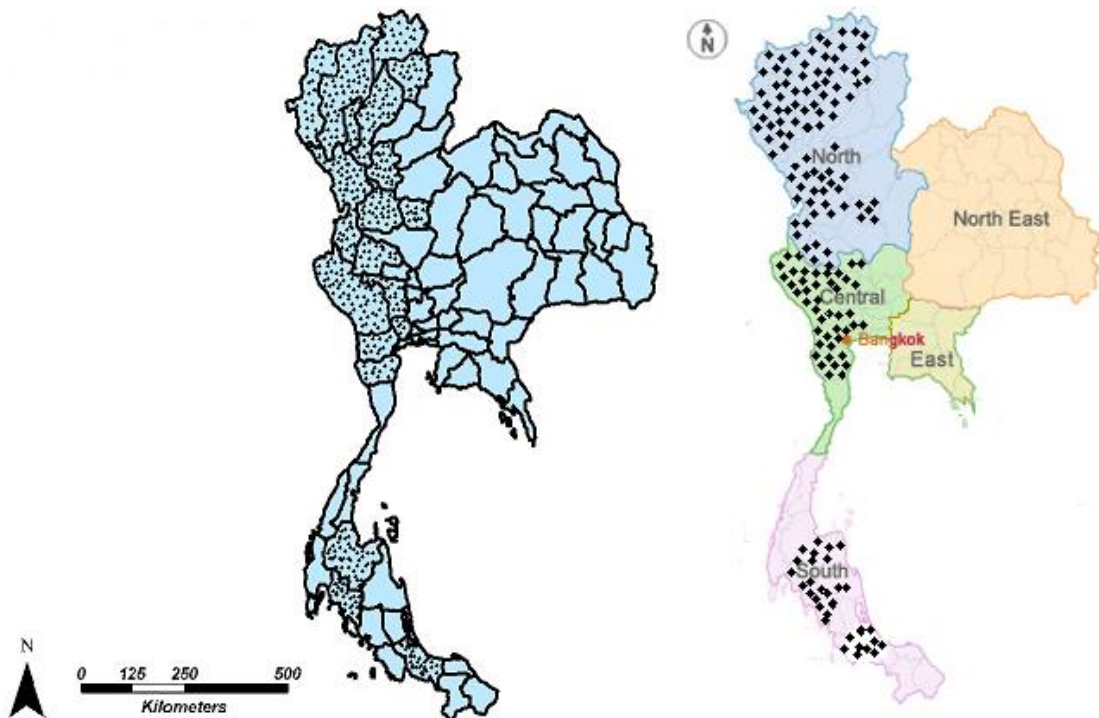


Figure 2.8 Map of Thailand showing dotted provinces as endemic fluorosis zones

Source: Modified from Mongkolnchai-arunya et al, [29]

In Lamphun Province 16 mg/l fluoride concentration was recorded, which is around 20 times higher than the Thai Drinking Water Standard (0.7 mg/l). Likewise, fluoride content of geothermal well water at Ban Pong Na Khum in Chiang Rai province was 37 mg/l [30]. People consuming the fluoridated water from artificial lake in Ban Mae Toen village in Lampang province have been facing the problems related to brain damage, deaf-mutism, or slow brain development and goiter. However, fluoride content varies among the regions and type of water. Most of the commercially-available bottled water in Bangkok contains negligible amounts of fluoride and the average F⁻ level in tap water meets the Thai Drinking Water Standard.

2.2 Technologies for Defluoridation of water

The choice of fluoride removal methods depend on the quality of water in the source. Boiling, UV disinfection, conventional filtration and most of the chemical treatment fails to remove fluoride from water. There are several in situ and ex situ conventional methods in practice for the treatment of fluoridated water.

2.2.1 Chemical Additive Methods

Fluoride can be removed by liming, co-precipitation or electrocoagulation-flotation (ECF) onto the formed precipitate. The precipitation and coagulation processes has been extensively investigated using activated alumina. The principle behind this process is that fluoride ions adsorb on the flocs, which are then removed in the succeeding treatment units like sedimentation, fixed beds or microfiltration units. In a study, ~ 69.5% removal was seen at 13.8 mg/l F⁻ solution and neutral pH by 4 g/l activated alumina. At alkaline pH, hydroxyl and silicates competed strongly with fluoride ions for the active alumina exchange sites, while at acidic condition soluble alumino-fluoro complexes resulted in presence of aluminum ions in treated water [31].

The fluoride removal efficiencies of Poly Aluminum Chloride (PAC) and alum were evaluated for treating the fluoridated drinking water. With 200 to 500 mg/l PAC, fluoride concentration decreased to 3.8 mg/l from 7.8 mg/l at pH 8.4, whereas alum dose of 200 to 500 mg/l lowered the F⁻ level to 2.3 mg/l [32]. In another study, fluoridated wastewater was treated by precipitation-flotation process. Calcium chloride was added to generate the precipitate followed by subsequent removal of fluoride as calcium fluoride (CaF₂). During the experiment, when [Ca²⁺]/[F⁻] ratio was increased to 1, 1.5 and 2, the F⁻ concentration dropped to 3.4, 2.9 and 2.8 mg/l from 610 mg/l and this trend continued as long as [Ca²⁺]/[F⁻] was greater than 1 [33]. The US EPA has regulated 4 mg/l F⁻ as the discharge standard for fluoridated wastewater.

The combined electrocoagulation-flotation (ECF) process forms an active coagulant for eliminating fluoride by precipitation and flotation in situ. The F⁻ level was decreased to < 2 mg/l at pH 6 from 15 mg/l concentration (after lime precipitation) by allowing 4.97 F/m³ charge loading. A residence time of 20 minutes was maintained in coagulation cell and the introduction of 50 mg/l Fe³⁺ or Mg²⁺ allowed the chemical sorption of fluoride by replacement of -OH from Al_n(OH)_{3n} flocs [34]. Similarly, for

improving the flotation in ECF, Sodium dodecyl sulfate (SDS) was used to treat fluoridated wastewater. The residual fluoride concentration (5 to 6 mg/l) was found to be lower than that of the dissolved air floatation method (10.3–10.9 mg/l) because the fluoride ion is co-precipitated or adsorbed onto the aluminum ions [35].

Nalgonda technique is commonly used defluoridation technique in both community and household levels. This process includes addition of lime, alum and bleaching powder (optional) in water, which is followed subsequently by coagulation, sedimentation, filtration, and disinfection [36]. This method was tested in Tanzania for the treatment of fluoride containing water. As a result, F^- concentration was dropped to 3.5 mg/l from 22.1 mg/l. If dose of alum was applied over 800 mg/l, the concentration could be reduced further [37]. In another study, Nalgonda technique was modified to cope with different degrees of water hardness for varying alum concentrations. Combination of 1000 mg/l alum and 60 mg/l lime was able to lower the fluoride to 1.4 mg/l from 5.6 mg/l with 0.43 g precipitate in tap water, and from 2.3 mg/l to 0.27 mg/l with 0.23 g precipitate in drinking water. The pH value of both water sources was found to be 7.4 (± 0.2). So, doubling the concentrations of alum and lime results in significant decrease of fluoride when compared to the existing Nalgonda technique [38].

Although precipitation-coagulation is widely used process, the main drawbacks of this process includes the difficulty in lowering residual fluoride concentration below the WHO regulated standard and there is sludge disposal problems as well. Likewise, the shortcomings of Nalgonda method are its moderate fluoride removal efficiency ($\sim 70\%$), high aluminum sulfate dose ($\sim 700\text{--}1200$ mg/l), increased pH and water hardness, and residual sulfate salinity and aluminum (2-7 mg/l) in treated water [15]. So, this technique is only desirable for lower concentration of dissolved solids (1500 mg/l) and 2-20 mg/l fluoride concentration at alkaline condition.

2.2.2 Filtration

The pressure driven membranes like Reverse Osmosis (RO), ultrafiltration (UF), nanofiltration (NF) and microfiltration (MF) uses hydrostatic pressure to force the fluoride contaminated water pass to through semi-permeable membrane. In a study, RO membrane was used to reduce the fluoride load to less than 1 kg/d under retention factor over 98%. This process was able to reduce the treated volume from 6 m³/d to

0.36 m³/d without any pretreatment or addition of some supplementary compounds. To treat 6 m³/d effluent volume containing 460 mg/l fluoride, the estimated membrane area was in the order of 10 m² [39]. Similarly, the effect of pH on F⁻ ion retention was evaluated using six NF and RO membranes (BW30, ESPA4, NF90, TFC-S, UTC-60, and UTC-80A). Fluoride retention was described on the basis of fluoride speciation, membrane and ion properties like hydrated size, Gibbs energy of hydration and charge. The process was dependent on pH and more than 70 % F⁻ ion was retained above pH 7. The charged F⁻ was dominant species at pH > 3.2, and the steric exclusion led to the strong retention of F⁻ by tighter membranes like BW30 and NF90 [40].

Nanofiltration has similar working principle as RO except that the operation is performed at low pressures with the same permeate flux. Evaluation for retention of halide salts by nanofiltration revealed that fluoride being a small ion is best retained under the reduced pressure. Fluoride retention is practically unaffected by the pressure as the passage of this ion is mainly controlled by diffusion. The filtered water had the salinity of 230 mg/l (initial salinity 2025 mg/l) and fluoride concentration was lowered to 0.7 mg/l from 13.5 mg/l [41]. Commercial thin-film composite membranes were used for treating high fluoride content water and membrane parameters affecting the process was discussed. The pure water permeability (L_p) values of all membranes followed the order of DS-5-DL (21.30×10^{-9} m³/m² s kPa) < SR-1 < DS-51-HL [42].

As microfiltration alone can't remove low molecular weight contaminants like fluoride, study was conducted to test the efficiency of coagulation/flocculation cum microfiltration process for removing fluoride from groundwater. Microfiltration tests were carried in micro/ultrafiltration unit (NETZSCH) with 0.45 µm porous membranes using cross-flow filtration mode after coagulation. The operating conditions were maintained at 5 mg/l F⁻ concentration, 5 g/l *Moringa Oleifera* Lam seeds, pH 7 and 2 bar pressure. The fluoride level was decreased to 1.03 mg/l with 79.3% removal efficiency [43]. *Moringa oleifera* seed was used for the coagulation of 10 mg/l fluoridated water, and later was separated by ultrafiltration membranes (mono 1, mono 2 and multi 1) under different pressures. After combined coagulation/filtration process, 83% fluoride was retained in mono 1 membrane at 1 bar pressure [44].

Despite having advantage of requiring no additives, membrane processes have numerous economical and technical restrictions. There is high chance of fouling,

scaling and membrane degradation (media for microbiological growth) and disposal of concentrated water becomes a problem. Besides, NF/RO systems is rarely installed for fluoride removal as their rejection depends on the type of membrane and they are less flexible than electro dialysis. The main drawback of RO for fluoride removal is that ~99% salts is rejected by membrane, i.e., all F^- ion is excluded during treatment [45].

2.2.3 Dialysis and Electro dialysis

Electro dialysis (ED) is the convenient technique for fluoride removal as this process is simple and easy to operate. The fluoride species is separated and removed by its selective transport through alternately aligned ion-exchange membranes. The negatively charged ions in the dilute stream migrate towards anode under the influence of electrical potential difference and is retained by the cation exchange membranes. This method differs from pressure-driven membrane processes as electrical current is utilized as major driving force for matter separation. Electro dialysis Reversal (EDR) is applied when ED is subjected to membrane fouling. In EDR, path of electric current is reversed to allow the separation and switching of dilution and concentration chambers.

The electro dialysis (ED) process was employed for treating of 7.72 mg/l fluoridated geothermal water with voltage of 10.02 V and 2.7×10^{-3} m/s linear flow rate. The removal of F^- (99%) and Cl^- (100%) was found to be higher than SO_4^{2-} (90.3%) ions because of the increased hydrated radius and ionic charges of this divalent ion resulting in slow transport. After 29 and 25 minutes of the experiment, fluoride concentration reduced to 0.06 mg/l and 0.07 mg/l with pH adjustment and chemical pretreatment [46]. Generally, the efficiency of electro dialysis depends on many factors such as pH, initial electrolyte concentration, applied current, flow rate, and coexisting ions. So, the effect of these experimental parameters was studied on fluoride removal [47]. The removal process was more effective when fluoride was the only anionic species present in water with high feed concentration. The operation time needed for maximum fluoride removal was much shorter on increasing the applied potential, while the flow rate didn't show any significant effect on removal process. Besides, fluoride and chloride ions competed strongly for the adsorption sites.

Likewise, ED process was used for removing F^- ions from artesian well water using anion-exchange membranes like AMP® (Asahi Glass Co.) and

photopolymer membranes MZA™. The AMP® membrane removed 69% fluoride under 0.1 A/dm² current density. On increasing current density to 0.7 A/dm², removal efficiency increased to 97%. On the other hand, MZA™ membrane could remove only 40% fluoride with the same current density [48]. Donnan dialysis utilizes counter-diffusion of two or more ions through ion-exchange membranes to separate target contaminants. In this context, two synthetic fluoridated water (9.5 mg/l and 6.1 mg/l) was treated using Donnan dialysis. The DSV anion exchange membrane (Asahi Glass) used in this study had 0.176 m² area and the compartment was 16 cm long, 11 cm wide and 0.12 cm thick. The receiver solution circulating in batch mode was able to lower fluoride level to the regulated norm (<1.5 mg/l). The most suitable operating conditions are: pH 5, 5×10⁻⁵ mol l⁻¹ F⁻ and 25×10⁻⁴ mol l⁻¹ Al³⁺ [49].

The main advantages of ED process includes its flexibility in operation, high selectivity, low chemical demand and higher recovery rates in comparison to other membrane processes. However, the disadvantages can be related to the formation of H₂ in the electrode rinse, specific power consumption for pumping, necessity of concentrate treatment, and disposal of brine might be a problem.

2.2.4 Ion Exchange Method

In this process, ions of equal charge is exchanged between the solution and an insoluble resin. Ion exchange and adsorption process are described using similar models as the exchange of ions takes place between solution and internal surface of the solid in both processes. Nonetheless, the materials should be interchanged in the ion-exchange membranes unlike adsorption processes.

In a research carried by Samadi et al, fluoride was removed from synthetic solution using strong-base anion resin of Polystyrene–divinylbenzene matrix. Maximum removal efficiency of 76, 78% and 80% was seen for 2.5, 3.5 and 4.5 mg/l F⁻ concentration at pH 7. For 4.5 mg/l F⁻ solution maintained at pH 5 or 7, the required time and amount of resin would be 60-90 min and 0.2 g/200 ml. The exchange capacity of the resin was 1.25-1.55 (eq/l) with the maximum uptake of 13.7 mg/g [50].

Despite having macro pore (~10² nm diameter) distributions, conventional ion exchange resins has very slow performance in removing fluoride ions, as the access to particle interior is often limited by diffusion. In this context, Zr (IV)-immobilized

resin prepared by surface-template polymerization was tested to treat the fluoridated tap water and industrial wastewater. Maximum capacity of the membrane (0.30 mmol/g) is attributed to large number of macropores (~300 nm) comparable to microfiltration membranes and high surface area (37 m²/g) of resin. High removal at pH 2 and 4 is due to F⁻ adsorption onto Zr – phosphate groups [51]. Yet, in this study problems were reported regarding slow binding kinetics and inaccessibility of fluoride to binding sites inside the polymer. Thus, for high-speed removal, the same authors modified adsorbent surface with large-macropores (10²~10³ nm diameter) and mesopores (2~50 nm diameter) by surface template polymerization using polystyrene as a porogen (PS 5 and PS 10). The specific surface area was constant at 35 – 40 m²/g and the adsorption capacities of PS 0 (reference polymer without polystyrene), PS 5 and PS 10 for 25 mg/l fluoride concentration are 0.30, 0.33 and 0.36 mmol/g, respectively [52].

But the selective uptake of fluoride from water by ion exchange method is not quite good. The coexisting anions present in real drinking water may interfere in the effective binding of fluoride in the resin. According to well-known Hoffmeister's selectivity series, selectivity of anion exchange resins to F⁻ over other co-existing anions like SO₄²⁻ and Cl⁻ is low (Citrate > SO₄²⁻ > oxalate > I⁻ > NO₃⁻ > CrO₄²⁻ > Br⁻ > Cl⁻ > formate > acetate > F⁻) [53]. Further shortcomings are associated with high costs, long detention time, secondary pollution (disposal of backwash water), low pH and high chloride in the treated water, and regeneration of resins.

2.2.5 Adsorption

Adsorption is a widely used process to remove soluble substances by using solid phase medium. This process is of fundamental importance to different physical, biological, and chemical processes occurring in environment. The selection of proper adsorbent requires rigorous trial for the efficient removal of target pollutants. Also, the adsorption capacity is an important factor to be considered for testing the adsorbents in real field applications. A variety of adsorbents like activated and amorphous alumina, bauxite, bone char, charcoal, calcite, clay, zeolite, biosorbents, agricultural by-products and rare metal-loaded polymeric resins have been screened for their utility in removing fluoride from aqueous solution. The commonly used adsorbents and the influence of various operational parameters on fluoride removal process are described below.

Alumina and aluminum-based adsorbents

These adsorbents are widely studied for defluoridation process in both community and domestic levels. Coprecipitation or adsorption may occur when Al (III) ion is added to the fluoridated water. Activated alumina contains aluminum oxide (Al_2O_3) grains which provides binding sites for fluoride with good sorptive surface. The fluoride interaction with aluminum hydroxide ($\text{Al}(\text{OH})_3$) and alumina (Al_2O_3) was studied at variable pH and fluoride concentrations. $\text{Al}(\text{OH})_3$ is a highly porous material and provides efficient coating for the surface modified adsorbents. Most of the amorphous gibbsite in solution forms AlF complexes at $\text{pH} < 6$ and $\text{F}^- : \text{Al}$ ratios > 2.6 [54]. Likewise, Activated alumina (AA) (Grade OA-25) was employed to remove fluoride in batch and continuous mode process with dose of 4 g/l. For continuous operation, 88 and 97% removal was noted for 5 mg/l and 2.8 mg/l F^- concentration [55].

Generally, low adsorption potential of commercial activated alumina have limited its use for removing fluoride from large volume of fluoridated water. So, alumina surface is modified in number of studies to enhance its adsorption efficacy either by coating, sieving or thermal treatment. Rare earth metal like Lanthanum, Neodymium, Yttrium and Zirconium are commonly used for impregnation purpose. In this context, Lanthanum hydroxide supported on alumina was able to lower the fluoride from 7 mM to 0.003 mM at pH 5.7-8. And, in case of industrial wastewater, fluoride level was lowered to 0.04 $\mu\text{g/l}$ from 3.2 $\mu\text{g/l}$ (more than 96%). The sorption selectivity shows that removal process is influenced by PO_4^{3-} and SO_4^{2-} ions but not by Cl^- , Br^- , I^- and NO_3^- ions [56]. Furthermore, the adsorption capacity of nanoscale aluminium hydroxide (nano- AlOOH) was evaluated and the adsorbent had superior adsorption ability than activated alumina (1.8-1.9 mg/g). For 20 mg/l fluoridated solution, 95% removal was seen at pH 7 and dose ≤ 1.6 g/l within 60 minutes [57]. However, the particles tend to aggregate in nanoscale operations which negates its other benefits.

For an effective utilization of nanoparticles, it should be encapsulated inside matrix of host material. So, hydroxyapatite-modified activated alumina (HMAA) was tested as hybrid adsorbent (incorporates properties of both nanoparticles and porous AA) for the removal of fluoride under batch and continuous operations. The hybrid adsorbent showed almost fivefold higher adsorption capacity than virgin-activated alumina (3.1 mg/g) due to dispersed phase of hydroxyapatite nanoparticles

[58]. In further studies, mesoporous alumina was coated by CuO and favorable condition was observed at 0.4 g/l adsorbent dose. More than 80% fluoride was removed from the solution comprising 1000 mg/l Cl^- , NO_3^- and SO_4^{2-} , whereas efficiency dropped to ~70% in presence of CO_3^{2-} and HCO_3^- ions above 200 mg/l [59].

Table 2.5 Fluoride adsorption capacity of Alumina/Aluminum based adsorbents

Adsorbents	Concentration Range (mg/l)	pH	Adsorption capacity (mg/g)	Ref.
Gibbsite ($\text{Al}(\text{OH})_3$)	1.9-19	5-7	16.3	[54]
Activated alumina (Grade OA-25)	2.5-14	7	1.45	[55]
Lanthanum hydroxide supported on alumina	133	5.7-8	6.65 (0.350 mM/g)	[56]
Nanoscale aluminum hydroxide (nano- AlOOH)	5-30	6-8	62.50	[57]
Hydroxyapatite-modified activated alumina (HMAA)	10	8	14.4	[58]
Copper oxide incorporated mesoporous alumina (COCA)	10	4-9	3.155	[59]

Activated alumina is an expensive adsorbent and high amount of toxic AlF complex is formed after the defluoridation process. Besides, frequent activation of alumina is required, which makes this technique much costly and also the adsorption efficiency eventually drops down with increasing number of usage-regeneration cycle.

Calcium-based adsorbents

Calcium derived compounds have high affinity for fluoride ions, thus can be effective adsorbents for removal of fluoride. Crushed limestone was employed for the treatment of fluoridated water in batch process. The highest removal was shown by smaller sized particles (150 μm) with 33.33 g/l dose, and the removal efficiency was proportional to the particles surface area. Surface-sensitive techniques like AFM and XPS and zeta potential values showed that both precipitation and adsorption were responsible for the removal of fluoride [60]. Similarly, fluoride was removed from 50 mg/l synthetic fluoride solution with activated and ordinary quick lime. Fluoride

removal efficiencies of these adsorbents were 80.5% and 35.7% at optimum conditions. There was almost threefold increment in surface area of adsorbent sample after thermal treatment (11.75 m²/g) than ordinary lime (4.19 m²/g) resulting in enhancement of adsorption capacity (16.67 mg/g). Nonetheless, this adsorbent is not suitable for water treatment applications in household level, as the fluoride concentration cannot be reduced to the standard value and also alkalinity of the water is increased [61].

Larsen and Pearce encompassed brushite and calcite suspension for making the fluoridated water applicable for domestic purposes after the treatment. Equal charges of 0.3-0.5 g brushite and calcite were boiled with 1 litre of fluoridated solution, allowing sedimentation of calcium salts. The fluoride concentration was reduced to 0.06, 0.4 and 5.9 ppm from 5, 10 and 20 ppm solution. The main purpose of boiling is to provide sufficient agitation for intimate contact to convert the two salts into apatite. The conversion of brushite to apatite incorporated fluoride in solution and subsequently increased phosphate concentration with the decrease in pH [62].

Table 2.6 Fluoride removal efficiency of Calcium based adsorbents

Adsorbents	Concentration Range (mg/l)	pH	Adsorption capacity/ Removal (%)	Ref.
Crushed Limestone	3-2100	7	90-99%	[60]
Quick Lime	10-50	-	16.67 mg/g	[61]
Brushite and calcite	5-20	7	~70.5%	[62]

In general, the addition of lime in fluoridated water results in calcium fluoride formation due to fluoride precipitation. Yet, the low soluble calcium hydroxide hinders the efficient fluoride removal process and the precipitates are also not settled. So, lime is generally added in the alum treatment to overcome this problem. The efficiency of these calcium based adsorbents depend on pH and the frequent adjustment of pH makes the process troublesome. The presence of co-ions in water will also interfere during the fluoride adsorption.

Iron-based adsorbents

Iron-based adsorbents like goethite and magnetite show strong likelihood for fluoride adsorption due to available active sites for adsorption. They are good for precipitation process and the released cations from iron compounds act as coagulants for fluoride removal. Granular ferric hydroxide (FeO(OH)) or goethite is a hydrous iron

oxide mineral and is environmentally friendly sorbent for fluoride. Over the pH 2–11, fluoride adsorption for 25 and 71 mg/l F⁻ concentrations was found to be overlapped. This indicated that there is no major role of surface electrostatic forces in fluoride removal. The presence of hydroxyl groups on adsorbent surface allowed fluoride adsorption indicative of an OH···F interaction [63].

The efficiency of synthetic siderite (FeCO₃) was tested for fluoride adsorption. Fluoride was adsorbed onto the fresh goethite after coprecipitation of ferric hydroxide. After adsorption, siderite was partially changed into goethite which shows high affinity for fluoride [64]. Furthermore, the interface interactions of fluoride onto laterite surface was studied with surface complex modelling. Laterite used in this study consist of 40% Fe₂O₃ as dominant species and 30 % aluminum with low amount of SiO₂. The adsorbent offered several binding sites ($\equiv\text{AlOH}$ and $\equiv\text{FeOH}$) for surface complexation, and the surface hydroxyl groups showed amphoteric behavior [65].

Table 2.7 Fluoride removal efficiency of Iron based adsorbents

Adsorbents	Concentration Range (mg/l)	pH	Adsorption capacity/ Removal (%)	Ref.
Goethite	10-105	7	~95% : 10 and 25 mg/l	[63]
Synthetic siderite (FeCO ₃)	20	6.86	1.775 mg/g	[64]
Laterite	25	5	-	[65]

However, the main drawbacks of these adsorbents are related to the high materials cost or time and energy consuming monotonous synthesis procedures. Also, some adsorbents have very small loading capacities and are less sensitive to pH.

Metal oxides/hydroxides/oxyhydroxides as adsorbents

Metallic elements have tendencies to donate valence electrons and acquire positive charges for attracting negatively charged fluoride. Two or multi-metal oxides/hydroxides can be combined to produce a new synthetic adsorbent and these metal oxyhydroxide coordinates metal ions and properties of oxide minerals. The metal hydroxides contain surface oxygen groups with differing number of coordinating metal ions which can effectively bind fluoride ions. Several studies have focused on the oxide ores like refractory grade bauxite, feed bauxite, manganese ore, and hydrated oxides of

manganese ores (WAD) to investigate their fluoride adsorption capacities. A new adsorbent, magnesia-amended silicon dioxide granules (MAS) was developed through the wet impregnation of SiO₂ with MgCl₂ solution for adsorption of fluoride. The area of SiO₂ was improved from 303.61 m²/g to 494.95 m²/g after magnesia loading, resulting in higher adsorption [66].

The nano-sized superparamagnetic zirconia material (ZrO₂/SiO₂/Fe₃O₄, SPMZ) was used as adsorbent to remove fluoride. Sorption at 0, 0.01 and 0.1 N NaNO₃ gave the equilibrium fluoride loadings of 10.6, 10.4 and 10.2 mg/g, respectively. The adsorption process was mainly due to the covalent interactions rather than ion pair formation. So, SPMZ have benefits like higher mass transfer rates, better selectivity, physicochemical stability, and also the particles can be detached from solution by high gradient magnetic separation [67].

Rare earth metals and titanium hydroxide-derived adsorbents are also used as fluoride adsorbing agents. The harmless rare earth metal-loaded adsorbents have high selectivity for fluoride due to their multi valence behavior and have easy operation procedure. The efficiencies of three adsorbents, TiO₂ (prepared through hydrolysis), Ti-Ce, and Ti-La hybrid oxides (prepared from hydrolysis-precipitation) were evaluated for the fluoride elimination. The synergistic effect was seen in hybrid adsorbents for fluoride sorption and this can be related to high zeta potential and their amorphous structures. High removal at acidic pH was related to electrostatic attraction process [68].

Table 2.8 Fluoride adsorption capacity of metal oxides/hydroxides

Adsorbents	Concentration Range (mg/l)	pH	Adsorption capacity (mg/g)	Ref.
Magnesia-amended silicon dioxide granules (MAS)	10	3	12.6	[66]
Superparamagnetic zirconia	10	4	14.7	[67]
TiO ₂	10	<5.7	1.7	[68]
Ti-Ce		<6.2	9.6	
Ti-La		<6.8	15.1	

The small amount of metals supported on cheaper materials significantly increase the fluoride removal. Nonetheless, the main problems related to the

implementation of these metal-based adsorbents is their cost. Besides, the alkali metals have the lowest electronegativity resulting in the formation of covalent bond.

Carbon-based adsorbents

Carbon-based adsorbents have been widely used in fluoride adsorption processes and most of them have very high internal surface area required for adsorption. The more the surface area, more will be the adsorption resulting in better removal efficiency. So, the fluoride removal efficiency of multi-walled carbon nanotubes (MWCNTs) was evaluated and compared with activated carbon and Fullerene C60 after treating fluoride contaminated drinking water in Iran. The performance of MWCNTs was found to be excellent than other two adsorbents because it could remove fluoride even at low concentrations. The removal was significant after 18 minutes of contact time. So, these tubular sheet of graphite have very good sorption potential due to their high surface area with uniform distribution of pores [69].

Fishbone charcoal was used for batch defluoridation of water in a moving media adsorption system and nomograph was developed based on the experimental results. The dose of 2 g/l could reduce 3 mg/l F⁻ to 1.5 mg/l within 240 minutes. The beakers were stirred at 100 rpm and 0.55 mm adsorbent size was considered for adsorption [70]. In another study, regenerated bone char media (0.50–1.0 mm) was optimized to use as adsorbent for treating fluoridated water in Tanzania. The removal of 70.64 % was reported, with bone char regenerated at 500°C. Residual fluoride varied from 17.43 mg/l at 2 min to 8.53 mg/l at 180 min. Filter column experiments showed slight differences in removal capacity between fresh and regenerated bone char [71].

Table 2.9 Fluoride removal efficiency of Carbon based adsorbents

Adsorbents	Concentration Range (mg/l)	pH	Adsorption capacity/ Removal (%)	Ref.
Carbon nanotubes (MWCNTs)	10	5	94%	[69]
Fishbone charcoal	3	8	0.75 mg/g	[70]
Regenerated bone char media	21.26	-	0.75 mg/g	[71]

Even though bone char is cost effective, it possess limitations for defluoridation of water due to unhygienic conditions and some traditional/religious

objections. Besides, activated charcoal (AC) is considered as universal adsorbent because of its wide applications and viability, but still the affinity of anions like fluoride towards most of the carbon-based adsorbents is low. Although some studies have focused on developing novel adsorbents utilizing surface area of AC and impregnating fluoride adsorbing metal, it can directly influence the cost for adsorbents preparation.

Natural materials as adsorbents

Naturally occurring adsorbents have been used for removing fluoride for decades due to their ease of availability. So, defluoridation of water samples by lignite (LN), fine coke (FC) and bituminous coal (BC) was studied at different adsorbent doses. Time required for equilibrium corresponded to 150 min for LN, 90 min for FC and 60 min for BC with 0.1 dose. The removal efficiencies of LN, FC and BC lied between 77 and 85% [72]. In another work, ground fired clay pot was used for fluoride adsorption. It was found that 120-240 g dose was enough to lower 6 l tap water to below 1.5 mg/l. The adsorbent was completely saturated after elution of 20 l fluoridated water [73].

An attempt was made to remove fluoride using natural materials like red soil (ferruginous lateritic clay), untreated charcoal, local powdered brick, fly ash and mineral serpentine ($Mg_6Si_4O_{10}(OH)_8$), of 2.5 ϕ mesh fraction. The main constituents of fly ash are Si, Al, Fe, Ti, Ca, $MgSO_3$ and alkalis. The oxides of aluminum and iron in red soil provide effective binding sites for F^- ions [74].

Table 2.10 Fluoride removal efficiency of Natural materials based adsorbents

Adsorbents	Concentration Range (mg/l)	pH	Adsorption capacity/ Removal (%)	Ref.
Lignite (LN)	90	5-10	7.09 mg/g	[72]
Fine Coal (FC)		Acidic	6.9 mg/g	
Bituminous Coal (BC)		pH	7.44 mg/g	
Ground fired clay pot	10	5-7	285 mg/kg	[73]
Red soil	10	-	99%	[74]
Untreated charcoal			9.5%	
Local powdered brick			50%	
Fly-ash			50%	
Mineral serpentine			59%	

In addition, various other clays like bauxite, palygorskite, Tunisian clays, activated kaolinite clay, chemically modified bentonite, attapulgite, algerian clay types, surface-tailored zeolite, metal loaded natural zeolites are used as promising adsorbents. Although fluoride removal capacity of these adsorbents is not much high in comparison to materials like activated alumina, some improvements in design configurations of packed column results in efficient fluoride removal. These locally available materials are valuable in improving drinking water supplies in the fluorosis endemic areas.

Nano-adsorbents

The small size and significant electrical conductivities of nano particles make them fit for various purposes. In this subject, nano-alumina (Al_2O_3) was tested for fluoride adsorption. More than 85% fluoride removal took place within 120 min and equilibrium was attained in 24 h at the speed of 220 rpm. The fluoride uptake process was highly affected by the phosphate, sulphate and carbonate ions in solution [75].

The amorphous Al_2O_3 supported on carbon nanotubes ($\text{Al}_2\text{O}_3/\text{CNTs}$) was used as adsorbent for fluoride, and its adsorption capacity was 13.5 times more than AC-300 carbon and four folds greater than $\gamma\text{-Al}_2\text{O}_3$ at 12 mg/l F^- solution. The workability at wide pH range makes $\text{Al}_2\text{O}_3/\text{CNTs}$ suitable adsorbent for fluoride [76]. Moreover, the feasibility of nano-scale aluminum oxide hydroxide (nano- AlOOH) was studied. At pH 6.8, the fluoride removal efficiency was 96.7% with 5 g/l dose. For the studied fluoride concentrations (6.06 mg/l, 11.39 mg/l, 24.04 mg/l), majority of sorption occurred within 30 minutes. The presence of SO_4^{2-} or PO_4^{3-} in solution was found to compete with the fluoride for the binding sites [77].

Table 2.11 Fluoride adsorption capacity of nano-sorbents

Adsorbents	Concentration Range (mg/l)	pH	Adsorption capacity (mg/g)	Ref.
Nano-alumina (Al_2O_3)	1-100	6.15	14	[75]
$\text{Al}_2\text{O}_3/\text{CNTs}$	50	6	28.7	[76]
Nano- AlOOH	13	6-8	3259 mg/kg	[77]

Adsorbents like granular Fe–Al–Ce adsorbent, superparamagnetic adsorbents of bayerite/ $\text{SiO}_2/\text{Fe}_3\text{O}_4$, magnetic nanosized adsorbent and nano-alumina has also been explored to assess their efficacy in fluoride removal.

Building materials based adsorbents

The efficiency of building materials towards fluoride removal has been evaluated in many defluoridation studies. The fluoride adsorption on light-weight concrete was analyzed at varying pH, shaking speed and temperature. The optimum values of sorption kinetics at 333 K and 60 min equilibrium time was 0.3, 0.255 and 0.147 g mg⁻¹ min⁻¹ at 235 rpm. The surface area of the adsorbent was 22 m²/g and also the hydroxylated surfaces of metal oxides such as Ca, Al and Si in the adsorbent reacted with H⁺ to form MOH₂⁺ ligand. This positive ligand interacts with fluoride and form MF compound and H₂O molecules [78].

Yadav and co-authors used brick powder (BP) as adsorbent for defluoridating groundwater and compared its efficiency with commercial activated charcoal (CAC). The equilibrium was reached within 60 minutes for both adsorbents. The F⁻ removal efficiency improved from 43.2 to 56.8% for 0.2–2.0 g/100 ml BP dose and 49.4–84.2% for the same dose of CAC [79]. In another study, hydrated cement (HC) was utilized for fluoride removal at various time. The adsorption capacity was considerable in acidic pH due to presence of alumina. Further, CO₃²⁻ and HCO₃⁻ had negative effect, while Cl⁻, NO₃⁻ and SO₄²⁻ didn't affect fluoride adsorption process [80].

Table 2.12 Fluoride removal efficiency of Building materials based adsorbents

Adsorbents	Concentration Range (mg/l)	pH	Adsorption capacity/ Removal (%)	Ref.
Light-weight concrete	120	6.9	2.6 mg/g	[78]
Brick powder (BP)	5	6–8	56.8%	[79]
CAC		4	84.2%	
Hydrated cement (HC)	6	6.7	75%	[80]

The success of these adsorbents in fluoride removal hinges on their good performance under variable operating conditions.

Apatite and hydroxyapatite as adsorbents

Apatite and hydroxyapatite are group of phosphate minerals having high concentration of OH⁻, F⁻ and Cl⁻ ions. So, the defluoridation capacities of various sorbents such as synthetic nano-hydroxyapatite (n-HAp), biogenic apatite (bone meal, B), treated biogenic apatite (bone meal prepared by H₂O₂ oxidation, BH₂O₂) and geogenic apatite (rock phosphate) were examined. The n-Hap had the maximum

defluoridation capacity followed by BH_2O_2 , B and rock phosphate. Bone usually comprises 30% organic compounds and 70% inorganic materials made of HAp, which makes it suitable adsorbent for fluoride removal [81]. In a likely manner, fluoride removal capacity of natural crystalline apatite was investigated at various laboratory conditions in Sri Lanka. The surface area and site density of apatite were $22 \text{ m}^2/\text{kg}$ and $2.7 \text{ sites}/\text{nm}^2$, thus the removal was almost 100% for increasing apatite suspensions [82].

Anionic clays and hydrotalcite-like compounds (HTICs) are drawing considerable attention in adsorption studies. Synthetic porous and crystalline calcium hydroxyapatite, Mg, Ni and Co calcined hydrotalcite-like compounds and CaF_2 bearing minerals are extensively used in lab and in real field experiments for fluoride removal. The kinetics of calcined MgAl-CO_3 layered double hydroxides (CLDH) was investigated for F^- ions removal. The fluoride depletion rate at various temperature reveals that the F^- removal rate of CLDH is enhanced with the rise in temperature. And, the results from experiment followed pseudo-second-order kinetics [83].

Table 2.13 Fluoride adsorption capacity of apatite and hydroxyapatite

Adsorbents	Concentration Range (mg/l)	pH	Adsorption capacity (mg/g)	Ref.
Nano-hydroxyapatite	10	5–6	2.311	[81]
Biogenic apatite			2.247	
Treated biogenic apatite			2.267	
Natural crystalline apatite	5-25	6	0.212	[82]
Calcined MgAl-CO_3 layered double hydroxides	100	6	100% removal	[83]

The main advantage of layered double hydroxides as adsorbents is that they don't produce toxic chemical sludge like precipitation methods and they can restructure themselves into the initial form after the adsorption of different anionic species.

Industrial by-products based adsorbents

Enormous solid waste is generated from many industrial applications as by-products. So, utilization of *malodorous* residues as adsorbents for defluoridation provide an alternative avenue and value-addition to these otherwise under/non-utilized materials. In this context, waste carbon slurry was used for treatment of fluoridated

groundwater and wastewater. With the rise in solution pH, the adsorption capacity was to 4.47 mg/g (52.1%) at pH 7.58, then the capacity reduced to 3.78 mg/g (39.4%) at pH 9.68. The breakthrough capacity of column was 4.155 mg/g at 1.5 ml/min [84]. Moreover, fly ash is emitted in large amount during combustion process and maize husk fly ash was tested for treatment of fluoridated solution. The optimum dose for maximum removal was 40 g/l and equilibrium was reached within 12 minutes [85].

Similarly, the performance of original waste mud (o-WM) and other two acid-activated (a-WM) and precipitated waste mud (p-WM) was assessed for removing F⁻ ions from water. The solution pH was varied from 2-8 by keeping all other parameters constant (400 rpm speed, 1 h, 10 g/l dose). The p-WM showed the highest removal followed by o-WM and a-WM [86]. The spent bleaching earth (SBE) from oil factory was recovered as an adsorbent and used to treat the fluoridated water (2.28 and 5.4 mg/l) in Kuhbonan regions of Iran. The optimum conditions maintained in the lab were verified with water of Kuhbonan. The residual fluoride met the WHO regulated standard with 10 g/l dose within 180 minutes [87].

Table 2.14 Fluoride adsorption capacity of Industrial wastes

Adsorbents	Concentration Range (mg/l)	pH	Adsorption capacity (mg/g)	Ref.
Waste carbon slurry	15	7.58	4.861	[84]
Maize husk fly ash	7	2	86% removal	[85]
Original waste mud	5.4-914	5	2.8	[86]
Acid-activated waste mud			4.2	
Precipitated waste mud			27.2	
Regenerated spent bleaching earth	2.5-8	7	0.6	[87]

One of the great advantage of using these adsorbents is associated with lower capital and operating costs, and only little processing is required to increase the adsorptive capacity of adsorbents. Further study is required to find practical applicability of industrial wastes as low-cost adsorbents at commercial scale.

Biopolymers and agricultural wastes based adsorbents

Biosorption is the physiochemical process where contaminants are allowed to passively concentrate and adhere onto the cellular structure of biomass. Biosorption is caused by various metabolism-independent process which depends on type of biomass. Like special ion exchange resins, biosorbents contain chemical active groups within their structures as shown in Table 2.15.

Table 2.15 Major binding groups responsible for the biosorption process

Binding group	Structural formula	pK _a	Ligand atom	Occurrence in biomolecules
Hydroxyl	-OH	9.5-13	O	PS,UA,SPS, AA
Carbonyl (Ketone)	>C=O	-	O	Peptide bond
Carboxyl	$\begin{array}{c} \text{-C=O} \\ \\ \text{OH} \end{array}$	1.7-4.7	O	UA,AA
Amine	-NH ₂	8-11	N	Cto, AA
Secondary amine	>NH	13	N	Cto, PG, peptide bond
Amide	$\begin{array}{c} \text{-C=O} \\ \\ \text{NH}_2 \end{array}$	-	N	AA
Imine	=NH	11.6-12.6	N	AA
Phosphonate	$\begin{array}{c} \text{OH} \\ \\ \text{-P=O} \\ \\ \text{OH} \end{array}$	0.9-2.1 6.1-6.8	O	PL
Phosphodiester	$\begin{array}{c} >\text{P=O} \\ \\ \text{OH} \end{array}$	1.5	O	TA, LPS

PS: Polysaccharides, UA: Uronic acids, SPS: Sulfated PS, Cto: Chitosan, PG: Peptidoglycan, AA: Amino acids, TA: Teichoic acid, PL: Phospholipids, LPS: lipoPS

Retrieved from Volesky, 2007 [88]

The non-metabolic mechanisms involved in biosorption process are complexation, chelation, coordination, ion exchange, precipitation and reduction. More than one binding processes can take place in a system at the same time due to the complexity of biopolymers. The binding takes place via simple ion-exchange followed

by complex formation (co-ordination compounds) which may be chelates. The complex formation is mainly through neutral trivalent nitrogen atoms and neutral divalent oxygen or sulfur atoms. The deprotonated ligands like -RCOO- acts as Lewis bases and competitive complex are formed. Besides, the amine groups can chelate the anions by electrostatic interaction or hydrogen bonding. The occurrence of outer-sphere complex is observed when at least one water molecule of hydration sphere of adsorbate molecule is retained during adsorption, while the inner-sphere complex occurs when anions bind directly to adsorbent without hydration sphere [89]. Chemical coordination and stereochemical characteristics are to be considered for attachment of target ions on available ligands, and this is important in explaining the biosorption capacity and respective uptake mechanisms.

Moreover, chitin and chitosan-derivatives are good examples of biosorbents because they contain larger number of amino and hydroxyl groups. Neodymium-modified chitosan was tested for its applicability as an adsorbent for fluoride removal. At neutral pH and 2 g/l dose, the fluoride level decreased from 20 mg/l to 0.37 mg/l, and its adsorption capacity was found to be 22.38 mg/g at 303 K and 50 min residence time. The rise in temperature increased mobility of F^- ions and enabled their penetration within the internal structure of chitosan due to swelling effect [90]. Moreover, natural biosorbents can be modified by introducing binding sites onto the adsorbents. So, the efficiency of protonated cum carboxylated chitosan beads (PCCB) was evaluated for defluoridation process. The capacity of modified adsorbent (1800 mg/kg) was found to be more than raw one (52 mg/kg) for 10 mg/l F^- at pH 7. Introduction of multifunctional groups by protonation and carboxylation enhanced adsorption capacity of chitosan [91].

Several kinds of biomass (e.g. agricultural residues, waste biomass, microbes, polysaccharide materials) have already been tested for fluoride removal, and it was proven that they can be promising adsorbents for complete abatement of fluoride from water. It was also found that when activated charcoal is infused with some metals, its capacity to adsorb F^- ions is enhanced 3-5 times than the plain coal. The details of biosorbents and their maximum fluoride adsorption capacities are listed in Table 2.16.

Table 2.16 Adsorption capacities of various plant parts and agricultural wastes

Adsorbents	Concentration (mg/l)	Dose (g/l)	pH	Time (min)	Adsorption capacity/Removal (mg/g or %)	Ref.
<i>Tinospora cordifolia</i>	1-7	140	7	120	25	[92]
<i>Ficus religiosa</i> (Peepal) Leaves	1-20	10	7	45	2.24	[93]
Tulsi Leaves	2.35	1	-	60	85.3 % removal	[94]
<i>Cynodon dactylon</i> based Carbon	2-10	12.5	7	105	4.702	[95]
Moringa indica based carbon	2-6	-	6.2	25	0.17	[96]
<i>Vitex negundo</i> based carbon	1-12	4	7	50	1.150	[97]
Rice Husk	5	6	2	180	83 % removal	[98]
Sweet Lemon Peel	10-30	14	4	40	0.744	[99]
H ₂ SO ₄ treated Coffee Husk	5-25	72	2	180	86 % removal from 10 mg/l F ⁻	[100]
Treated <i>Citrus limonum</i> leaf	2-15	200	2	145	70 % removal from 2 mg/l F ⁻	[101]
Zrimpregnated groundnut shell carbon	2-10	0.02	3	180	2.32	[102]
Al modified peanut shell	0-40	20	7	180	98.9 % removal from 10 mg/l F ⁻	[103]

Local agricultural biomass are renewable and readily available in abundance, thus they provide viable option as adsorbent materials. Yet, there are inadequate studies carried out on the application of adsorbents from sewage sludge,

marine bivalve mollusk shells and banana and litchi peel for the defluoridation processes. It is hoped that with continuity in current trends, these technologies would be well developed in a practical scale in times to come.

2.3 Adsorption Isotherms

Adsorption isotherms are mathematical expressions describing distribution of adsorbate among solution and the adsorbent, based on set of assumptions mostly associated with the heterogeneity/homogeneity of adsorbents, type of coverage and the possibility of interaction between adsorbates [104]. So, sorption of a material at the surface boundary of two different phases can be clearly understood from the adsorption isotherms. The isotherm models used for characterizing the adsorption phenomena varies from two parameter models like Langmuir, Freundlich, Dubinin-Radushkevich, Flory–Huggins, Temkin and Hill to complex multi-component models like Redlich–Peterson, Sips, Khan, Radke–Prausnitz, Koble–Corrigan and Toth models. Langmuir and Freundlich are commonly used isotherms in adsorption of fluoride due to their simplicity and apparent usefulness, and can be used at constant temperature and pH.

2.3.1 Langmuir Adsorption Isotherm

Langmuir isotherm model provides a clear concept of monomolecular adsorption where all energetically active sites have equal affinity for adsorbate. The area of each site responsible for adsorption is determined exclusively by geometry of adsorbate. Basically, this model is based on the following three assumptions:

- (a) Adsorption occurs only at finite number of identical localized sites and maximum adsorption corresponds to saturated monolayer of adsorbate molecules with uniform thickness on the adsorbent surface;
- (b) This isotherm model signifies that the adsorption is homogeneous, where each molecule possesses constant enthalpies and adsorption activation energy;
- (c) There is no transmigration of adsorbate in surface plane and binding to adsorbent e occurs mostly by physical forces [105, 106].

Langmuir model has good agreement with experimental results and it is expressed in non-linear form as:

$$q_e = \frac{Q_0 b C_e}{1 + b C_e} \dots\dots\dots (i)$$

where, C_e is equilibrium concentration of adsorbate (mg/l), q_e is amount of adsorbate adsorbed per unit mass of the adsorbent (mg/g), Q_0 and b are Langmuir constants indicating measures of monolayer adsorption capacity (mg/g) and adsorption rate (L/mg). Graphically, it is characterized by plateau in which an equilibrium saturation point is obtained where there is no more adsorption once the site has been occupied. This indicates q_e approaches Q_0 asymptotically as C_e approaches infinity. Even though non-linear method provides better result, the linear least-square method is favored due to its uncomplicatedness and expediency. So, Equation (i) can be converted into various linear forms as shown in Table 2.17 to calculate the adsorption capacities for the given fluoride concentrations. For fitting nonlinear isotherm models to linear models, the dependent and independent variables are transformed accordingly.

Table 2.17 Linear forms of Langmuir isotherm model

Name	Linear forms	Plot	Slope	Intercept
Langmuir-1	$\frac{C_e}{q_e} = \frac{1}{bQ_0} + \frac{C_e}{Q_0}$	$\frac{C_e}{q_e}$ vs C_e	$\frac{1}{Q_0}$	$\frac{1}{bQ_0}$
Langmuir-2	$\frac{1}{q_e} = \frac{1}{Q_0} + \frac{1}{bQ_0C_e}$	$\frac{1}{q_e}$ vs $\frac{1}{C_e}$	$\frac{1}{bQ_0}$	$\frac{1}{Q_0}$
Langmuir-3	$q_e = Q_0 - \frac{q_e}{bC_e}$	q_e vs $\frac{q_e}{C_e}$	$\frac{1}{b}$	Q_0
Langmuir-4	$\frac{q_e}{C_e} = bQ_0 - bq_e$	$\frac{q_e}{C_e}$ vs q_e	B	bQ_0

Retrieved from Foo & Hameed, 2010 [107]

2.3.2 Freundlich Adsorption Isotherm

Freundlich model encompasses heterogeneous surface of the adsorbents and possess non-uniform distribution of adsorption energies. The stronger sites are occupied in the beginning and then the energy of adsorption decreases exponentially upon the completion of adsorption process. The total amount adsorbed is the summation of adsorption on all sites and is not restricted to monolayer formation unlike Langmuir model. So, the adsorption process is non-ideal and reversible with multilayer

adsorption. But Freundlich isotherm lacks major thermodynamic law and does not approach Henry's law at vanishing concentrations [107, 108]. The non-linear form of this model is expressed as:

$$q_e = K_F C_e^{1/n} \dots\dots\dots (i)$$

The logarithmic form of this equation can be represented as,

$$\log q_e = \log K_F + \frac{1}{n} \log C_e \dots\dots\dots (ii)$$

where, K_F and $1/n$ are characteristic parameters of sorbent-sorbate system and indicates the adsorption capacity and adsorption intensity, respectively. If $n = 1$, the partition between two phases are independent of fluoride concentration. The higher value of n (smaller value of $1/n$) signifies strong interaction among adsorbents and fluoride, while $1/n$ equal to 1 denotes linear adsorption leading to equal adsorption energies for all the sites. The exponent, $1 < n < 10$ represents beneficial adsorption [109].

Table 2.18 shows values of the Langmuir and Freundlich isotherm models constants for fluoride adsorption using various adsorbents reported in literature.

Table 2.18 Isotherm Constants and Correlation Coefficients for the adsorption of fluoride using different adsorbents at 298 K

Adsorbents	Langmuir			Freundlich			Ref.
	b	Q _o (mg/g)	R ²	K _F	N	R ²	
Banana peel	0.993	2.283	0.989	1.037	2.314	0.914	[99]
Groundnut shell	0.359	3.344	0.979	0.893	1.709	0.959	
Sweet lemon peel	0.544	1.037	0.971	0.500	4.291	0.883	
Cow Dung Carbon	0.500	111.11	0.767	36.14	1.45	0.912	[110]
<i>Pleurotus eryngii</i> ATCC 90888	1.5	66.6	0.998	36.72	2.33	0.976	[111]
Nano-hydroxyapatite	1.316	4.575	0.9909	1.764	2.966	0.9544	[81]
Biogenic apatite (B)	0.821	4.99	0.9353	1.413	2.857	0.9833	
Treated biogenic apatite (BH ₂ O ₂)	0.74	6.849	0.9737	1.662	2.937	0.9637	
Geogenic apatite	<0	0.014	0.105	0.034	<0	0.2588	

2.4 Adsorption Kinetics

Adsorption equilibrium and kinetic studies play significant role in controlling the process efficiency and provides a basis to gain insight into underlying mechanisms [112]. Sorption kinetics is generally based on rate law, thus a good knowledge of molecular details, interatomic distance and individual molecular steps involved in chemical reaction is necessary. The simplest means of understanding the experimental data from batch kinetic study is to get an idea about residual fluoride concentration in liquid phase at equilibrium time. Although several models like homogeneous surface diffusion model, pore diffusion model, and heterogeneous diffusion model (also known as pore and diffusion model) are extensively used in batch adsorption, the mathematical complexity have limited their use for practical purposes [113].

So, simple kinetic models like pseudo-first-order model, pseudo-second-order model, Weber and Morris intraparticle diffusion model, and Elovich's equation are most commonly investigated for describing adsorption kinetics data.

2.4.1 Weber and Morris Intraparticle Diffusion Model

The Weber and Morris intraparticle diffusion model is used to test the significance of internal diffusion as a rate limiting step in adsorption process. In a sorbent-sorbate system, fractional uptake of solute on adsorbent differs depending on the fraction of diffusivity within particle and its radius. A process is controlled by diffusion if its rate depends on diffusion of the components towards each other. Adsorption diffusion models consist of one or more consecutive steps:

- (a) transfer of solute from bulk liquid phase through hypothetical hydrodynamic boundary layer/film covering the particle (external diffusion or film diffusion);
- (b) migration of solute from adsorbent surface to internal active adsorption sites in pores or along pore walls (internal diffusion or intraparticle diffusion);
- (c) interaction of solute with adsorption sites, i.e., adsorption and desorption between adsorbate and the sites (mass action/chemical reaction) [114, 115].

The first two steps is fast until adequate shaking time is provided for avoiding formation of concentration gradient in the solution. The final phase is the mass action, which occurs very quickly in physical adsorption process, thus can be neglected in kinetic studies. If film diffusion controls the rate of reactions, the diffusion constant

varies inversely with particle size and film thickness [116]. The solute uptake in Weber Morris model is proportional with $t^{1/2}$ than with contact time, t . The linear form of this equation is given as:

$$q_t = k_{int}t^{1/2} + C \dots\dots\dots (i)$$

$$k_{int} = \frac{6qe}{R} \sqrt{\frac{D}{\pi}} \dots\dots\dots(ii)$$

where, k_{int} is intra particle diffusion rate constant ($\text{mgg}^{-1}\text{min}^{-0.5}$) calculated from slope of graph plotted between q_t Vs. $t^{1/2}$, C is a constant related to boundary layer thickness, R (cm) is particle radius and q_e (mg/g) is solid phase concentration at equilibrium.

The plot of q_t vs. $t^{1/2}$ can represent multi-linear portions and indicating the presence of two or more steps in adsorption process. For most cases, transportation of fluoride through 'surface film' limits the rate if necessary turbulence is maintained. The pore diffusion may limit the reaction rate for a vigorously mixed batch reactor. For the porous adsorbents, the physical meaning of rate constants helps in understanding the transfer mechanisms. Molecular size plays an important role if adsorption rate is controlled by intraparticle diffusion, as the reaction rate is faster for smaller sized adsorbate. Table 2.19 shows the Weber and Morris models parameters for different adsorbents selected from literature.

Table 2.19 Weber and Morris model parameters of various adsorbents for 5 mg/l F^-

Adsorbents	k_{int} , $\text{mg g}^{-1} \text{min}^{-0.5}$	C	R^2	Ref.
<i>Vitex negundo</i> bark carbon	0.066	0.567	0.874	[97]
Norit ROW 0 commercial carbon	0.002	0.003	0.987	[117]
<i>Pleurotus eryngii</i> ATCC 90888	0.002	0.209	0.923	[111]
<i>Abutilon indicum</i> carbon	0.053	0.344	0.921	[118]
Mangrove plant leaf powder	0.023	0.0275	0.991	[119]
Almond tree bark powder	0.019	-0.014	0.972	
Pineapple peel powder	0.03	-0.019	0.96	
Chiku leaf powder	0.05	-0.006	0.904	
Toor plant leaf powder	0.047	0.054	0.985	
Coconut coir pith	0.058	-0.011	0.997	

Adsorption reaction models, on the other hand doesn't consider the steps as of diffusion models and is based on whole adsorption process. The commonly used adsorption reaction models are pseudo-first order and pseudo-second order models.

2.4.2 Pseudo First-Order Kinetic Model or Lagergren's equation

Lagergren rate equations applies best for solute adsorption from solution and is based on solid adsorption capacity [120]. Pseudo-first-order is the earliest known model which is intuitively related to the one-site occupancy directed by surface reaction rate. The reaction rate is limited by only one mechanism and all the sites are dependent on time. The kinetic data is very well represented by this model at negligible sorbate interactions. The general rate expression of pseudo-first order equation is expressed as:

$$\frac{dq_t}{dt} = k_1(q_e - q_t) \dots \dots \dots (i)$$

where q_e and q_t (mg/g) are adsorption capacities at equilibrium and time, t (min), and k_1 (min^{-1}) is pseudo-first-order rate constant. The value of q_e is highly dependent on operational conditions like pH, ionic strength and initial adsorbate concentration. The parameter $k_1(q_e - q_t)$ doesn't denote the number of available binding sites.

Integrating equation (i) with boundary conditions of $q_t = 0$ at $t = 0$ and $q_t = q_t$ at $t = t$, yields:

$$\ln\left[\frac{q_e}{q_e - q_t}\right] = k_1 t \dots \dots \dots (ii)$$

Equation (ii) can be rearranged as:

$$\log(q_e - q_t) = \log q_e - \frac{k_1}{2.303} t \dots \dots \dots (iii)$$

This equation is only applicable when the measured concentration is equal to the surface concentration. The parameter $\log(q_e)$ can be adjusted and usually it is not equal to the intercept of plot between $\log(q_e - q_t)$ and t . Both the cases of diffusion through boundary liquid film and adsorption kinetics as chemical phenomenon can be interpreted as pseudo-first order rate equation of Lagergren [116]. In summary, pseudo-first order model is appropriate only for rapid initial adsorption phase rather than entire adsorption process. Table 2.20 shows the pseudo-first-order kinetic model parameters of several adsorbents for 5 mg/l F^- concentration.

Table 2.20 Pseudo-first-order kinetic model parameters of various adsorbents for 5 mg/l F⁻

Adsorbents	q _e (exp), mg/g	K ₁ , min ⁻¹	q _e (cal), mg/g	R ²	Ref.
Tea Ash	2.07	0.002	0.23	0.005	[121]
Sawdust	3.65	0.0495	1.26	0.9984	[122]
<i>Citrus documana</i> peel carbon	0.3910	0.06955	0.2447	0.990	[123]
<i>Citrus medica</i> peel carbon	0.3800	0.06425	0.1898	0.9824	
<i>Citrus aurantifolia</i> peel carbon	0.3660	0.07554	0.217	0.9692	
Mangrove plant leaf powder	0.45	0.051	0.194	0.981	[119]
Almond tree bark powder	0.128	0.058	0.156	0.997	
Pineapple peel powder	0.2	0.06	0.25	0.983	
Chiku leaf powder	0.34	0.081	0.441	0.974	
Toor plant leaf powder	0.381	0.085	0.573	0.962	
Coconut coir pith	0.409	0.078	0.716	0.923	

2.4.3 Pseudo Second-Order Kinetic Model

When the use of pseudo-first order kinetics equation turn out to be untenable, generalization for two-sites-occupancy adsorption system is proposed, which is known as pseudo-second-order kinetic equation [124]. The main assumptions for this model is that two reactions are occurring simultaneously. The first one is fast and reaches equilibrium quickly, while the second one is slower and continue for longer time covering the entire adsorption process. Pseudo-second order kinetics is a lump sum parameter of chemical reaction and physical diffusion process, and is given as:

$$\frac{dq_t}{dt} = k_2 (q_e - q_t)^2 \dots \dots \dots (i)$$

where q_e and q_t (mg/g) denote the solute uptake at equilibrium and at time t (min), and k₂ is pseudo-second-order rate constant (g mg⁻¹ min⁻¹). The driving force (q_e-q_t) is directly proportional to the available fraction of active binding sites. The rearrangement of Eq. (i) gives the following equation:

$$\frac{dq_t}{(q_e - q_t)^2} = k_2 dt \dots\dots\dots (ii)$$

Integrating above equation for boundary conditions $t = 0$ to $t = t$ and $q_t = 0$ to $q_t = q_t$,

$$\frac{1}{(q_e - q_t)} = \frac{1}{q_e} + k_2 t \dots\dots\dots (iii)$$

This equation is known as integrated rate law for pseudo-second order reaction [125] and the linear forms of this kinetic model is given in Table 2.21.

Table 2.21 Pseudo-second-order kinetic model linearized forms

Type	Linearized form	Plot	Effects of linearization
Linear 1	$\frac{t}{q_t} = \frac{1}{k_2 q_e^2} + \frac{1}{q_e} t$	t/q_t vs. t	-Reversal of relative weights of data because of $1/q$ in dependent variable - t in both dependent and independent variables, thus spurious correlation
Linear 2	$\frac{1}{q_t} = \frac{1}{q_e} + \frac{1}{k_2 q_e^2} \frac{1}{t}$	$1/q_t$ vs. $1/t$	- Reversal of relative weights of data because of $1/q$ in dependent variable -Independent variable is $1/t$, leading to distortion of error distribution
Linear 3	$q_t = q_e - \frac{1}{k_2 q_e} \frac{q_t}{t}$	q_t vs. q_t/t	- q in both dependent and independent variables, thus spurious correlation - Presence of q in independent variable introduces error, violating the basic assumption in method of least squares - $1/t$ in independent variable, leading to distortion of error distribution
Linear 4	$\frac{q_t}{t} = k_2 q_e^2 - k_2 q_e q_t$	q_t/t vs. q_t	- q in both dependent and independent variables, thus spurious correlation - Presence of q in independent variable introduces error, violating the basic assumption in method of least squares

Retrieved from Yuh-Shan Ho [126]

Linear 1 type of pseudo-second order model is most popularly used in adsorption process. The values of k_2 and q_e can be obtained from intercept and slope

from the plot of (t/q_t) and t . Table 2.22 represents the pseudo-second-order kinetic model parameters of various adsorbents for 5 mg/l fluoride concentration.

Table 2.22 Parameters of Pseudo-second-order kinetic model of various adsorbents for 5 mg/l F⁻

Adsorbents	q_e (exp), mg/g	K_2 , g mg ⁻¹ min ⁻¹	q_e (cal), mg/g	R^2	Ref.
Mangrove plant leaf powder	0.45	0.494	0.471	0.981	[119]
Almond tree bark powder	0.128	0.268	0.166	0.997	
Pineapple peel powder	0.2	0.186	0.257	0.983	
Chiku leaf powder	0.34	0.193	0.401	0.974	
Toor plant leaf powder	0.381	0.21	0.438	0.962	
Coconut coir pith	0.409	0.114	0.505	0.923	
<i>Tea Ash</i>	2.07	0.08	2.11	0.99	[121]
Sawdust	3.65	0.066	3.76	0.9997	[122]
<i>Citrus documana</i> peel carbon	0.3910	0.35065	0.4503	0.9946	[123]
<i>Citrus medica</i> peel carbon	0.3800	0.47403	0.4214	0.9971	
<i>Citrus aurantifolia</i> peel carbon	0.3660	0.46028	0.4098	0.9970	

2.4.4 Elovich Equation

The kinetic equation of chemisorption onto heterogeneous surface was established by Zeldowitsch (1934) for describing adsorption rate of CO onto MnO₂, which decreases exponentially with the increase in quantity of the adsorbed gas [112]. This equation is limited only to the explanation of limiting property reached by kinetic curve. In recent years, the equation is used for describing the uptake of target pollutants from aqueous medium, which is expressed as;

$$\frac{dq_t}{dt} = \alpha \exp(-\beta q_t) \dots\dots\dots (i)$$

This equation is commonly known as Elovich equation and is based on adsorption capacity of adsorbents. So, in this equation q_t is the adsorption capacity at time t (mg/g), α (mg g⁻¹ min⁻¹) is initial rate of adsorption such that $\frac{dq_t}{dt}$ is equivalent to

α when adsorption capacity at time t , q_t is zero. The parameter β (g mg^{-1}) signifies the extent of surface coverage and is also referred to activation energy required for chemisorption (also called constant of desorption).

To simplify the above (Eq.i), Chien and Clayton (1980) made an assumption that the parameter, $\alpha\beta \gg 1$. So, the integration of rate equation (Eq. (i)) at same boundary conditions of $q_t (t = 0) = 0$ and $q_t (t = t) = q_t$ gives simplified and linearized form of Elovich equation:

$$q_t = \frac{1}{\beta} \ln(\alpha\beta) + \frac{1}{\beta} \ln(t) \dots\dots\dots (ii)$$

If this equation applies, it should give a straight line from the plot of q_t vs. $\ln t$ with slope of $\frac{1}{\beta}$ and intercept of $\frac{1}{\beta} \ln(\alpha\beta)$. The calculated parameters of Elovich equation for the treatment of 5 mg/l fluoridated water using different adsorbents is given in Table 2.23.

Table 2.23 Elovich model parameters of adsorbents for 5 mg/l F^-

Adsorbents	α ($\text{mg g}^{-1} \text{min}^{-1}$)	B (g mg^{-1})	(R^2)	Ref.
<i>Vitex negundo</i> bark carbon	0.689	4.83	0.874	[97]
Norit ROW 0 commercial carbon	0.576	111.1	0.936	[117]
<i>Abutilon indicum</i> carbon	0.307	6.17	0.921	[118]
Mangrove plant leaf powder	2.65	17.857	0.978	[119]
Almond tree bark powder	0.012	20.8333	0.993	
Pineapple peel powder	0.02	13.333	0.972	
Chiku leaf powder	0.04	7.9365	0.958	
Toor plant leaf powder	0.062	8.8496	0.987	
Coconut coir pith	0.0457	7.04225	0.986	

Chapter 3

Methodology

This chapter provides experimental procedure for treating fluoridated water by the selected low cost adsorbents. The experimental approach consisted of adsorbents preparation followed by batch adsorption studies of fluoride including the equilibrium isotherm modeling and analysis of kinetics. The schematic outline (Figure. 3.1) highlights the experimental activities undertaken during the study.

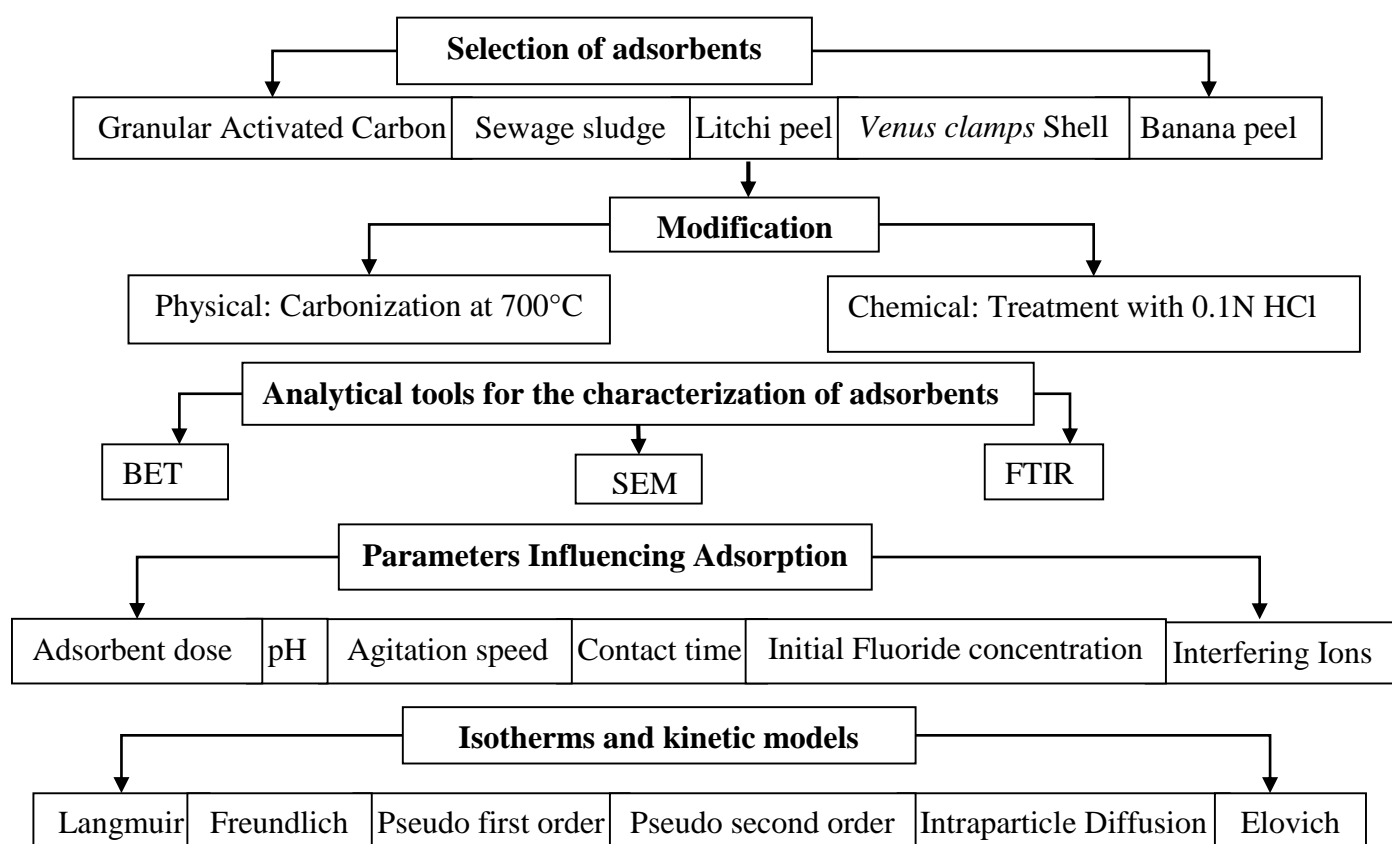


Figure 3.1 Research Framework

3.1 Materials

The materials used in this study comprises of agro-industrial residues to prepare adsorbents. The agro-industrial waste includes renewable lignocellulosic materials like peels and other solid by-product with varying composition.

3.1.1 Raw materials to prepare adsorbents

The important attributes of adsorbents include its capacity, selectivity, regenerability, kinetics, compatibility and cost. Agricultural wastes are preferred as raw materials for adsorbent preparation because they can be used with minimum processing and, thus reduces the costs of production. The raw materials selected in this study for fluoride removal are activated sewage sludge, sea shell, litchi peel and banana peel. Granular activated carbon (GAC) with suitable pore structure and high surface area has good value realization, commercial acceptance and hence, it is chosen as a baseline adsorbent. Besides, sewage sludge can be a highly promising feedstock to make adsorbents and its conversion signifies attractive alternative to the existing sludge disposal and reuse routes. Sludge is generally composed of exhausted biomass and minerals like calcite (CaCO_3), quartz (SiO_2) and gismondine ($\text{CaAl}_2\text{Si}_2\text{O}_8 \cdot \text{H}_2\text{O}$).

Venus clams belong to the Veneridae family and are among the favorite seafood. But improper disposal of post-consumption residues causes a significant level of environmental problem. The exoskeleton of bivalve shell is formed by biomineralization and is composed of aragonite (CaCO_3), which can readily swap out its Ca atoms in favor of anions, locking them into the solid form. Additionally, *Litchi chinensis* is an exotic tropical and subtropical fruit native to Southeast Asia. World production of litchi is around 2.11 million tons [127]. Likewise, banana peel covers ~40% total weight of fruit and is considered as major horticultural by-product. Particularly, Kluai Namwa is the most widely disseminated ABB cultivar grown as favorite cooking banana, and includes almost 70% of all bananas that are cultivated in Thailand [128]. Because of the extreme consumption of these fruits, high amount of peels is usually discarded as waste which has no practical utility. It can cause a severe problem in the community due to gradual fermentation and releasing off odors. The reason for choosing waste peel as adsorbents is their non-toxic properties, cost effectiveness and non-availability of any literatures based on the development of such adsorbents for fluoride removal.

The anaerobically digested sludge was collected from wastewater treatment plant, near Asian Institute of Technology, Thailand. The litchi peel, banana peel and the sea shells were collected from local vegetable and seafood market in Bangkadi, Thailand.

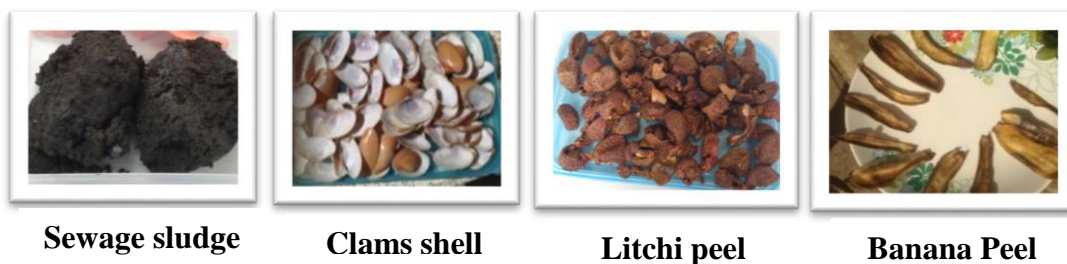


Figure 3.2 Agro-industrial Residues for preparing the adsorbents

3.1.2 Reagents and Chemicals

The list of AR grade chemicals used in this study are listed in Table 3.1.

Table 3.1 List of Reagents and Chemicals

Chemicals/Reagent	Supplier	Purity	Application
Anhydrous Sodium Fluoride (NaF)	Sigma-Aldrich	99.99%	To prepare adsorbate solution
Hydrochloric acid (HCl)	-	Analytical Reagent	For the treatment of Litchi Peel Powder
Sodium hydroxide (NaOH)	Sigma-Aldrich	>97%	To prepare buffer solution for pH adjustment
Sodium Chloride (NaCl)	-	99%	Electrolyte solution for zero point charge
Anhydrous Sodium Sulfate (Na ₂ SO ₄)	-	>99%	Chloride and sulfate solution to study effect of co- ions
SPADNS (Sodium 2-(parasulphenylazo) 1, 8 dihydroxy-3,6 naphthalenedisulphonate)	Sigma-Aldrich	Analytical Reagent	For analyzing fluoride ion in solution by UV spectrophotometer
Zirconyl chloride octahydrate (ZrOCl ₂ *8H ₂ O)	Sigma-Aldrich	98%	
TISAB Tablets	ExStik [®] (Thailand)	-	Control solution pH and ionic strength

3.2 Preparation of Adsorbate Solution

Stock solution of 1000 mg/l was prepared by dissolving 2.21 g anhydrous NaF in 1000 ml flask followed by dilution with de-ionized (DI) water up to the mark. Sodium fluoride appears as an odorless and colorless white powder, with 4% water solubility at 15°C and pH 7.4. The normal fluoride concentration in groundwater of most areas is ~ 5 mg/l. So, the test solution of 5 mg/l was prepared by serial dilution from fresh stock solution. The efficiency of six adsorbents were tested for 5 mg/l F⁻ solution and banana peel (BP) was used to treat 10 mg/l fluoride solution.

3.3 Preparation of Buffer Solution

From the normality calculation, 8.1774 ml of 37.5 % concentrated HCl was diluted with 1000 ml DI water to prepare 0.1 N HCl. Likewise, 0.1 N NaOH was prepared by dissolving 4 grams of NaOH in 1000 ml DI water and stored in refrigerator till next use. The pH of working solution was adjusted by adding this buffer solution.

3.4 Experimental Methodology for Adsorbents Preparation

Corresponding to the anionic state of fluoride, different types of adsorbents were selected and their methods of preparation varied accordingly.

3.4.1 Preparation of powdered sewage sludge

The collected sludge was washed thoroughly with DI water for removing the coarse impurities and was dried in oven at 60 °C for 24 h. The dried material is suitable for long-term storage as it is less subject to decay. High temperature and prolonged contact causes the contraction of sludge which might result in narrowing or closing of pore entrances. The dried sludge was ground and sieved through 150 mesh size (100 µm 225 µm), as the powdered adsorbent is more suitable for batch adsorption studies. Finally, the prepared adsorbent was stored in a sterilized air tight container.



Figure 3.3 Preparation of powdered activated sludge adsorbent

3.4.2 Preparation of clams shell powder

The shell was separated from edible part and washed with tap water to remove the remnants. Then, it was dried in sunlight for 7-8 hours and washed with DI water to remove soluble impurities. It was next dried in convection oven at 50 °C overnight and the following day it was ground and screened through 250 mesh sieve (60 μm 375 μm). The powdered shell was stored in a tight container until further use.



Figure 3.4 Preparation of clams shell powder adsorbent

3.4.3 Preparation of untreated litchi peel powder (ULP)

The collected litchi peel was washed with tap water for the removal of pulpy residues and dried in sunlight for 8 hours. It is supposed that pre-drying have positive influence on BET surface area. The dried peel was washed thoroughly with DI water to remove adhering dirt and was dried at 80 ± 2 °C overnight in oven. Then the peel was ground and sieved through 250 BSS (375 μm) mesh size, and stored in air tight container for further applications.



Figure 3.5 Preparation of untreated litchi peel powder adsorbent

3.4.4 Preparation of carbonized litchi peel powder (CLP)

The lignocellulosic biomass are good initiators for preparing carbonaceous adsorbents. In this context, a part of oven-dried litchi peel was separated for carbonization process and was thermally activated at 700 ± 5 °C in muffle furnace for 2

h in presence of air. It should be considered that the excessive heat energy given at high temperature for long duration is known to reduce the overall surface area of biochar due to knocking and breaking of some porous wall. The ash content was removed from the char with DI water followed by drying in oven at 110 ± 5 °C for 24 h. Finally, the char was sieved by 150 BSS mesh (225 μm) and the as-received biochar without further treatment was tested for fluoride removal.



Figure 3.6 Preparation of carbonized litchi peel powder adsorbent

3.4.5 Preparation of acid treated litchi peel powder (ALP)

Chemical modification by acid treatment is useful especially to increase the number of positive charges on adsorbent surface. Taking this into consideration, about 50 g of untreated litchi powder (ULP) was soaked in 200 ml of 0.1 M HCl for 24 hours. Meanwhile, the acids used for treating cellulosic biomass waste have to be in dilute form. The following day, it was filtered and rinsed with DI water until filtrate pH was near neutral. The residual peel powder in the filter paper was dried in oven at 100 °C all night and kept in an air tight container thereafter.

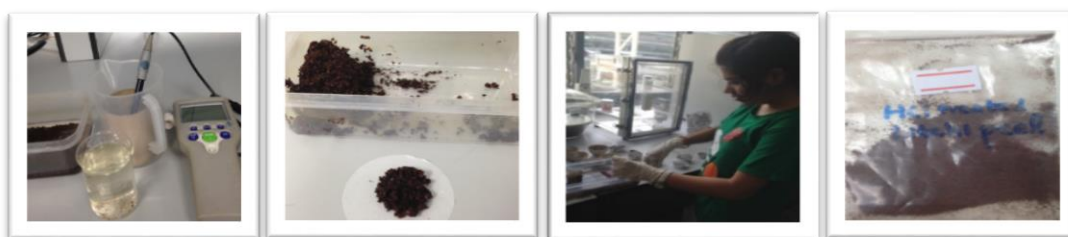


Figure 3.7 Preparation of acid treated litchi peel powder adsorbent

3.4.6 Preparation of banana peel powder (BP)

After the peels were collected, they were washed with tap water to remove adhering dust and dried in sunlight for two consecutive days. Considering the energy

consumption for drying, 80-100 ° C was chosen as the most suitable temperature for drying banana peels. So, peels were dried for 36 h and later on mashed into powder and sieved through 250 BSS, mesh size (375 μm).



Figure 3.8 Preparation of banana peel powder adsorbent

3.5 Characterization of adsorbents

The prepared adsorbents were characterized by means of various techniques to analyze their physical and chemical properties. Owing to different nature of original starting material in preparing the adsorbents, the surface characterization is necessary in order to understand the sorption mechanisms in detail.

3.5.1 Nitrogen Adsorption Desorption Isotherms

The most widely used technique for determining surface area of adsorbents involve measurement of gas physically adsorbed onto solid surface at a temperature close to the gas boiling point. In this context, the surface area, pore volume and pore diameter of prepared adsorbents was determined by single point BET surface area analyzer supplied by MicrotracBEL, Japan Inc. The detail procedure for sample preparation and surface area measurement is provided in Appendix-A. The measurement was automatically done by Belsorp Adsorption/Desorption Data Analysis Software - Version 6.3.2.0 available within the instrument. The total pore volume of adsorbents was estimated by liquid volume of nitrogen at 0.98 cm³/g relative pressure.

3.5.2 Scanning Electron Microscopy

In this study, the microstructural appearance of adsorbents were examined and analysed by SEM (KEYENCE VE 8800) operating under low voltage at variable pressure (VP) mode. The surface texture, pore structure and pore arrangements of prepared adsorbents before and after fluoride adsorption were also viewed. The

experiment was carried out by the bombardment of electrons on target sample particle spread earlier over a 10 mm aluminum stub with the help of carbon adhesive doubled edged tape. Then the surface was coated with platinum film (120 s, Argon atmosphere). The electrons interact with atoms in sample, producing various signals containing information of sample's surface topography. The structures and surface characteristics of the sorbents were compared at different magnifications.

3.5.3 Fourier Transform Infrared Spectroscopy (FTIR)

In Fourier transform infrared (FTIR), the infrared radiation is passed through sample. This is an essential tool to analyze surface functional groups present on adsorbents surface. The adsorbent samples was mashed into very fine powder and mixed with spectral-grade potassium bromide KBr in the ratio of 1:10. The mixture was then pressed with the aid of manual bench press under high vacuum pressure to obtain transparent pellets. These disks were directly placed in between the paper holder inside the analysis chamber of spectrophotometer. The spectra were then measured from 500 to 4000 cm^{-1} at 4 cm^{-1} resolution (Thermo Nicolet 6700) using 200 scans. The analysis was done automatically by OMNIC version 7.3 software attached to the system. When the infrared radiation is passed through sample, some is absorbed by sample and some is transmitted. The resulting spectrum thus indicates molecular absorption and transmission, creating molecular fingerprint of sample.

3.6 Experimental set up for Batch Adsorption Studies

The equilibrium experiments were carried out for batch adsorption of fluoride onto the selected adsorbents. All tests were conducted in 250 ml Erlenmeyer flasks with 50 ml test solution at room temperature (25 ± 3 °C). The freshly prepared solution was placed in the flasks with glass stoppers. The definite amount of adsorbents were weighed in Mettler Toledo balance and placed into the flasks. The flasks were shaken in the NB-101 M Orbital shaker (N-Biotek Inc., Gyeonggi-Do, Korea) at 150 rpm for a certain period of time.

This study mainly focused on the factors influencing adsorption process like adsorbent dosage, pH, agitation speed, contact time, initial fluoride concentration and effect of co-existing ions (for BP adsorbent only). As these factors play a vital role in

fluoride uptake, optimization of each parameter is done to evaluate the maximum removal efficiency, equilibrium time and for the isotherm selection. For optimizing certain parameter, all other variables were kept constant and only one specific parameter was varied. The average values of duplicate runs were recorded for reproducible results with an error of < 3%.

The uptake capacity and percentage removal is often based on material balance of adsorption system. The amount of fluoride uptake at equilibrium contact time, q_e (mg/g) was calculated using Equation (i) and the percentage removal of fluoride was obtained using Equation (ii).

$$q_e = \frac{C_i - C_e}{W} \times V \dots\dots\dots (i)$$

$$\text{Removal (\%)} = \frac{C_i - C_e}{C_i} \times 100 \dots\dots\dots (ii)$$

where, C_i and C_e (mg/l) are liquid-phase F^- concentrations at initial and equilibrium time, W is dry weight of adsorbent (g) and V is the volume of fluoride solution (l).

3.6.1 Effect of Adsorbent Dose

A dosage study is a crucial parameter as it defines adsorbent capacity for certain fluoride concentration under given set of operating conditions. For this purpose, specific dose range was selected for each adsorbent, and was added to the test solution of pH 7 prior to shaking in rotary shaker. The flasks were constantly agitated at 150 rpm for 2 hours. At last, minimum dose required for maximum removal is considered as optimum dose. The dose range used for each adsorbents is given in Table 3.2.

Table 3.2 Variation of adsorbent doses at constant operating parameters

Adsorbents	Adsorbent dose range (g/l)	Fluoride Concentration (mg/l)
GAC	2 to 12 (2, 4, 6, 8, 10, 12)	5
Sludge	1 to 6 (1, 2, 3, 4, 5, 6)	
ULP		
CLP		
ALP		
Shell	1 to 7 (1, 2, 3, 4, 5, 6,7)	10
BP	0.5 to 5 (0.5, 1, 1.5, 2, 2.5, 3, 3.5, 4, 4.5, 5)	

3.6.2 Effect of pH

Fluoride adsorption depends on solution pH which influences electrostatic binding of ions to the functional groups present in adsorbents. The influence of pH was studied in the range of 2-10. For this purpose, 50 ml of test fluoride solution was maintained at varying pH values (2, 3, 4, 5, 6, 7, 8, 9, 10) by adding drops of 0.1N HCl and 0.1N NaOH. Then, optimum dose of each adsorbent was added in the flasks and agitated at 150 rpm for 2 hours. Finally, the residual fluoride concentration was measured and the optimum pH value was chosen for each adsorbents. The pH was measured with HANNA digital pH meter. The standard glass-combination electrode pH meter was calibrated against commercial buffer solutions of known pH.

The effect of pH on fluoride adsorption can be described more clearly with the zero point charge (pH_{PZC}) of adsorbents and it was determined by the solid addition method. For estimating pH_{PZC} , 0.5 g (dry) adsorbent powder was added separately to 50 ml NaCl (0.01 M) solutions maintained at the initial pH values (pH_i) of 2-10. The mixture was continuously agitated at 120 rpm for 24 h at 35 °C and final pH (pH_f) of supernatant liquid was noted. The resulting pH change, ΔpH ($pH_i - pH_f$) was then plotted against initial pH. The value of ΔpH that left the pH of solution unchanged is considered to be the estimate of pH_{PZC} .

3.6.3 Effect of Agitation Speed

The effect of agitation in fluoride removal was monitored at low, medium and high agitation speeds (100, 150, 200, 250, 300 rpm). The selected dose of each adsorbent was added in 50 ml working solution maintained at neutral pH value. The flasks were shaken at 100-300 rpm for 2 hours and optimum speed was determined.

3.6.4 Effect of Contact Time

It is important to evaluate the influence of residence time for designing batch adsorption experiments. For determining equilibrium time for each adsorbents, the kinetics of fluoride uptake was examined as a function of shaking time (40, 80, 120, 160, 200, 240, 280, 320 min) at 25 ± 3 °C. The test solution maintained at neutral pH and adsorbent dose was shaken at specified speed for the required time intervals. Then, the optimum residence time was evaluated after the attainment of equilibrium.

3.6.5 Effect of Initial fluoride concentration

The required adsorbent dose, contact time and pH to bring the fluoride to permissible level depends on initial fluoride concentration of sample. Once all the optimum parameters were identified for adsorption, finding the effect of increasing fluoride concentration becomes important. So, 5 to 40 (5, 10, 20, 30, 40) ppm fluoride solutions was prepared by serial dilution of fresh stock fluoride solution. With addition of required dose of adsorbents in the fluoride solution of pH 7, the shaker was agitated at best derived speed for optimum time interval. Since, the ExStik FL700 fluoride meter has the maximum fluoride detection limit of 10 ppm, the residual fluoride concentration after adsorption was diluted accordingly. Besides, the residual fluoride concentrations for six different adsorbents (GAC, sludge, shell, ULP, CLP, and ALP) at varying fluoride concentrations was measured by UV-Visible Spectrophotometer (Thermo scientific, Genesys 10 UV) at 570 nm. The details of the measurement procedure and the obtained calibration curve is provided in Appendix B.

3.6.6 Effect of co-existing ions

In addition to fluoride, aqueous solution may contain several anions like Cl^- , SO_4^{2-} , CO_3^{2-} , HCO_3^- , PO_4^{3-} and NO_3^- at varying concentrations and they may impede the fluoride removal process. So, the concentration of anions like sulfate and chloride were kept at much higher concentration than fluoride, so that the synthetic solution resembles real groundwater sample. The concentration of each anion (chloride and sulfate) was maintained at 50 to 250 mg/l in presence of 10 mg/l fluoride at pH 7. Then, fluoride removal efficiency of banana peel (BP) adsorbent was evaluated under the optimum reaction conditions.

3.7 Adsorption Isotherms

Modeling of adsorption data is essential for evaluating the performance of various adsorbents. The adsorption isotherm study was done by fitting experimental equilibrium data to the two parameter isotherm models: Langmuir and Freundlich models. These models are chosen in this study because of their simplicity and also they are easily linearized. The study was carried out using variable fluoride concentrations of 5 mg/l to 40 mg/l (5, 10, 20, 30 and 40) at pH 7 with the optimum adsorbent doses.

The equilibrium value of fluoride adsorption by given adsorbents was plotted against equilibrium fluoride concentration to evaluate the suitability of these models.

3.7.1 Langmuir Adsorption Isotherm

This isotherm assumes monolayer coverage of fluoride over homogeneous adsorbent surface. To determine uptake capacity for given fluoride concentrations, Langmuir-1 linear equation was used.

$$(C_e/q_e) = (1/Q_0b) + (C_e/Q_0) \dots\dots\dots (i)$$

where, C_e is equilibrium concentration of fluoride (mg/l), q_e is amount of fluoride adsorbed per unit mass of adsorbent (mg/g), Q_0 and b are Langmuir constants related to measures of monolayer adsorption capacity (mg/g) and adsorption rate (L/mg). The constants Q_0 and b was determined from slope of the linear plots, C_e/q_e vs C_e . Q_0 denotes the practical limiting adsorption capacity when the adsorbent surface is covered fully with fluoride. Also, this parameter allows comparison of adsorption performance, when the adsorbents cannot reach its full saturation in the experiments.

The isotherm shape was used as an indicator to predict if fluoride adsorption process is “favorable”. The characteristics of Langmuir isotherm was interpreted with the separation factor, R_L by plotting a graph between R_L Vs. C_i .

$$R_L = \frac{1}{1+bC_i} \dots\dots\dots (ii)$$

where, C_i = Initial F^- concentration (mg/l) and b is reciprocal of concentration at which half saturation of adsorbent is attained. The R_L value shows adsorption to be either unfavorable ($R_L > 1$), linear ($R_L = 1$), favorable ($0 < R_L < 1$) or irreversible ($R_L = 0$) [129].

3.7.2 Freundlich Adsorption Isotherm

The relationship between the amounts of fluoride adsorbed per unit mass of adsorbent, q_e (mg/g), and equilibrium fluoride concentration, C_e (mg/l) was expressed in terms of linearized Freundlich isotherm model.

$$\log q_e = \log K_F + (1/n) \log C_e \dots\dots\dots (i)$$

where, and K_F and $1/n$ are empirical constants, indicating the adsorption capacity and adsorption intensity. The slope ($1/n$) represents adsorption intensity or surface heterogeneity and its value lies between 0 and 1. This expression reduces to linear

adsorption isotherm when $1/n = 1$ [109]. The values of n and K_F was obtained from slope and intercept of linear plot between $\log q_e$ vs. $\log C_e$. Freundlich isotherm is widely used but does not provide any information on monolayer adsorption capacity.

The suitability of these equations to describe experimental data was adjudged by correlation coefficient, R^2 values. According to regression analysis, higher the R^2 value (closer to unity), the better is the model for depicting isotherm parameters.

3.8 Batch Kinetic Studies

The kinetics studies is needed to select the residence time of the adsorbents for full scale batch or continuous fluoride removal. The methodology for evaluation of kinetic parameters is identical to that of batch equilibrium experiments. It basically helps in describing the fluoride adsorption rate which helps to determine the residence time of fluoride at adsorbent-solution interface. The samples were drawn out at predetermined time and residual fluoride concentration was measured. The amount of fluoride adsorbed at any time t , q_t , (mg/g), was derived from following equation:

$$q_t = \frac{C_i - C_t}{W} \times V \dots\dots\dots (i)$$

where, C_i and C_t (mg/l) are liquid-phase concentrations of fluoride at initial and at any time t , W is mass of adsorbent (g) and V is volume of fluoride solution (l).

Adsorption of fluoride onto adsorbent surface is a time dependent process. So, the kinetic parameters were evaluated from the batch adsorption of 10 ppm fluoride for BP adsorbent and 5 ppm fluoride for remaining six adsorbents at neutral pH. The time was varied from 40 min to 320 min depending on adsorbents and fluoride removal percentage was calculated. The experimental data from the time against % removal curves were fitted to pseudo-first order, pseudo-second order, Weber and Morris intraparticle diffusion model and Elovich equation by linear regression analyses.

3.8.1 Weber and Morris intraparticle diffusion model

In order to test the role of diffusion in fluoride removal process, the kinetic data was modelled with Intraparticle diffusion model given as:

$$q_t = k_{int}t^{1/2} + C \dots\dots\dots (i)$$

where, k_{int} is intra-particle diffusion rate constant ($\text{mgg}^{-1}\text{min}^{-0.5}$) obtained from slope of straight line plotted between q_t Vs. $t^{1/2}$, and C is a constant that gives idea about boundary layer thickness. The plot of q_t against $t^{1/2}$ should give straight line passing through origin when the intra-particle diffusion is the only rate limiting step [130].

3.8.2 Pseudo First-Order Kinetic Model or Lagergren's equation

The experimental kinetic results from batch process was analyzed by using the pseudo-first order model, which is expressed as:

$$\log (q_e - q_t) = \log q_e - \frac{k_1}{2.303}t \dots \dots \dots (i)$$

where q_e and q_t (mg/g) are adsorption capacities at equilibrium and time, t (min), and k_1 (min^{-1}) is pseudo-first-order rate constant for the kinetic model. The values of the rate constant was calculated by plotting $\log (q_e - q_t)$ vs t for various fluoride concentrations. For fitting this equation, equilibrium sorption capacity of adsorbents, q_e , must be known beforehand.

3.8.3 Pseudo Second-Order Kinetic Model

The adsorption kinetics was also explained with the help of pseudo-second order process by using the following equation:

$$\frac{t}{q_t} = \frac{1}{h} + \frac{1}{q_e} t \dots \dots \dots (i)$$

where, h ($\text{mg}/(\text{g}\cdot\text{min})$) is equal to $k_2 q_e^2$ and refers to the initial adsorption rate. Here, 'k₂' is rate constant of sorption ($\text{g}/\text{mg min}$), q_e is the amount of fluoride adsorbed at equilibrium (mg/g) and q_t is amount of fluoride on the adsorbents surface at any time t (mg/g). The constants related to this equation were found experimentally by plotting the graphs of t/q_t against t .

3.8.4 Elovich Equation

The linear graph of (q_t) vs. $\ln (t)$ at different contact times was obtained to confirm the applicability of Elovich equation, and this equations is given as:

$$q_t = \frac{1}{\beta} \ln (\alpha\beta) + \frac{1}{\beta} \ln (t) \dots \dots \dots (i)$$

where, q_t is sorption capacity at time t (mg/g), α ($\text{mg g}^{-1} \text{min}^{-1}$) is initial adsorption rate, and β (g mg^{-1}) is related to the extent of surface coverage. The graph of (q_t) vs. $\ln(t)$

should give straight line so that the value of α and β could be easily obtained from intercept and slope.

3.9 Analysis of samples

After completion of experiments, the solution was filtered with Whatman no. 42 filter paper and filtrate was analyzed for residual fluoride using ExStik FL700 Fluoride meter. The sensing electrode is a europium doped lanthanum fluoride single crystal that has been incorporated into removable sensing module and houses reference electrode and temperature measurement system. The FL700 allows the users to follow the American Society for Testing and Materials (ASTM) and EPA standard methodology using total ionic strength adjustment buffer (TISAB) reagents and standards. There are four main constituents of TISAB, namely CDTA (cyclohexylenedinitrilotetraacetate), sodium hydroxide, sodium chloride and acetic acid (ethanoic acid), which are all dissolved in DI water. The TISAB is a buffer solution which increases ionic strength of solution to a relatively high level and is commonly applied for fluoride ion analysis. So, for the measurement of residual fluoride concentration, one TISAB reagent tablet was mixed with 20 ml of unknown sample and after 35 seconds, the instrument displayed the fluoride concentration.



Figure 3.9 Steps for analyzing residual fluoride solution in the sample using Fluoride Ion-selective electrode

Chapter 4

Results and Discussion

This chapter presents the results based on batch adsorption experiments of fluoride using seven selected adsorbents. The various techniques used for the characterization of the prepared adsorbents are briefly discussed. Further, the optimum parameters to achieve the highest fluoride removal efficiency for each adsorbents are investigated. The experimental data is tested with different isotherm and kinetic models.

4.1 Characterization of adsorbents

Characterization of adsorbents is important as it helps us to understand their properties and interaction behaviour with fluoride. The performance of adsorbents is greatly influenced by their physical and chemical properties. In this study, all adsorbents were characterized for their physical characteristics by determining surface area, total pore volume and mean pore diameter. SEM analysis was done to study surface morphology of adsorbents, which also gives idea about the sorption mechanism of fluoride ions onto their surface. Besides, the FTIR spectra provided information about the surface functional groups in the adsorbents.

4.1.1 Surface area and Pore Characteristics

The knowledge of surface area gives information about the likelihood of interactions happening in the adsorbents. Surface area is usually measured by inferring the monolayer coverage within an adsorbent with known density and molecular dimensions. The structural heterogeneity of porous material is characterized in terms of pore size distribution, representing a model of solid internal structures. The pore dimensions intuitively correlate with the capacity and kinetics of the adsorbents. The porosity isn't an intrinsic property of solids, but in fact it depends on the treatment procedure involved in preparation of adsorbents. According to International Union of Pure and Applied Chemistry (IUPAC), pores are classified on the basis of pore diameter as micropores ($d_p < 20 \text{ \AA}$), mesopores ($20 \text{ \AA} \leq d_p < 500 \text{ \AA}$), and macropores ($d_p \geq 500 \text{ \AA}$). The pore characteristics and surface area of adsorbents calculated by Belsorp

Adsorption/Desorption Data Analysis Software-Version 6.3.2.0 is presented in Table 4.1.

Table 4.1 Surface area and pore characteristics of prepared adsorbents

Adsorbents	Sample weight (g)	Surface Area (m ² /g)	Total pore Volume (cc/g)	Mean Pore diameter,(Å)
Granular activated carbon (GAC)	0.175	884.66	0.3877 at P/P _o = 0.324	17.531
Sludge	0.2725	2	0.00097266 at P/P _o = 0.327	19.453
Shell	0.353	2.05	0.002446 at P/P _o = 0.990	45.430
Untreated Litchi Peel (ULP)	0.4292	1.56	0.00015549 at P/P _o = 0.370	15
Carbonized Litchi Peel (CLP)	0.3406	3.02	0.0012975 at P/P _o = 0.990	20.035
Acid treated Litchi Peel (ALP)	0.3502	2.12	0.0028743 at P/P _o = 0.990	29.142
Banana Peel (BP)	0.3210	1.87	0.000748 at P/P _o = 0.301	16.143

As seen from Table 4.1, none of the adsorbents had macropores. The distinct pore volume of GAC shows that majority of pores were microporous in nature. The ULP and BP have low surface area but the pores are predominantly microporous. The higher content of cellulose in fruit peels might have resulted in the formation of micropores. In addition, low surface area of BP adsorbent signifies the characteristic of its fibrous nature and presence of carbonaceous materials [131].

In any cellulosic precursors, lignin is the main constituent for char formation, while cellulose and hemicellulose are degraded and emitted as tars during the pyrolysis process. So, CLP comprises of both micropores and mesopores due to the added porosity in peel's morphology. Since CLP is produced without any further chemical activations, its BET surface area seems to be quite small in comparison to

GAC. The sludge and ALP have the mesoporous structures including some micropores, as the high adsorbed volume at low relative pressure was observed because of the micropores. In shell, mesopores was present all over the surface along with some open voids. The pores have heterogeneous distribution of slit widths which is attributed to the plate-like particles or layered structure of CaCO_3 like in clay materials [132].

So, the location of binding sites is important for the proper functioning of adsorbents. The adsorbed molecule is first transported through the macropores to mesopores, and finally to the micropores. The micropores generally constitutes the largest portion of internal surface and contributes the most to the total pore volume.

4.1.2 Surface Morphology

Adsorption is surface phenomenon, so the surface morphology of adsorbents is of significance in adsorbent-adsorbate interactions. The surface of adsorbents can be characterized either as external or internal depending on their depth and width ratio. According to Gregg and Sing, the external surface usually comprises bulges or cavities with higher width to depth ratio, while the internal surface includes pores and cavities having depth larger than width [133]. From the micrographs, pore development and changes in surface texture of adsorbents is clearly visible. The SEM images of the dried samples of sludge before and after adsorption of fluoride is shown in Figure 4.1. The pores of the sludge differ in their sizes and basically have irregular shapes with the adherence of small size particles onto the larger ones. After the adsorption, the surface covered with adhered substances were suspected to be the fluoride ions.

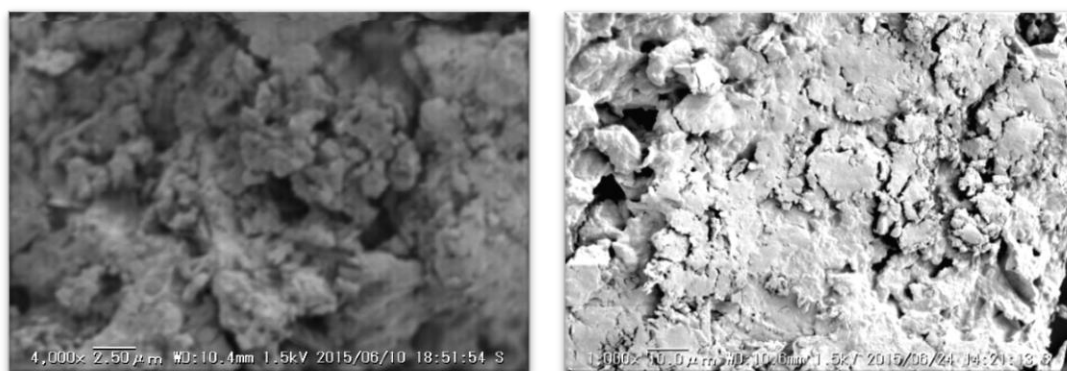


Figure 4.1 SEM images of sludge before (left) and after (right) defluoridation (4000x)

The shell powder is non-conducting material, and thus microphotographs were taken at low vacuum mode to obtain the sharp images. The sample showed porous structure with the mixture of plate like oblong particles and some ribbon-like tubules going through the layers. After adsorption of fluoride, the surface became smoother with adhesive appearance.

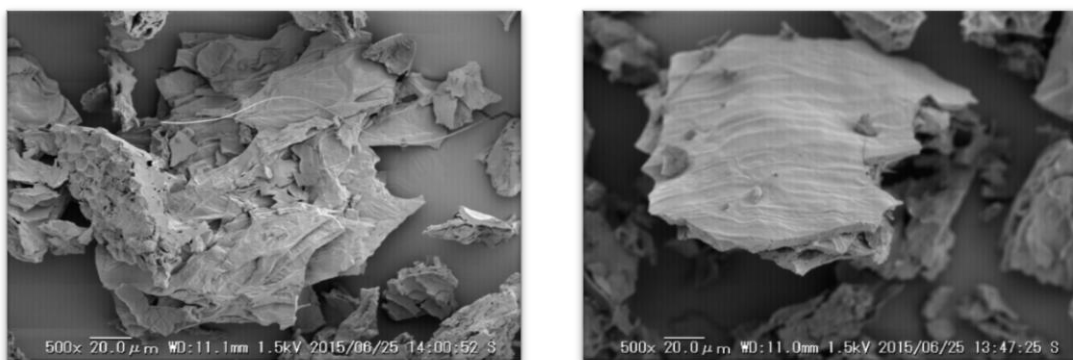


Figure 4.2 SEM images of shell before (left) and after (right) defluoridation (500 x)

Figure 4.3 shows the SEM images of untreated litchi peel (ULP) before and after the defluoridation process. The images before adsorption showed the pores with different appearance on the surface of ULP. But after fluoride adsorption, there was reduction in the number of pores, pore space and the available surface area. The rough texture is suitable for the surface adsorption and the fibers provides adsorption sites that aid in fluoride adsorption.

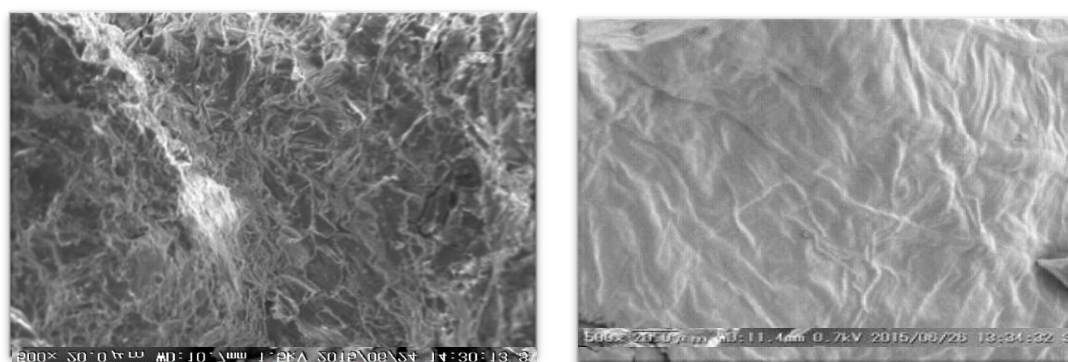


Figure 4.3 SEM images of ULP before (left) and after (right) defluoridation (500 x)

The microphotographs of the acid treated litchi peel (ALP) powder before and after fluoride adsorption is presented in Figure 4.4. The images showed more irregular and heterogeneous surfaces after the acid treatment of ULP powder. Some of the interesting morphological changes were extended surface arrangement with

repeating structures, plant vessel orientations, subsistence of crater-like pores of comparable shapes and sizes, and the availability of smallest openings for fluoride adsorption. It seems that fluoride could easily penetrate through pores or channels and further be adsorbed at interior sites/acidic centers. But once the fluoride ions were adsorbed onto the active sites of ALP, the probability of hydrogen bridge generation between carboxyl and hydroxyl groups was reduced, and this resulted in a regularly arranged biomass structure.

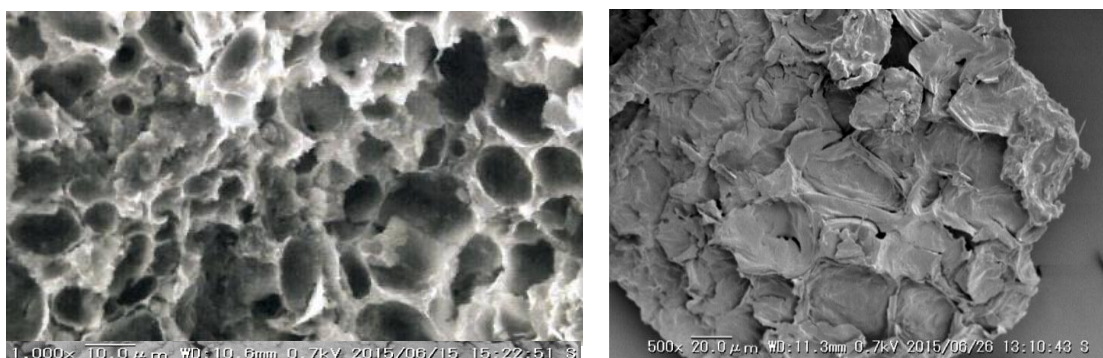
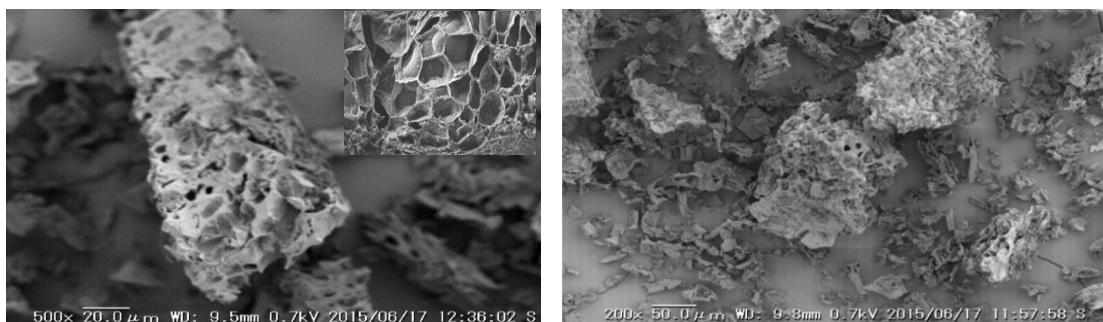
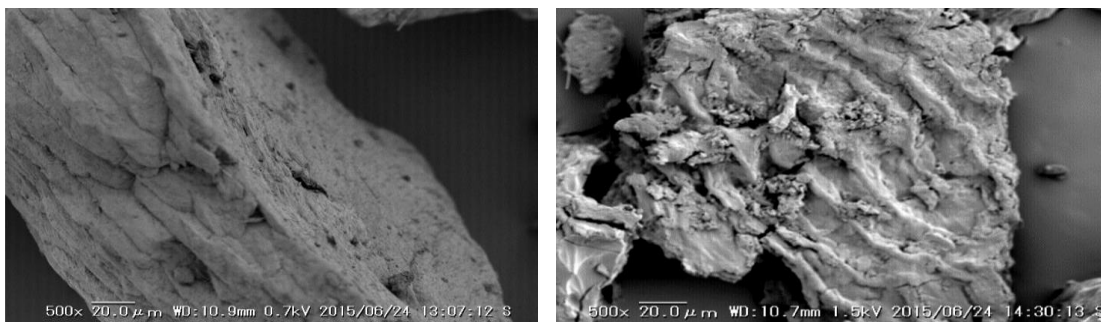


Figure 4.4 SEM images of ALP (left) and after (right) defluoridation (500 x)

The litchi peel char (CLP) morphology before and after fluoride adsorption is presented in Figure 4.5. The pores formed after carbonization are narrow, tapered and some of them are even blocked by tarry substances. The heterogeneous and rough surface with honeycombed like structures provided large surface area for adsorption, which favored the diffusion of fluoride ions into the center of biomass. The active binding sites on the surface of CLP is covered after the adsorption of fluoride.



(a)



(b)

Figure 4.5 SEM images of CLP (a) before and (b) after defluoridation (500x)

Figure 4.6 represents SEM images of banana peel (BP) powder before and after fluoride adsorption at a resolution of 500 X. Before fluoride adsorption, the adsorbent exhibited irregular and rough porous surface with heterogeneous voids and plate like structures. These structures act as the reactive adsorption centers for fluoride. After the adsorption, the peel powder appears to have dense smooth surface as the pores and caves were partially covered by fluoride.

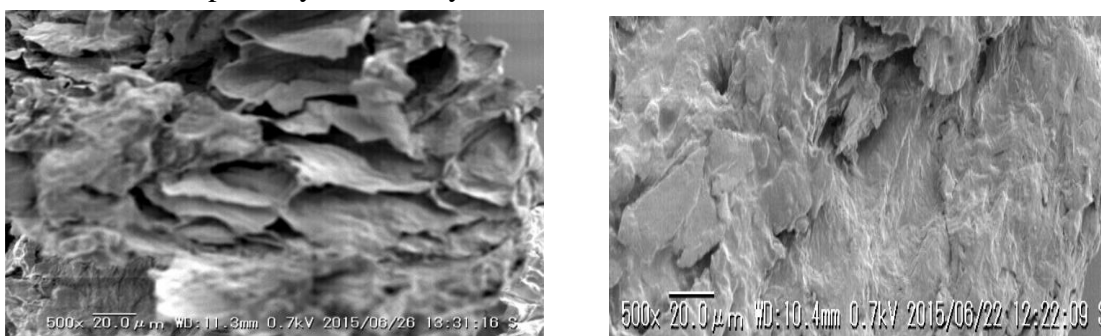


Figure 4.6 SEM images of BP before (left) and after (right) defluoridation

4.1.3 FTIR spectra of adsorbents

The adsorption characteristics of adsorbent is predominantly influenced by surface functional groups. The spectra of the seven adsorbents obtained from FTIR spectroscopy is presented in Appendix C. The simple spectra is generally obtained from the adsorbents with few IR active covalent bonds.

The FTIR spectra of sewage sludge is presented in Appendix C. In comparison to primary sludge, secondary activated sludge has lower content of grease,

fats and higher content of nitrogen, phosphorus and protein [134]. The major peaks pertaining to different groups present in sewage sludge are given in Table 4.2.

Table 4.2 Wavenumber (cm^{-1}) for dominant peaks from FTIR study of sewage sludge

Wavenumber (cm^{-1})	Major functional groups
3401.7	O-H stretching of hydroxyl groups and adsorbed water
2924.8 – 2853.2	Asymmetrical and symmetrical stretching of aliphatic methylene group indicating the presence of lipids
1653.5	C=O vibration of amide I
1540.1	N-H in plane bending in amide II
1457.6	Cellulose owing to the discharge of toilet paper
1034.5	Si-O stretching of clay minerals or Si-O-Si structures associated with pronounced concentration of silicon in the sludge sample
668.4 – 797.8	C-H structures originating from aromatic compounds

The amine group present in the adsorbent is cationic, which is responsible to attract fluoride anions during adsorption. Summing up, it can be concluded that Si–O–C, Si–O–Si, Al–O–(OH)–Al structures, carboxyl and hydroxyl groups, polysaccharides, lipids and cellulose were found on surface of anaerobically digested dewatered sewage sludge. So, sewage sludge is a complex matrix of inorganic minerals and organic matters from residual solids produced during wastewater treatment.

The prismatic layer of sea shells usually contain organic matrices of chitin and proteins. Aragonite (CaCO_3) is the dominant inorganic biomaterial of marine life, while calcite is preferentially present in terrestrial organisms as most stable polymorph. The FTIR spectra of the clams shell powder is presented in Appendix C and the detail is provided in Table 4.3. The infrared spectroscopy provided much more information about functional groups present on shell surface and to some extent their mineralogy could also be predicted. The comparison of *Venus clams* spectra with the spectra of calcite and aragonite from the literature [135] reveals that its characteristics resembles with aragonite.

Table 4.3 Wavenumber (cm^{-1}) for dominant peaks from FTIR study of shell powder

Wavenumber (cm^{-1})	Major functional groups
2918.6 – 3401.2 (3412.9)(Broad band)	Stretching vibrations of O-H or N-H groups
2522.6 (2521.7)	Aromatic C-H bond
1475.9	Characteristic peak of carbonate group
1082.8	Symmetrical and asymmetrical stretching vibration of sulfonic acid
856.9	Characteristic aragonite symmetric stretching vibration of carbonate and external plane bending vibration of carbonate
712.8 (Narrow peak) and 699.7	Internal plane bending mode of aragonite

The absorption peaks at 712.8, 856.9 and 1082.8 cm^{-1} show that the CaCO_3 in nacreous layers of clams shell is basically aragonite crystalline structure [136]. The external plane bending vibration mode is infrared active for all three polymorphs: aragonite, calcite and vaterite.

The FTIR spectra of untreated (ULP), acid treated (ALP) and carbonized litchi peel (CLP) are shown in Appendix C and the functional groups favorable for fluoride adsorption is listed in Table 4.4. The most distinct absorptions peaks are observed in both ULP and ALP, whereas the peaks are comparatively different for CLP.

Table 4.4 Wavenumber (cm^{-1}) for dominant peaks from FTIR study of ULP, ALP and CLP

Wavenumber (cm^{-1})			Major functional groups
ULP	ALP	CLP	
3409.9 (Broad band)	3390.9 (Broad band)	3386.3 (Number of erratic bands)	Bounded hydroxyl ($-\text{OH}$) and amine ($-\text{NH}$) groups
2926.4	2924.7	2922	Aliphatic C–H stretching vibration related with alkane groups
Narrow band at 1734.8	Narrow band at 1732.6	–	C=O bond of non-ionic carboxylic acids; C=O stretching of acetyl and uronic ester groups of polysaccharides, such as pectin, lignin and hemicelluloses Note: The disappearance of stretching band in CLP confirms removal of non-cellulosic materials from the litchi peel
1632.9	1622.1	1613.4	C=O stretching vibration; Aldehydes and ketones from simple and complex carbohydrates, esterified carboxylic acids
1448.4	1450.5	1435.4	CH_2 bending vibration
1375.1-1261.4	1377.1-1249.1	1316.5	Aliphatic C–H and amide groups
1054.4	1053.1	-	C-O and C-H stretching vibration: Confirms structure of cellulose
Below 1000	Below 1000	Below 1000	Aliphatic C–H groups

The appearance and disappearance of some peaks as well as the shift in absorption bands of spectrum concluded that litchi fruit peel was successfully modified in both acid treated form and carbonized form. The surface chemistry of adsorbents is

explained on the basis of acidic and basic character of their surface. It is quite well established that acidic behavior is associated with oxygen-containing functional groups like carboxyl, carboxylic anhydrides, lactones and phenols [137]. So, among the active groups, carboxyl and hydroxyl groups could assist in fluoride adsorption.

The fruit peels are lignocellulosic feedstock mainly comprising polymers like pectin, cellulose, hemicellulose, and small content of lignin [138]. In this context, banana peel (BP) powder not only have the well-developed biological cell structure but also contains rich organic functional groups. The FTIR spectra in Appendix C displayed the major functional groups in the BP. The FTIR spectra displayed number of peaks, indicating the complex nature of adsorbent. BP contains significant amount of oxygen from carbohydrates and fiber. The functional groups corresponding to the absorption bands is given in Table 4.5.

Table 4.5 Wavenumber (cm^{-1}) for dominant peaks from FTIR study of BP powder

Wavenumber (cm^{-1})	Major functional groups
3424.5	-OH stretching of hydroxyl group
2919.3	C-H stretching of alkane and alkene
1758.5	C-H and C=O bond of carboxylic acids and ester
1638.4	Secondary amine NH stretch
1456.5	Organic sulfate stretch
1384.4	C-O carboxyl band resulting from complexation of the carboxyl oxygen
1044.4 – 1090.8	Si-O stretching and Si-O bending of silica
Below 900 (884.6)	N-H deformation of amines
569.8-800	Aromatic C-H out-of plane

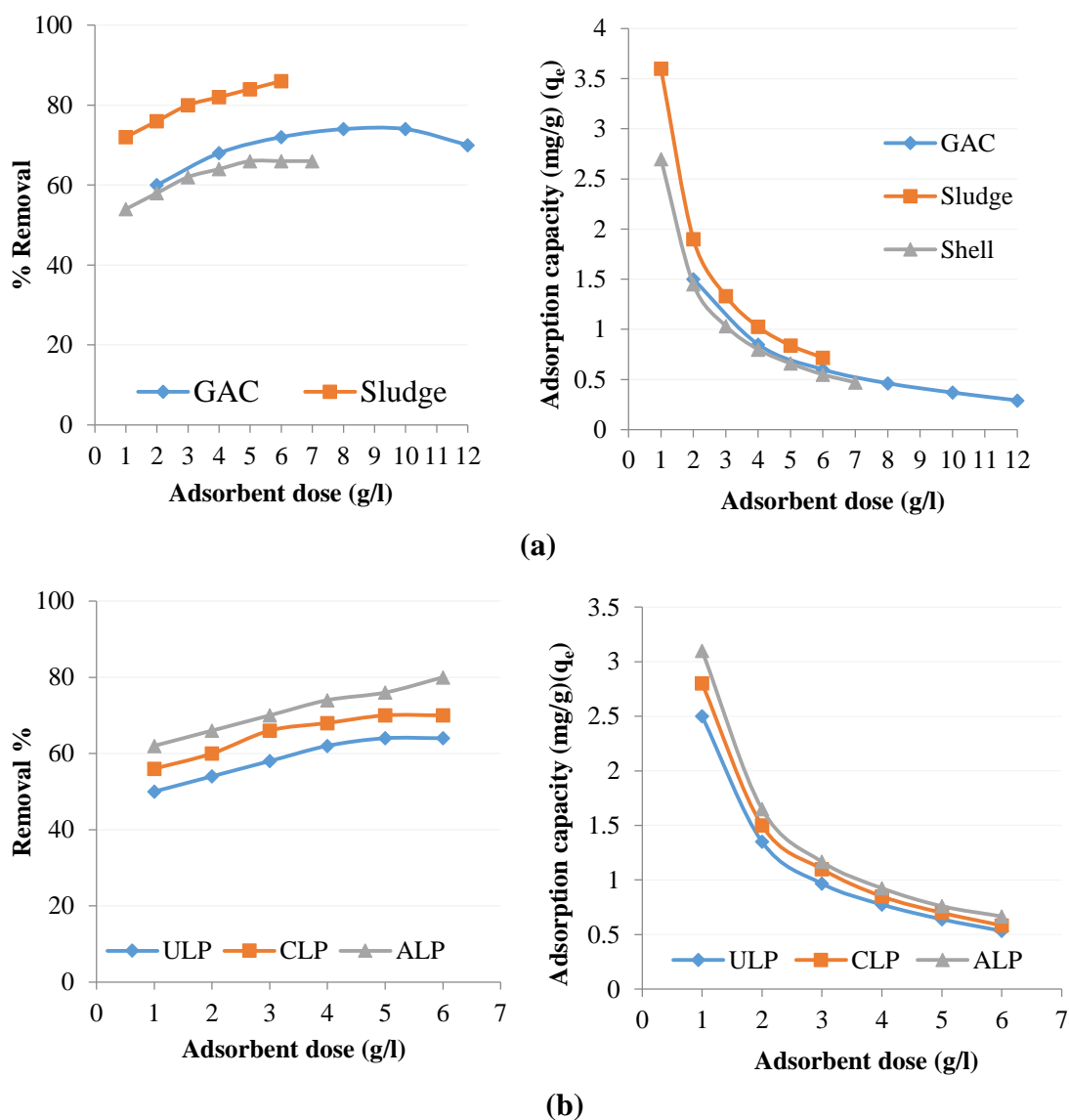
Additionally, the absorption bands at around 1637.4 to 1384.4-1456.5 cm^{-1} were characteristics of C=C in aromatics rings. The actual mechanism by which these fruit peels remove fluoride from the aqueous medium is not clearly understood. Yet, their selectivity for fluoride is related to presence of calcium, magnesium, hydroxyl and amine groups present in plant biomass. These groups are responsible for Van der Waals forces, interparticle bridging, hydrogen bonding, substitution, and columbic interactions between the adsorbents and fluoride ions.

4.2 Batch Adsorption Studies

The idea of the optimum operating conditions would represent better design and modelling adsorption processes. So, the results of batch studies to address the influence of adsorbent dose, pH, agitation speed, contact time, initial fluoride concentration, and effect of co-existing ions (for BP adsorbent only) are explained briefly under the following sections.

4.2.1 Effect of Adsorbent dose

The response of adsorbent dose on fluoride removal by the adsorbents is presented in Figure 4.7.



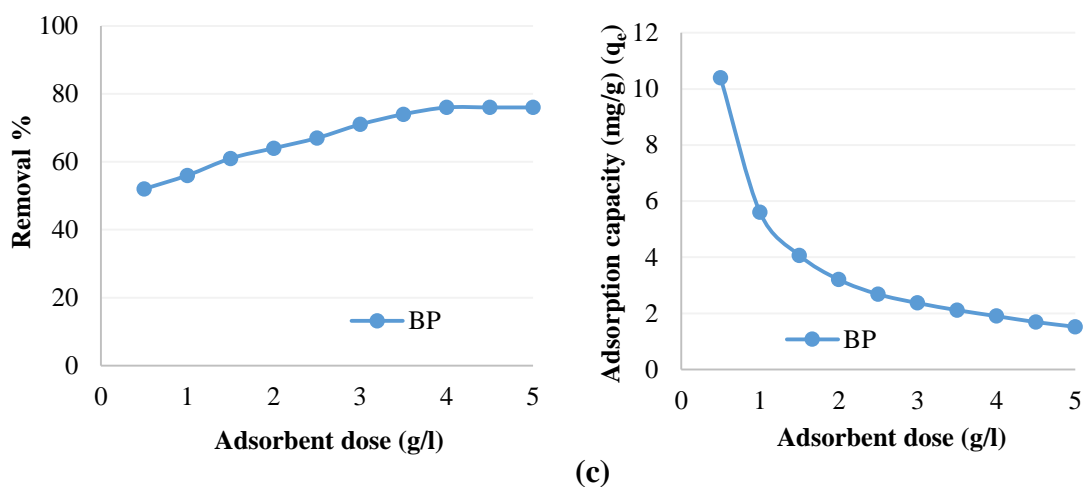


Figure 4.7 Effect of adsorbent dose on the removal of fluoride by (a) GAC, Sludge and Shell (b) ULP, CLP and ALP (c) BP (Process conditions: Initial F^- concentration: 5 mg/l for GAC, sludge, shell, ULP, CLP and ALP; 10 mg/l for BP, Neutral pH)

As seen from Figure 4.7, fluoride removal efficiency increased from 60 to 74 % for 2 to 10 g/l dose of GAC, 72 to 86% for 1 to 6 g/l sludge, 54 to 66% for 1 to 7 g/l shell powder, and finally 52 to 76% for 0.5 to 5 g/l BP powder. Similarly, at 6 g/l dose of ULP, CLP and ALP, the maximum defluoridation efficiency of 64%, 70% and 80% was observed. However, after addition of 4 g/l GAC, shell and ULP no significant removal was observed. Similar case was recorded after adding 3g/l sludge and CLP in the test solution during the experiment. The fluoride removal efficiency of adsorbents must be directly proportional to available surface area of adsorbents. This is because the larger surface area provides better sorbent-sorbate interaction due to increased number of sorption sites. But at lower dose, amount of fluoride is relatively higher compared to the availability of adsorption sites, resulting in the lower removal efficiency. The flattening of curves at higher adsorbent doses is because of the reduction in net surface area due to overlapping of binding sites [139, 140].

In contrary, with increment of the adsorbent dosage, the adsorption capacity of adsorbents was decreased. The adsorption capacity dropped from 1.5 to 0.29167 mg/g when GAC dose was increased from 2 to 12 g/l. Likewise, for sludge, shell, ULP, CLP and ALP, the equilibrium uptake capacity fell down drastically from 3.6 to 0.71667 mg/g, 2.7 to 0.47143 mg/g, 2.5 to 0.53333 mg/g, 2.8 to 0.53333 mg/g,

and 3.1 to 0.66667 mg/g, when the dose was increased from 1 to 6 g/l for the respective adsorbents. In case of banana peel (BP), the uptake capacity decreased from 10.4 to 1.52 mg/g for 10 mg/l F⁻ concentration with the rise in dose from 0.5 to 5 g/l. With the escalation of adsorbent dose, there is less commensurate increase in adsorption because of the lower adsorptive capacity utilization of adsorbent. This is termed as 'solid concentration effect' related to the overcrowding of particles [141]. Such kind of aggregation would result in reduction of total surface area of adsorbents and finally the diffusional path length is increased.

To maintain the maximum uptake and high removal efficiency, the surface loading (mass ratio of fluoride to adsorbent dose) must be less than optimum value. So, in order to ensure effective adsorption at lower adsorbent dose, 3 g/l is chosen as the applicable dosage for ULP, CLP, ALP and shell. At this dose, the fluoride removal efficiency of these adsorbents was 58 %, 66%, 70% and 62%, respectively. Although sludge is a cost effective adsorbent with high defluoridation efficiency, it still possess limitations like harboring bacteria and hence unhygienic conditions. So, 2 g/l dose is chosen to be appropriate which resulted in 76% efficiency. Considering the high cost of commercial activated carbon, 2 g/l GAC was chosen for further adsorption studies from economical viewpoint and 60% efficiency was recorded at this dose. Since, banana peel is an eco-friendly adsorbent without any negative health impacts, 4 g/l is chosen as suitable dose, at which 76% of removal occurred for 10 mg/l F⁻ solution.

4.2.2 Effect of pH

The influence of solution pH on fluoride removal is likely to be controlled both by the properties of adsorbate and adsorbents. When the adsorbent is mixed in solution, it forms a colloidal suspension carrying electrical charges. So, it is possible to know if the adsorbent surface is positively or negatively charged depending on pH. At a characteristic pH value, the surface charge density of adsorbents become zero, and this corresponds to the same number of positive and negative groups on adsorbents surface. The pH needed for adsorbents to have a net neutral charge on the surface is labeled as point of zero charge (pH_{PZC}) [111]. The understanding of pH_{PZC} is useful to hypothesize the ionization of functional groups present in adsorbents and their

interaction with ionic species in solution. Figure 4.8 shows the influence of pH_{PZC} of seven adsorbents on the percentage removal of fluoride as a function of pH.

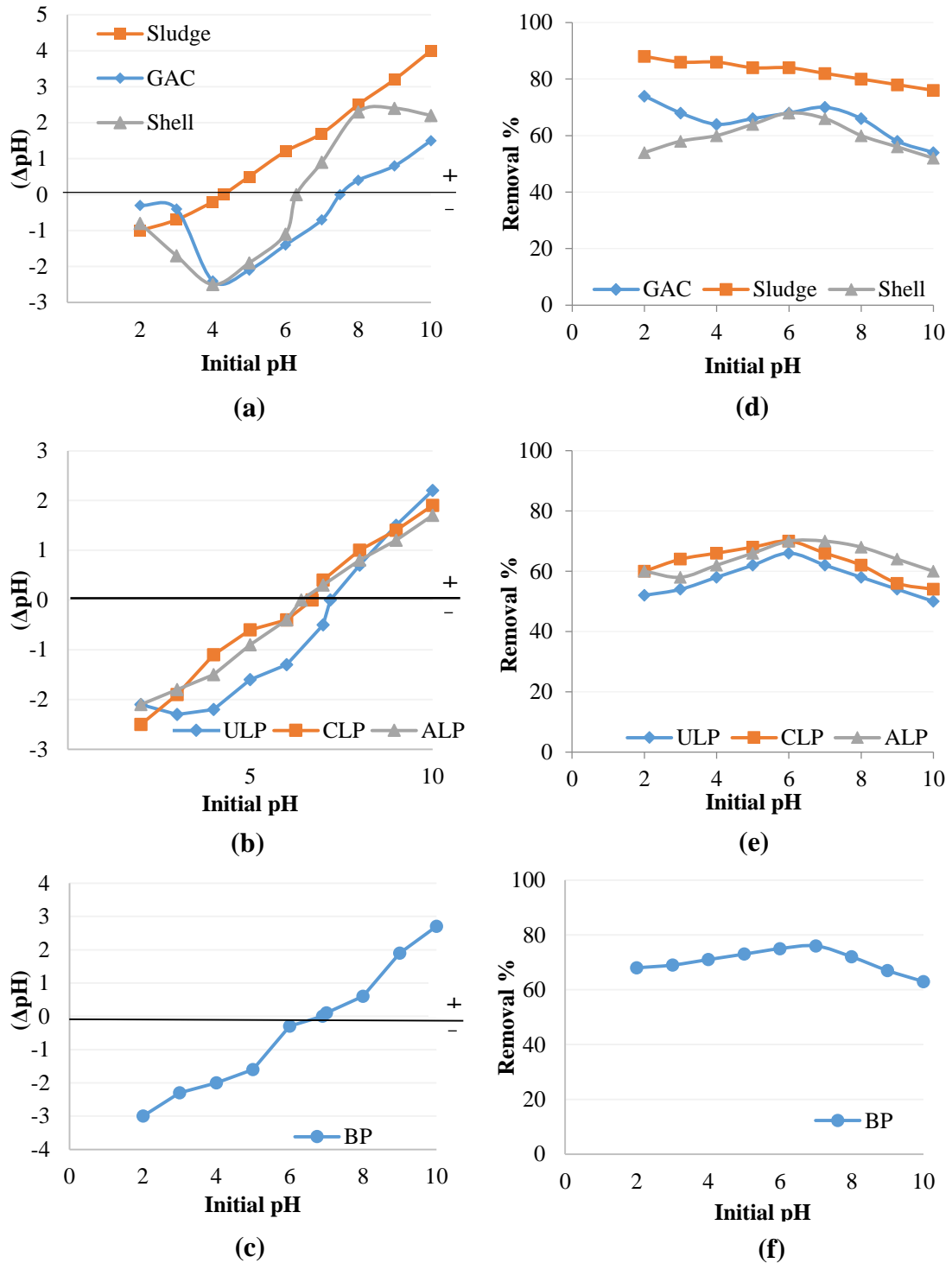


Figure 4.8 Zero point of (a) GAC, Sludge and Shell (b) ULP, CLP and ALP (c) BP; Effect of solution pH on the removal of fluoride by (d) GAC, Sludge and Shell for 5 mg/l F^- (e) ULP, CLP and ALP for 5 mg/l F^- (f) BP for 10 mg/l F^- , Neutral pH

Note: The symbol + and – in Figure 4.12 (a), (b) and (c) stands for the positively and negatively charged surface, respectively.

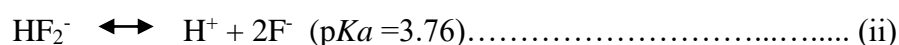
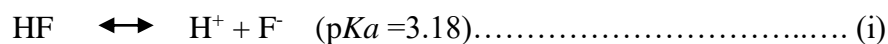
As seen from Figure 4.8 (d), (e) and (f), the adsorption of fluoride increased from acidic to near neutral value of pH and decreased slowly with the further increment in pH. For GAC and sludge, 74% and 88% of fluoride was removed at pH 2, while for shell, ULP, CLP, and ALP, the maximum fluoride removal efficiency of 68%, 66%, and 70% was recorded at pH 6. Likewise, BP showed a significant removal of 76% at neutral pH. The higher sorption rate at acidic medium could be due to the strong coulombic attraction between adsorbent surface and fluoride ions. But in alkaline condition, the competition between fluoride and negatively charged hydroxyl ions for binding sites resulted in the lower removal efficiency [139, 142]. This result can be discussed further based on the point of zero charge of adsorbents. The pH_{PZC} values of seven adsorbents obtained from the above graphs is listed in Table 4.6.

Table 4.6 Zero Point Charge (pH_{PZC}) values of prepared adsorbents

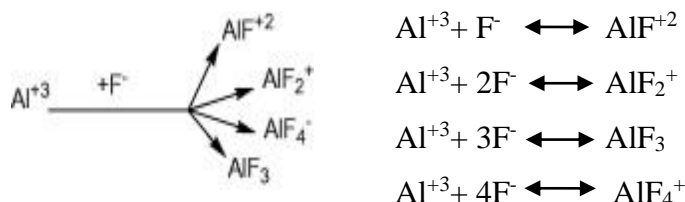
Adsorbents	Point of zero charge (pH_{pzc})
GAC	7.5
Sludge	4.3
Shell	6.3
ULP	7.2
CLP	6.7
ALP	6.4
BP	6.9

The surface functional groups do not contribute to the pH of solution at pH_{PZC} values and it is very important for adsorption processes. For higher concentration of acidic functional groups, the pH_{PZC} value of adsorbents is less. Normally, the adsorbent surface would be positively charged upto $pH < pH_{PZC}$, heterogeneous and neutral surface exists upto certain level higher than pH_{PZC} , and finally the surface becomes negatively charged when $pH > pH_{PZC}$ [143]. So, fluoride removal is favorable when the pH of solution is lower than pH_{PZC} of adsorbents ($pH < pH_{PZC}$). In this study, pH value favorable for the adsorption was lesser than the point charge for all selected adsorbents, and hence the fluoride ions could be easily associated with adsorbent

surface. The positively charged surface allows electrostatic binding of fluoride to the corresponding groups in adsorbents. However, at extremely low pH values the formation of weakly ionized hydrofluoric acid retards fluoride adsorption [144]. The deprotonation reactions of hydrogen fluoride (HF) and bifluoride (HF_2^-) is given as:



The solution pH can significantly influence the ionization of adsorbate in the solution. According to fluoride speciation, neutral HF is dominant at $\text{pH} < 3.18$, whereas fluoride exists as F^- ion at pH above 3.18 [145]. So, low sorption capacity of the adsorbents below pH 3 is due to existence of fluoride as HF which is not adsorbed. The highest fraction of HF_2^- formation is $< 0.5\%$ if the total dissolved fluoride is below 10 mg/l, and hence presence of bifluoride ions can be neglected [146]. In the case of sludge, multivalent metal cations like Al^{+3} are released from their surface at acidic pH which are able to capture and complex with the fluoride ions. At pH 5-7, most of the fluoride exists as soluble fluoro-aluminate complexes (AlF_i^{3-i}) and the fluoro-alumina interaction is more pronounced [147, 148].

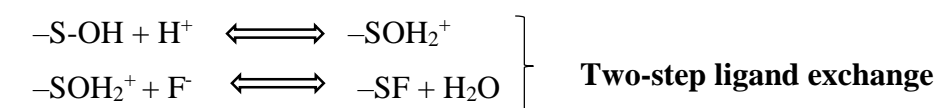


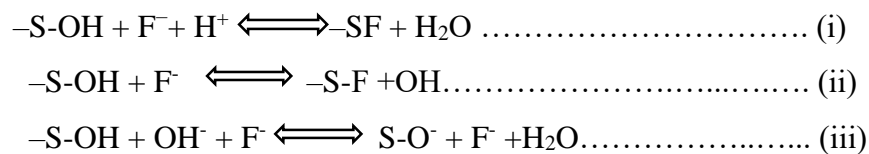
The inorganic metal oxides present in the sewage sludge undergoes surface hydroxylation as a result of acid base dissociation at varying pH. The hydroxylated surface of the Al, Ca, Mg, Si oxides acquire the charges through this amphoteric dissociation, which helps in the adsorption and net catching reactions of fluoride [149]. The silica present in the sludge has high surface reactivity and can anchor the fluoride ions with desirable selectivity. So, the most probable adsorption mechanism of F^- ions on the metal oxides present in sludge can be inferred as either surface complexation or electrostatic adsorption or a combination of both. Fluoride adsorption was changing at varying pH values possibly due to electrostatic interaction between alumina surface and dominant fluoride species. With the rise in pH, the increased concentration of hydroxyl ions hinders the free exchange of adsorbent structural OH^- for the fluoride ions resulting in the lower removal efficiency.

Moreover, the sea shells basically comprises of CaO with a trivial amount of other oxides [150]. The surface chemistry of an oxide in solution is determined mainly by the deprotonation or hydroxyl ion association reaction. Decreasing the solution pH provides positively charged species like Ca^{2+} , CaHCO_3^+ and CaOH^+ in solution. So, the increased number of positive sites leads to pronounced fluoride removal in acidic medium. Besides the surface sorption of fluoride on calcite, precipitation as insoluble CaF_2 also favors the fluoride removal. Unlike in acidic medium, exposure of deprotonated carbonate ligands results in the increment of negative charge density on shell surface at alkaline pH [151].

As seen from the FTIR analysis, oxygenated functional groups are present all over the solid surface of CLP, unlike some activated carbons where these groups are present only on the porous surface. At normal condition, these groups contain lone pairs of electrons and cannot adsorb F^- ions efficiently. So, as pH of the solution is lowered, surface group protonation can occur and the hydrated fluoride ions are easily adsorbed. Additionally, these functional groups contributes in the penetration of water and results in the char swelling. The $\text{H}_3\text{O}^+\text{F}^-$ hydrated ion pairs diffuse into char walls and fluoride is exchanged with the protonated groups. Fluoride removal process is thus attributed to chemical adsorption driven primarily by the C–F bond formation and hydrogen bonding between fluoride and protonated surface groups of CLP [152]. But as pH is increased, there will be lesser number of protonated sites and the exchange process is not much effective.

In lignocellulosic biomass, the protonation of existing ligands like amino, hydroxyl, and carboxyl groups at low pH values could benefit for the removal of fluoride. In case of ALP, the negative charges on adsorbent is counterbalanced by higher H^+ ion concentrations as a result of acid treatment. This in turn reduces the hindrance for the diffusion of fluoride onto the positively charged sites. The protonation of these functional groups contributed to the adsorption because of the electrostatic interactions between functional groups and F^- anion [153]. The reasonable reaction mechanisms for fluoride removal by lignocellulosic adsorbents like ULP, ALP and BP at acidic, neutral and alkaline conditions are described as:





Here, S denotes the adsorbent surface. It is clearly understood that the adsorbent surface have higher number of positive charges (mainly S-OH₂⁺ groups) in the acidic condition and can adsorb more fluoride ions. The removal mechanism appears to be ion exchange where the fluoride becomes the immobilized counter ion in the protonated sorption sites. This mechanism was further supported by the increment in the pH values after sorption reaction [154]. The change in pH values after the experiments signifies that adsorption occurs through dissociation of functional groups on adsorbents surface, and it consequently will create shift in kinetic reactions and equilibrium characteristics. With increment of the pH values, HF dissociation increases and the positive charge density of adsorbents also gradually decreases. Also, S-O⁻ groups in the adsorbent surface tends to inhibit the fluoride adsorption. For all these processes, corresponding number of OH⁻ must be produced or H⁺ be consumed to maintain the electroneutrality of solution [155].

Therefore, the adsorption of fluoride onto the selected adsorbents is strongly pH-dependent. In most of the cases, removal of fluoride was through isomorphic substitution of OH⁻ groups in the adsorbents surface. This substitution is iso-electronic in nature, as both the ions have similar size and ionic radii [156]. Moreover, the extreme pH values for the sake of maximum fluoride removal will result in the higher costs for post treatment. In addition, from a drinking water point of view adsorption at neutral pH is considered as optimum pH for all the selected adsorbents at which, 70%, 82%, 66%, 62%, 66%, 70% and 76% fluoride was removed by GAC, sludge, shell, ULP, CLP, ALP from 5 mg/l F⁻ and BP from 10 mg/l F⁻ solution, respectively. High removal efficiency at neutral pH demonstrates the practical applicability of these adsorbents.

4.2.3 Effect of Agitation Speed

The effect of agitation speed on fluoride removal by the given adsorbents is presented in Figure 4.9.

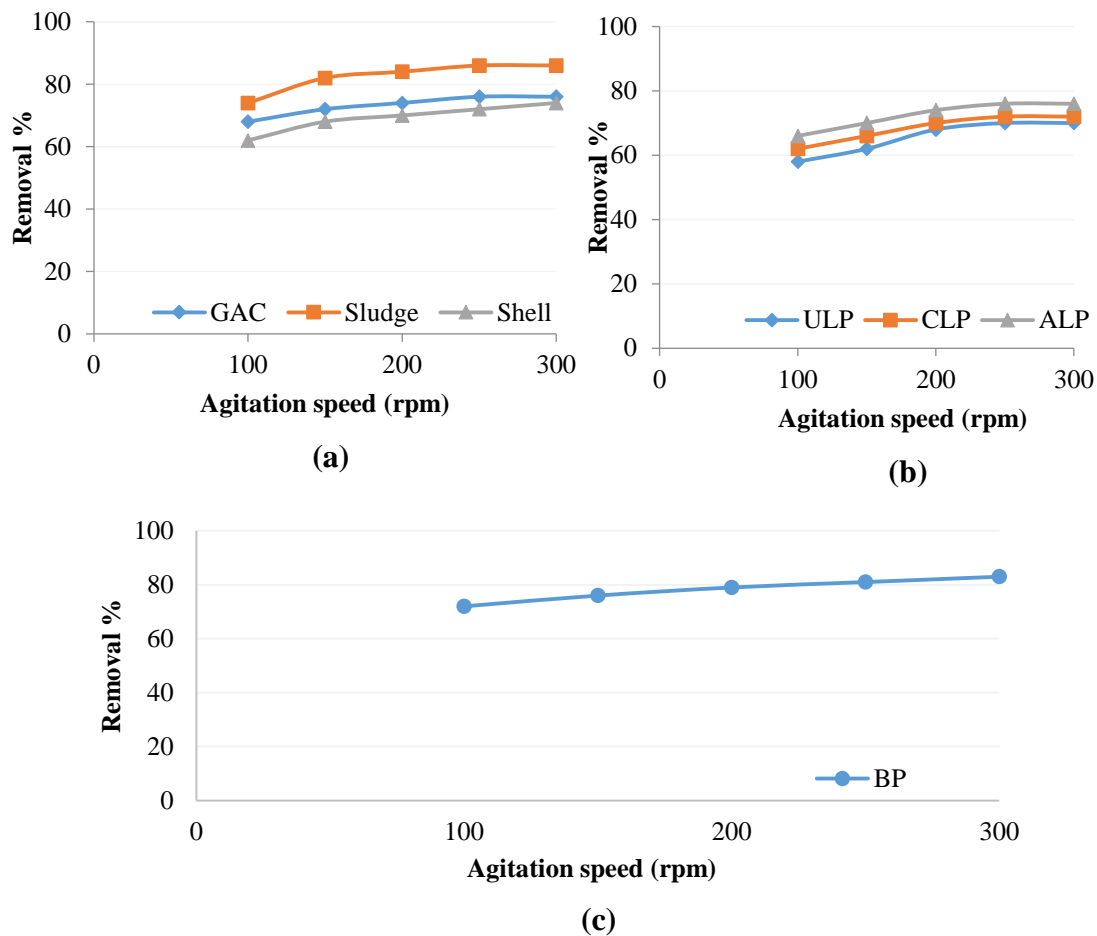


Figure 4.9 Effect of agitation speed on the removal of fluoride by (a) GAC, Sludge and Shell (b) ULP, CLP and ALP (c) BP (Process conditions: Initial F^- concentration: 5 mg/l for GAC, sludge, shell, ULP, CLP and ALP; 10 mg/l for BP, Neutral pH)

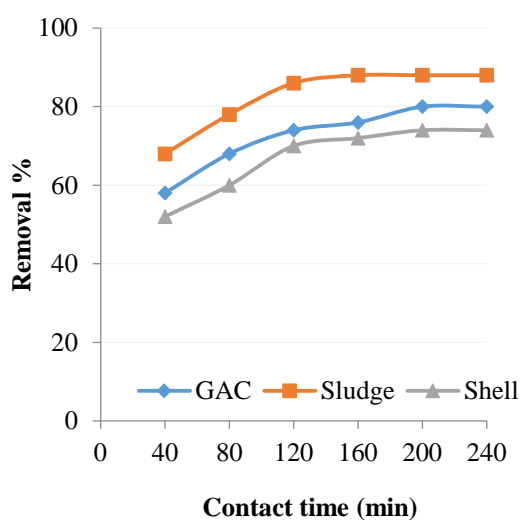
Under static condition, there was no movement between the solution and adsorbents. At lower speeds, the adsorbents accumulate at the flask bottom, which resulted in the burial of active sites under the layers of adsorbents. Because of this, the fluoride is removed only by the uppermost layers and the buried layer doesn't take part in the sorption process. This also affects the time required for adsorbents to attain the equilibrium. But once the shaking speed of the reactor was increased, fluoride removal efficiency increased proportionately. From Figure. 4.13, it was observed that for GAC, sludge, ULP, CLP and ALP, maximum removal of 76%, 86%, 70%, 72%, and 76% occurred at 250 rpm. The removal was almost constant thereafter and no uptake was recorded for further increment of shaking speeds. Likewise, for shell and BP a linear relationship was obtained for fluoride removal with respect to agitation speed and at

300 rpm, 74% and 83% fluoride was removed from the system. This is because the degree of agitation reduces the film thickness and increase the diffusion of fluoride ions. Also, better contact between adsorbents and fluoride is possible at higher speeds [139, 157]. But it should be considered that random spreading of adsorbent particles at high speeds may not allow sufficient time for binding the fluoride ions.

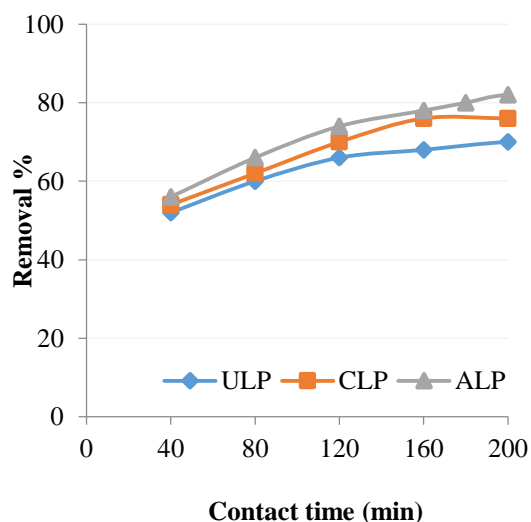
The major driving force for fluoride removal is the reduction of interfacial force (surface tension) between solution and adsorbents. The collision frequency between adsorbents and F^- ions increased with increasing speed and fluoride ions were electrostatically bound onto the surface of adsorbents. The increase in removal with agitation speed confirms the influence of external diffusion on sorption kinetics [158]. However, higher speed may damage the physical structure of adsorbents and there is high tendency of F^- desorption as high energy input and shear force can break the bonds between fluoride and adsorbents. Thus, speed of 200 rpm is sufficient to guarantee that all active adsorption sites are readily available for fluoride adsorption.

4.2.4 Effect of Contact Time

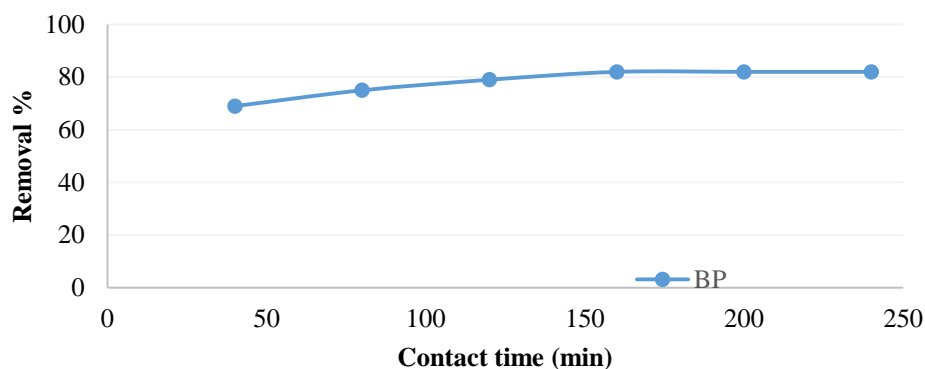
The percentage removal of fluoride by different adsorbents as a function of contact time is presented in Figure 4.10.



(a)



(b)



(c)

Figure 4.10 Effect of contact time on the removal of fluoride by (a) GAC, Sludge and Shell (b) ULP, CLP and ALP (c) BP (Process conditions: Initial F^- concentration: 5 mg/l for GAC, sludge, shell, ULP, CLP and ALP; 10 mg/l for BP, Neutral pH)

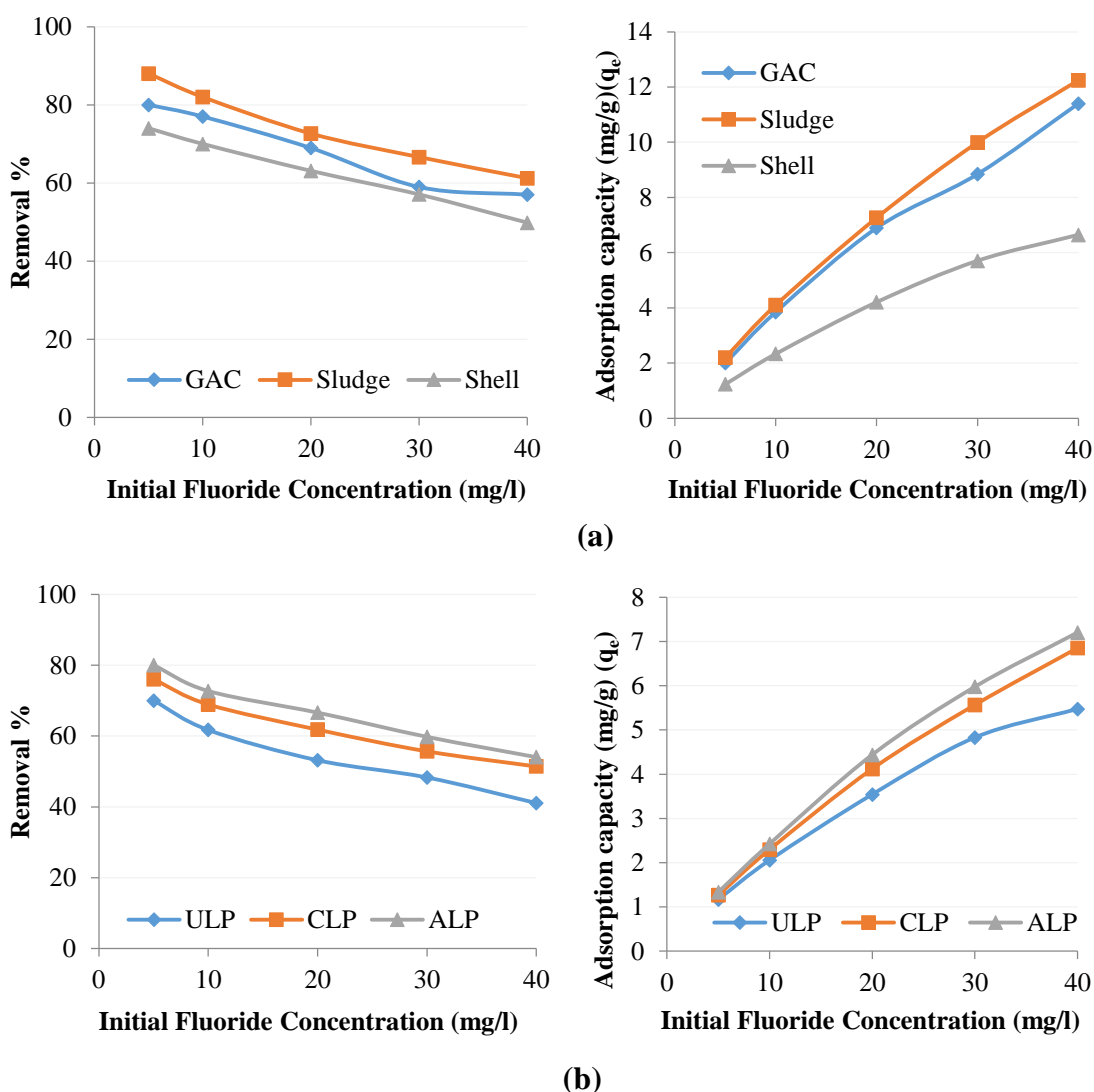
It is quite evident from Figure 4.10 that fluoride adsorption increased with prolonged contact time. The curves obtained for all seven adsorbents represented three distinct phases, where the initial peak represents the high fluoride uptake. In the beginning, there is large number of vacant sites in the adsorbents and fluoride is adsorbed instantaneously onto these binding sites. This instantaneous sorption of fluoride could be the result of specific chemical interaction or other driving forces like diffusion. The second phase of the graph indicates slow uptake of fluoride where all the active sites over the adsorbent surface are utilized before saturation. The fall in adsorption rate is because of the relocation of F^- ions from boundary layer to the interior porous surfaces [159]. So, transportation rate of the ions from exterior to interior sorption sites determines the rate of adsorption in following phases. Later on, the binding sites became limited and remaining sites were not occupied because of the repulsive forces between fluoride on solid surface and the bulk phase [160]. Finally, fluoride removal rate levelled off significantly, which denotes the equilibrium phase.

The fluoride removal curves with respect to time are single and continuous which indicates the probability of monolayer coverage of F^- ions onto the adsorbents. The intra-particle diffusion is more prominent in the inner surface of adsorbents due to constant agitation speed in the reactor. With the lapse of time, the removal gradually reached the constant values of 80%, 88%, 72%, 70%, 76%, 82%, and 80% for GAC,

sludge, shell, ULP, CLP, ALP for 5 mg/l F⁻, and BP for 10 mg/l F⁻, respectively. This denotes the attainment of equilibrium at the corresponding time of 180 min, 180 min, 160 min, 200 min, 160 min, 200 min and 160 min, respectively for the above listed adsorbents in sequential order. However, it should be considered that the accumulation of F⁻ ions with increasing time makes it difficult to diffuse deeper into highest energy sites on adsorbent surface. First the mesopores is filled up by the fluoride which later on hinders the diffusion of accumulated ions. Consequently, the mass transfer rate between solution and solid phase decreases with lapse of time [161].

4.2.5 Effect of Initial Fluoride Concentration

Figure 4.11 represents the influence of varying fluoride concentration on the fluoride removal process by seven adsorbents.



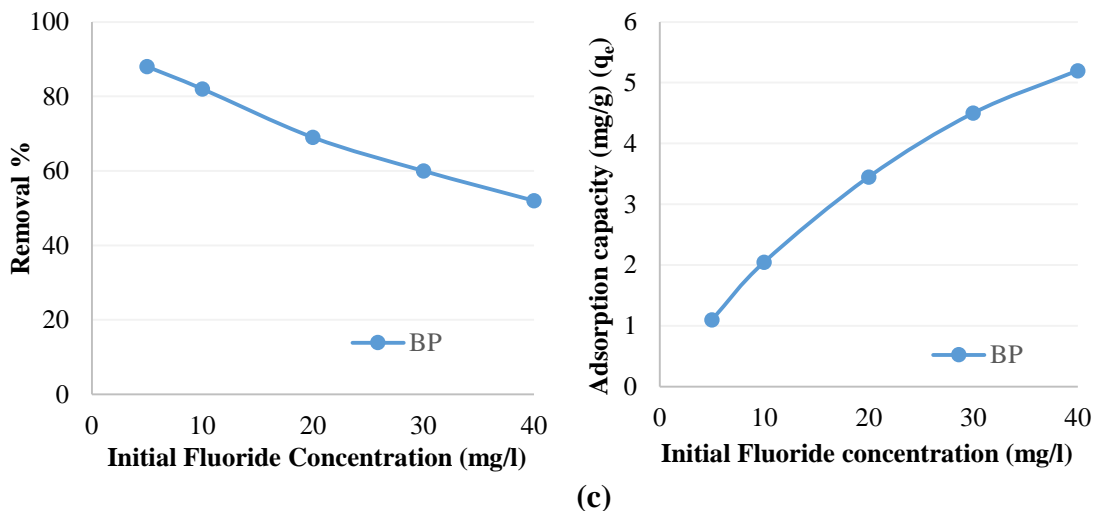


Figure 4.11 Effect of initial fluoride concentration on the removal of fluoride by (a) GAC, Sludge and Shell (b) ULP, CLP and ALP (c) BP at neutral pH

Initial concentration of fluoride offers essential driving force for improving the mass transfer resistances between solution and solid phase medium. The fluoride removal decreased with the rise in the fluoride concentration. From Figure 4.11, it can be seen that 80%, 88%, 74%, 70%, 76%, 80%, and 88% fluoride was removed by GAC, sludge, shell, ULP, CLP, ALP, and BP from 5 mg/l fluoride solution, respectively which shows that all fluoride ions in solution interacted with the available active sites. Higher removal efficiencies at low fluoride concentrations is because of higher ratio of the surface area to the total fluoride ions, resulting in utilization of more energetically active sites [100].

But removal rate drastically fell down to 57%, 61.225%, 49.85%, 41.075%, 51.4%, 54.025%, and 52% by the respective adsorbents for 40 mg/l fluoride concentration. The reason for sharp reduction in removal efficiency with the rise in fluoride concentration is because of the less surface area to accommodate the increased fluoride ions. So, more fluoride is left unabsorbed as the binding sites become saturated. In other ways, it can be said that the fixed number of active sites can adsorb only fixed amount of fluoride [162]. Also, the competition between fluoride ions for the remaining low energy sorption sites result in the decrement of removal efficiency.

Moreover, with the increment in fluoride concentration the main driving force for migration of fluoride from bulk to adsorbent surface increases. This results in

more adsorption of fluoride per unit mass of the adsorbent. In present study, adsorption equilibrium, q_e increased from 2 to 11.4 mg/g for GAC, 2.2 to 12.245 mg/g for sludge, 1.233 to 6.646 mg/g for shell, 1.166 to 5.476 mg/g for ULP, 1.266 to 6.853 mg/g for CLP, and 1.333 to 7.203 mg/g for ALP, with the rise in fluoride concentration from 5 to 40 mg/l. For BP, the value of q_e decreased for 5 mg/l concentration (1.1 mg/g) but increased from 2 to 5.2 mg/g with the increase in fluoride concentration from 10 to 40 mg/l. The initial direction of curve shows that adsorption becomes easier with the rise in concentration. So, it can be concluded that both removal percentage and equilibrium adsorption capacity is highly dependent on initial fluoride concentration.

4.2.6 Effect of co-existing ions

Figure 4.12 shows the influence of various co-ions like chloride and sulfate on the fluoride removal process by banana peel (BP) powder. The plots showed that maximum F^- removal is seen when all operating variables are set at optimum values (Fluoride Concentration: 10 mg/l, Adsorbent dose: 4 g/l, Neutral pH, Agitation speed: 200 rpm, Contact time: 160 min).

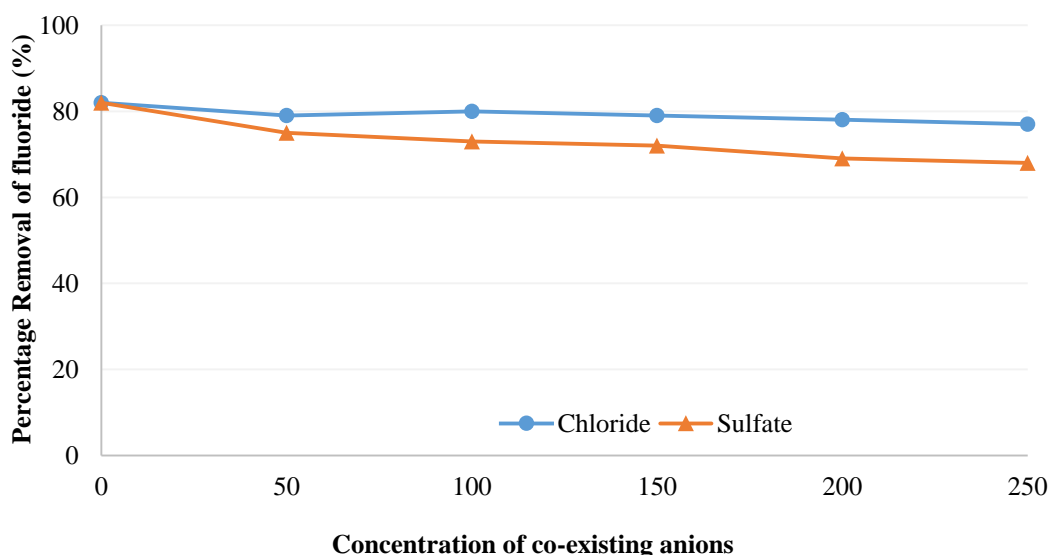


Figure 4.12 Effect of anions on fluoride adsorption onto BP

It can be inferred from Figure 4.12 that there was no significant impact on fluoride removal in presence of monovalent chloride ions, while the presence of divalent sulfate at higher concentrations resulted in decrease of fluoride removal efficiency. The F^- ion removal reduced from 79% to 77% and 75% to 68% on increasing

the chloride and sulfate concentration from 50 to 250 mg/l, respectively. This is because chloride ion is basically low affinity ligand and their adsorption mechanism is through the formation of weaker bonds with active sites at outer-sphere complexation. Hence, F⁻ ion is adsorbed via the formation of strong bonds with accessible binding sites at inner-sphere complexation. Sulfate ions, on the other partially forms the inner and outer sphere complexes [163, 164]. Besides, there might be competition between fluoride and sulphate ions for sorption sites, as high columbic repulsion might reduce the interactions of fluoride with the binding sites [110].

Thus, the expected effect of chloride ions on fluoride adsorption is less significant than the sulphate ions. The competition between reactive species for the adsorption sites is influenced by factors such as chemistry of fluoride, solution pH and nature of binding sites, number of available sorption sites, adsorbate concentrations, and the selectivity of biomass to bind the certain species.

4.3 Batch Adsorption Isotherms

Adsorption equilibrium gives an elementary physiochemical statistics for determining the process parameters of adsorption process under the predetermined reaction conditions. The equilibrium isotherms for fluoride adsorption were measured during experiments and the outcomes are described briefly under following sections.

4.3.1 Langmuir Isotherm Model

The data from the adsorption experiments was analyzed by linear regression of Langmuir isotherm equation and the graphs are plotted as shown in Figure 4.13. The best fitting of curve is obtained using Langmuir-1 isotherm because of minimal deviations from the fitted equation resulting in best error distribution.

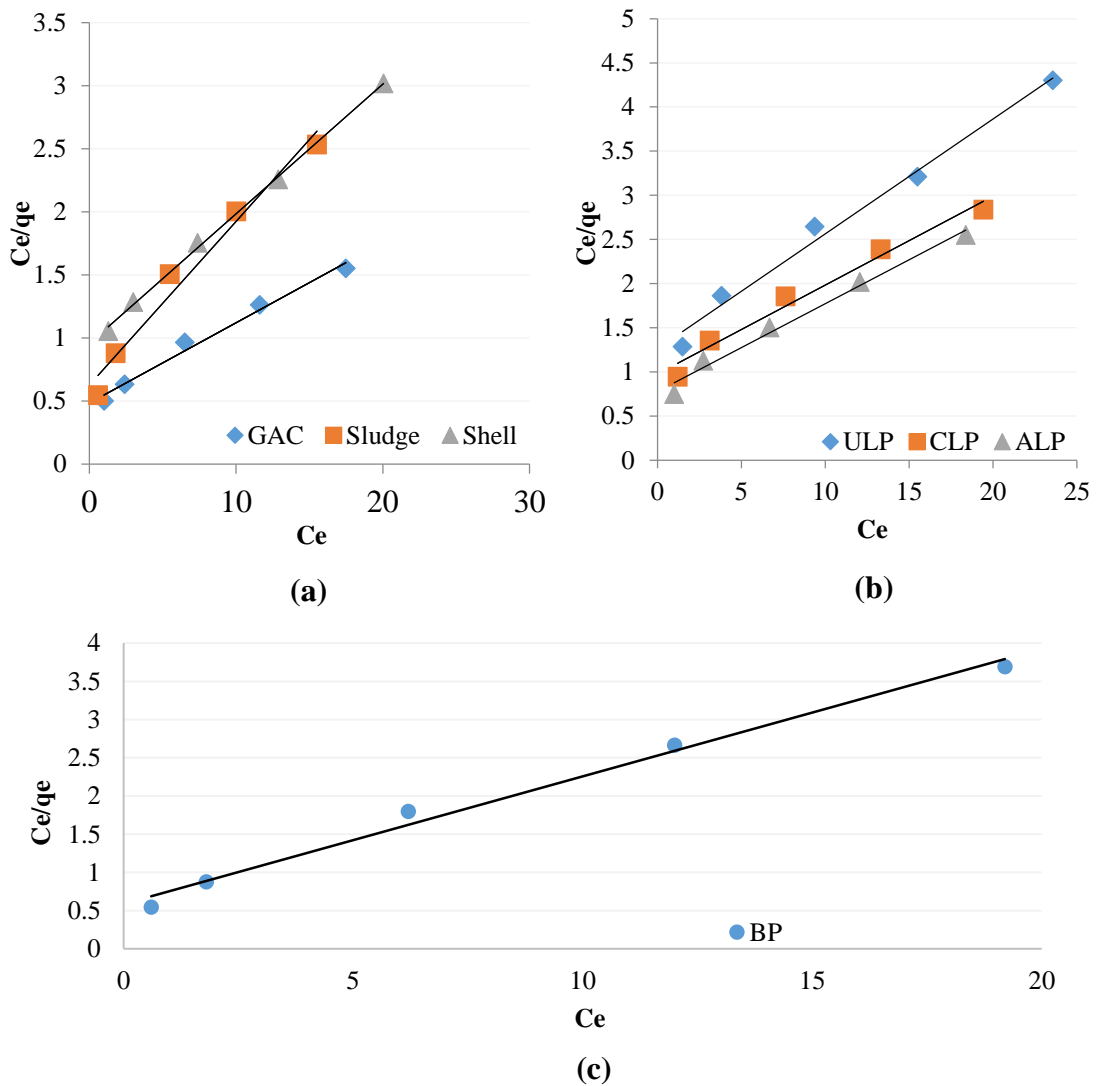


Figure 4.13 Langmuir adsorption isotherm for (a) GAC, Sludge and Shell (b) ULP, CLP and ALP (c) BP at neutral pH and 298 K

From Figure 4.13, we can see that the graph of C_e/q_e versus C_e produced a linear line, which confirmed applicability of Langmuir isotherm. The Langmuir constants, Q_0 and b are calculated from intercept and slope of obtained plots, and is listed in Table 4.7. These characteristic parameters give idea about the surface properties and affinity of sorbent at fixed pH (7) and temperature (298 K).

Table 4.7 Calculated parameters of Langmuir isotherm for the selected adsorbents

Adsorbents	Equations	Correlation coefficient (R ²)	Surface energy (b)	Monolayer adsorption capacity (Q _o)
GAC	$y = 0.063x + 0.486$	0.986	0.129	15.87
Sludge	$y = 0.129x + 0.626$	0.972	0.206	7.75
Shell	$y = 0.102x + 0.956$	0.998	0.107	9.72
ULP	$y = 0.130x + 1.261$	0.987	0.103	7.68
CLP	$y = 0.100x + 0.978$	0.977	0.102	9.96
ALP	$y = 0.099x + 0.777$	0.985	0.128	10.05
BP	$y = 0.166x + 0.587$	0.990	0.283	6

The R² values of Langmuir model approaching to one denotes excellent linear relationship between C_e/q_e and C_e. GAC showed highest monolayer adsorption capacity followed by ALP, CLP, shell, sludge, ULP and BP. The Langmuir model provided the estimated value for maximum fluoride adsorption capacity where the adsorbents could not be reach in experiments. The isotherms showing an increase in adsorption capacity at lower concentration range and an apparent plateau on the achievement of monolayer is related to comparatively strong adsorbent-adsorbate interactions [165]. A steep initial slope i.e., higher value of ‘b’ signifies the existence of stronger bonds between fluoride and adsorbents, and revalidates that one of the dominant modes of adsorption is chemisorption. The calculated values of separation factor, R_L for the respective adsorbents is listed in Table 4.8.

Table 4.8 Separation factor (R_L) for the selected adsorbents

(C _i)	R _L (GAC)	R _L (Sludge)	R _L (Shell)	R _L (ULP)	R _L (CLP)	R _L (ALP)	R _L (BP)
5	0.607	0.492	0.651	0.660	0.662	0.609	0.414
10	0.436	0.326	0.483	0.492	0.495	0.438	0.261
20	0.279	0.195	0.318	0.326	0.328	0.280	0.150
30	0.205	0.139	0.237	0.244	0.246	0.206	0.105
40	0.162	0.108	0.189	0.195	0.196	0.163	0.081

As seen from Table 4.8, the R_L value for each adsorbents was found to lie between 0 and 1 for 5-40 mg/l fluoride concentrations. This indicates the fluoride adsorption by all seven adsorbents was favorable under optimum conditions [129]. In addition, a graph was plotted between the separation factor (R_L) values and initial fluoride concentrations (C_i) for each adsorbents in order to explain the crucial features of Langmuir isotherm as shown in Figure. 4.14.

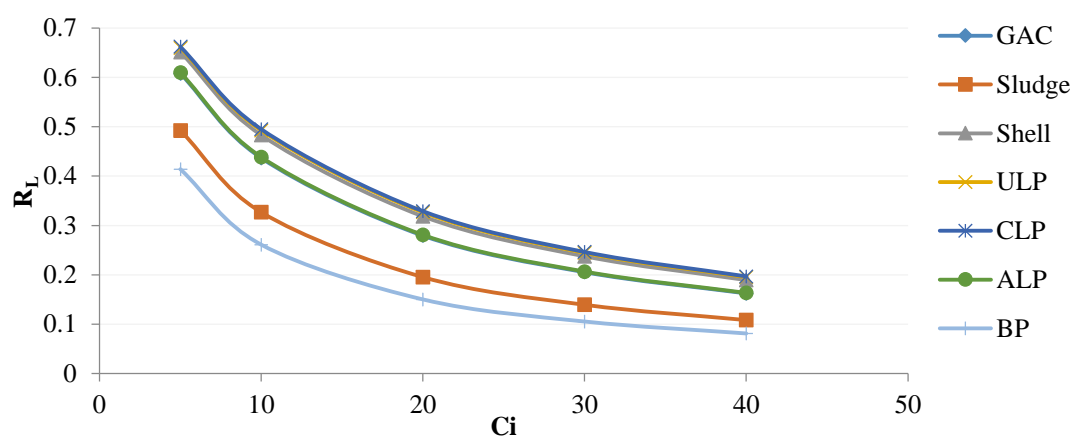


Figure 4.14 Separation factor R_L values versus initial fluoride concentration (C_i)

The steeper isotherms suggest that the tested adsorbents are more effective for fluoride removal. The irreversible isotherm is highly favorable isotherm, and the amount adsorbed does not depend on decreasing concentrations to very low values; unlike unfavorable isotherms, which have low adsorption capacities at low equilibrium concentrations resulting in concave forms [166].

4.3.2 Freundlich Isotherm Model

The relationship between the amount of fluoride adsorbed per unit mass of the adsorbents (q_e) and equilibrium fluoride concentration (C_e) was obtained from the Freundlich isotherm models as shown in Figure 4.20.

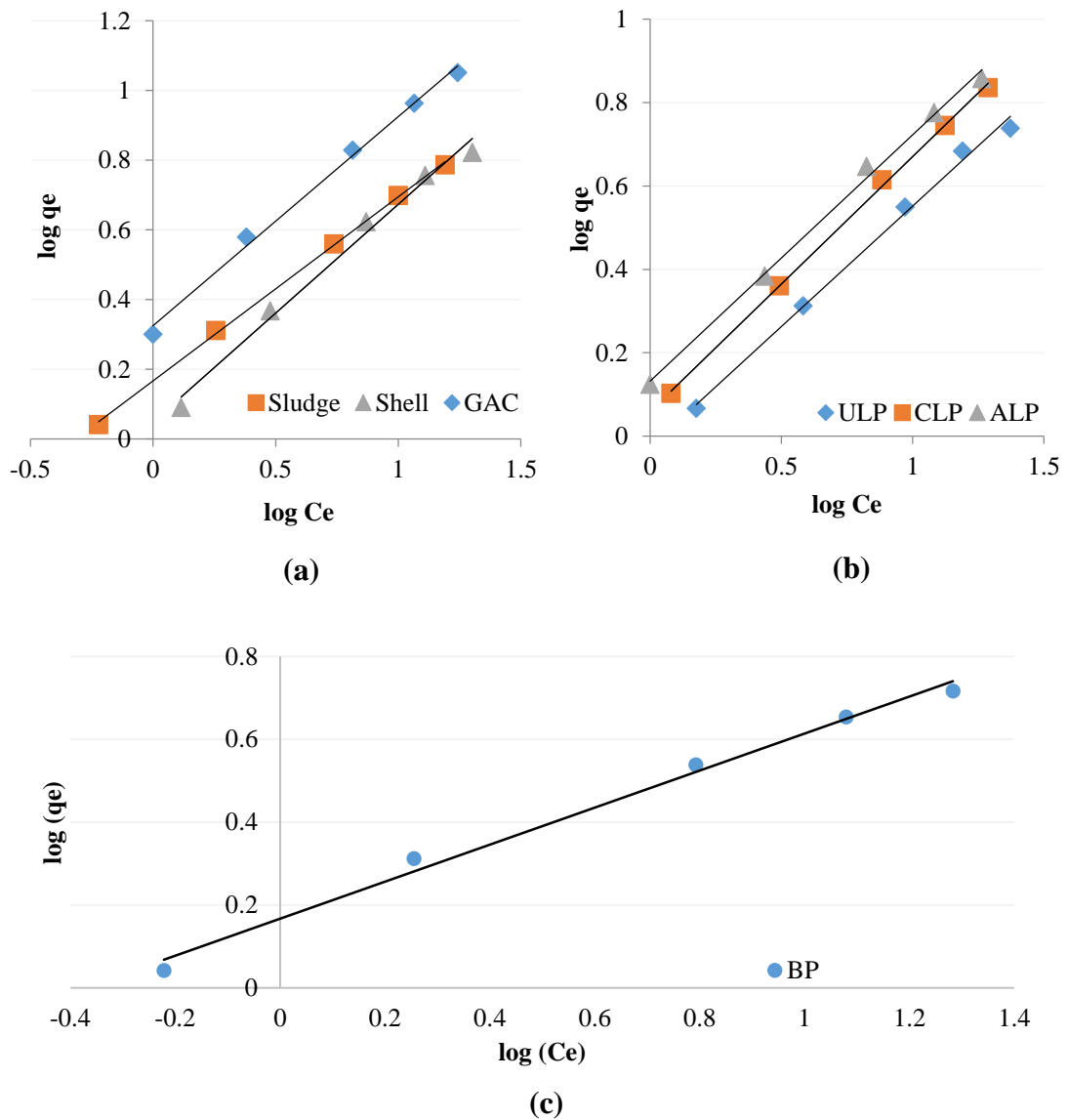


Figure 4.15 Freundlich adsorption isotherm for (a) GAC, Sludge and Shell (b) ULP, and ALP (c) BP at pH 7 and 298 K

As seen from Figure 4.15, the graphs of $\log q_e$ vs. $\log C_e$ resulted in a straight line. When the value of C_e equals to one, $\log K_F$ becomes equal to $\log q_e$. Additionally, if the experimental data obeys Freundlich isotherm, it gives a concise analytical expression for the experimental facts, rather than a clear picture of the adsorption mechanisms. The values of the slope (n) and intercept (K_F) generated from the given plots are presented in Table 4.9.

Table 4.9 Calculated parameters of Freundlich isotherm for the selected adsorbents

Adsorbents	Equations	(R ²)	(K _F)	1/n	(n)
GAC	$\log y = \log (0.65x) + \log (0.263)$	0.997	1.832	0.65	1.538
Sludge	$\log y = \log (0.528x) + \log (0.166)$	0.999	1.465	0.528	1.893
Shell	$\log y = \log (0.624x) + \log (0.049)$	0.988	1.119	0.624	1.602
ULP	$\log y = \log (0.577x) - \log(0.025)$	0.995	0.942	0.577	1.731
CLP	$\log y = \log (0.610x) + \log (0.059)$	0.998	1.147	0.610	1.638
ALP	$\log y = \log (0.590x) + \log (0.132)$	0.996	1.355	0.590	1.693
BP	$\log y = \log (0.446x) + \log (0.167)$	0.991	1.469	0.446	2.239

The R² value of the Freundlich model approaching unity denotes very worthy linear relationship between $\log (C_e)$ and $\log (q_e)$. The magnitudes of K_F and n indicated easy removal of fluoride ions and verified that the adsorption process is favorable. The value of slope (1/n) lied between 0 and 1 for all seven adsorbents and this indicates the increase in the bond energies with the increase in surface density. The surface will become more heterogeneous as the 1/n value approaches zero. The 1/n value less than one implies chemisorption process, while above unity it is indicative of cooperative adsorption [107]. For adsorbents having a highly heterogeneous surface in terms of both geometrical (e.g., different pore sizes and shapes) and chemical (e.g., functional groups, impurities) properties, Freundlich isotherm better fits the experimental data.

Therefore, in this study the R² values shows that the fluoride adsorption isotherms fitted well to both Langmuir and Freundlich models, emphasizing the probability of mono and heterolayer formation on adsorbents surface. The presence of functional groups with varying intensity and non-uniform distribution may cause differences in energy level of sorption sites, thus affecting their adsorption capacity. The sites with higher energy tend to form heterolayer due to strong chemical bonding, whereas sites with low energy induces monolayer due to the electrostatic forces [167].

4.4 Batch Kinetic Studies

Adsorption kinetics describes the fluoride removal rate as a function of equilibrium contact time.

4.4.1 Weber and Morris intraparticle diffusion model

The Weber- Morris intraparticle diffusion model was tested for given adsorbents and the variance of adsorption capacity was studied with respect to time. The representative plots of intraparticle diffusion model for GAC, sludge, shell, ULP, CLP and ALP for 5 mg/l F⁻ and BP for 10 mg/l F⁻ at 298 K is shown in Figure 4.16.

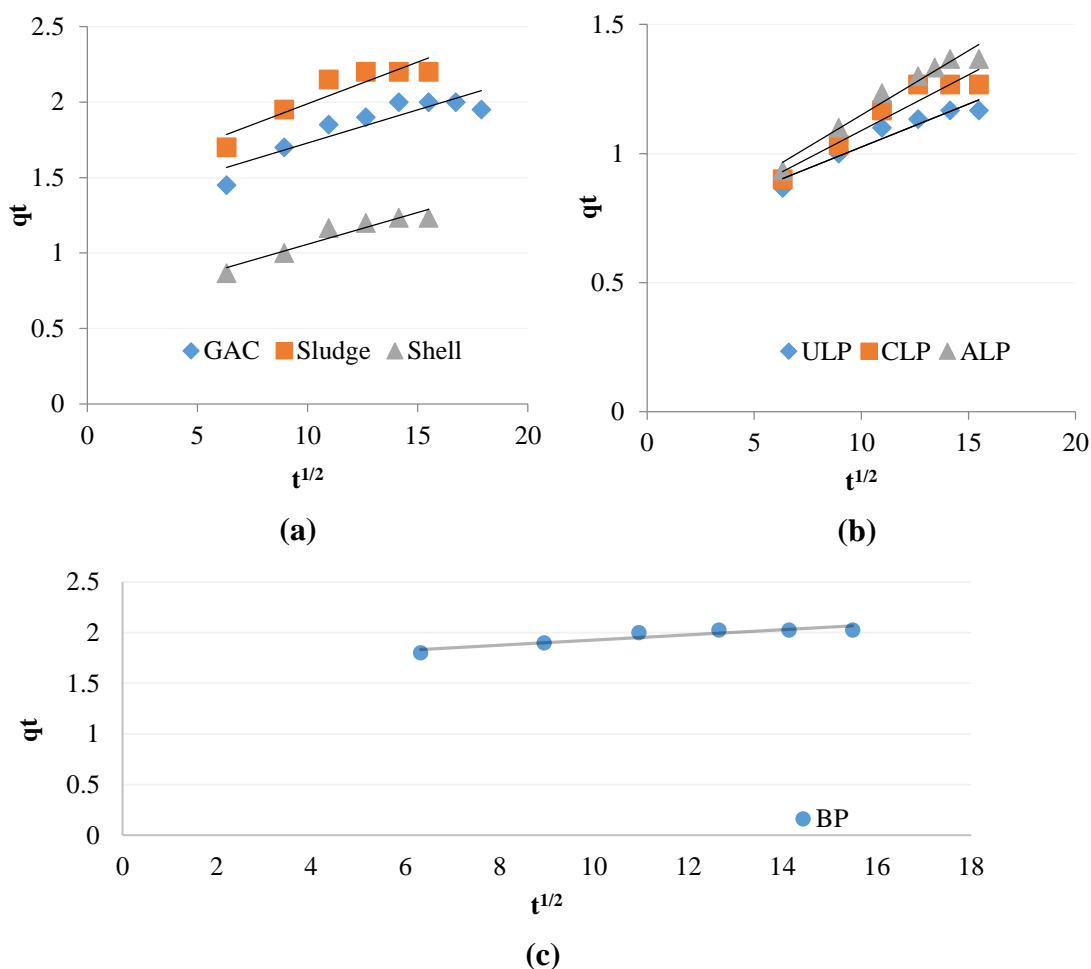


Figure 4.16 Intraparticle diffusion model for (a) GAC, Sludge and Shell at 5 mg/l F⁻ (b) ULP, CLP and ALP at 5 mg/l F⁻ (c) BP at 10 mg/l F⁻ at pH 7

As seen from Figure 4.16, the plots are not linear over whole time range. The curves for all adsorbents represented three phases during adsorption process. For instance, in case of GAC, first linear portion implied external surface adsorption and boundary layer diffusion effect (stage 1) during the first 120 minutes. Then a gradual adsorption stage of intraparticle diffusion (stage 2) was reached which continued up to 200 min, and finally an equilibrium adsorption (stage 3) was attained. In the third stage, diffusion rate starts to slow because of the extremely less fluoride concentration in

solution. The adsorbents are surrounded by the film of water molecules through which the F⁻ ions must diffuse prior to adsorption. Then, the ions were transported through diffusion into adsorbents and finally was retained in internal pores [168]. Thus, fluoride removal rate can be described by the assumption of initial film-transfer dominance, eventual surface-diffusion dominance, and a period at which both mechanisms might influences adsorption rate.

Meanwhile, the adsorbents are continuously shaken during adsorption period, so it is reasonable to predict that the mass transfer from bulk solution to external surface of adsorbents does not limit the rate. Even though the intraparticle diffusion plots rendered linear lines, they fail to pass through origin in each case. This variation from origin or near saturation might be because of the difference of mass transfer in initial and final stages of adsorption [169]. The data exhibited multi-linear plots, and thus is assumed that other mechanisms are also involved together with intraparticle diffusion. This concludes that the sorption process is ‘complex’ including more than one mechanisms. Hence, adsorption kinetics of fluoride could be controlled by both surface adsorption and intraparticle diffusion simultaneously when slope is not equal to zero. The various parameters of this model are calculated and listed in Table 4.10.

Table 4.10 Calculated parameters of Intraparticle diffusion model for selected adsorbents

Adsorbents	Equations	Correlation coefficient (R ²)	Intraparticle diffusion rate constant (K _{int})	C
GAC	$y = 0.044x + 1.289$	0.814	0.044	1.289
Sludge	$y = 0.055x + 1.437$	0.843	0.055	1.437
Shell	$y = 0.042x + 0.635$	0.909	0.042	0.635
ULP	$y = 0.033x + 0.691$	0.922	0.033	0.691
CLP	$y = 0.043x + 0.658$	0.915	0.043	0.658
ALP	$y = 0.049x + 0.651$	0.960	0.049	0.651
BP	$y = 0.025x + 1.672$	0.856	0.025	1.672

The linear plots in this study yielded a reasonably good correlation coefficient for every adsorbents. It is found that particle size plays a vital role in kinetic reactions as fluoride removal rate increased for smaller particle size. This is in

accordance with higher diffusion rate of fluoride for smaller particle size of sludge and CLP. For smaller particle size, there exists a smaller diffusion distance between the layers and faster adsorption velocities is preferable for batch adsorption. Higher value of 'C' for GAC, sludge and BP signifies higher boundary layer effect and there is greater attribution of surface adsorption in rate determining step [119].

4.4.2 Pseudo-First Order Kinetic Model

The adsorption rate of seven adsorbents were estimated on the basis of their adsorption capacity by using pseudo-first-order kinetic model. The graphs obtained for GAC, sludge, shell, ULP, CLP and ALP for 5 mg/l F⁻ and BP for 10 mg/l F⁻ at 298 K and neutral pH are shown in Figure 4.17.

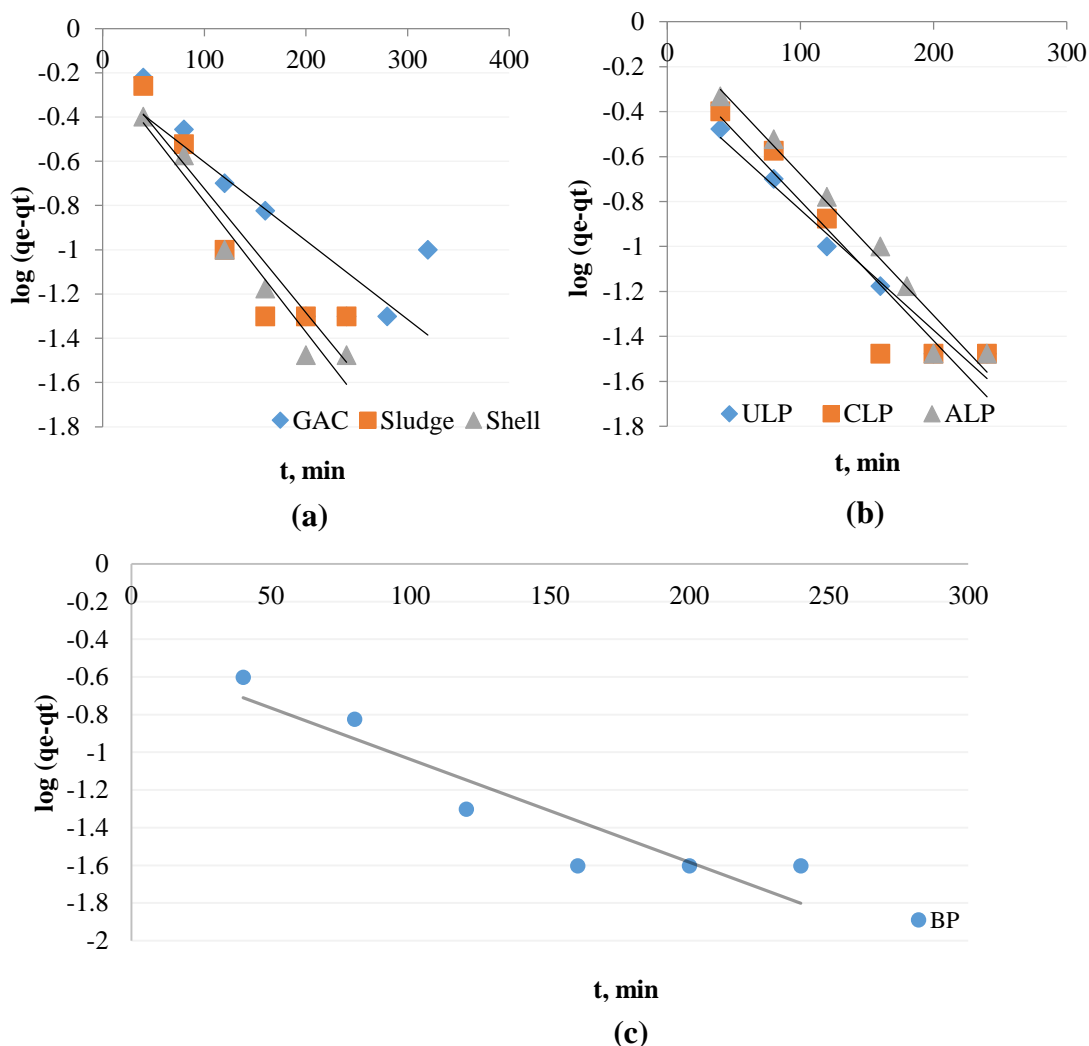


Figure 4.17 Pseudo first-order kinetic model for (a) GAC, Sludge and Shell at 5 mg/l F⁻ (b) ULP, CLP and ALP at 5 mg/l F⁻ (c) BP for 10 mg/l F⁻ at pH 7

As seen from Figure 4.17, the equilibrium data were well represented by Lagergren-first order model only in initial stage where the adsorption rate of fluoride is very rapid. So, trial and error method is used to find the equilibrium adsorption capacity, q_e to analyse these kinetic models. The values of pseudo-first-order rate constant (k_1) and adsorption capacities of tested adsorbents is given in Table 4.11.

Table 4.11 Calculated parameters of Pseudo first order kinetic model for selected adsorbents

Adsorbents	Equations	(R ²)	First order rate constant (k_1)	$q_{e,cal}$	$q_{e,exp}$
GAC	$y = -0.003x - 0.247$	0.712	0.0008	0.565	2.05
Sludge	$y = -0.005x - 0.163$	0.852	0.0128	0.686	2.25
Shell	$y = -0.005x - 0.188$	0.952	0.0135	0.647	1.26
ULP	$y = -0.005x - 0.300$	0.965	0.012	0.501	1.2
CLP	$y = -0.006x - 0.175$	0.880	0.014	0.667	1.3
ALP	$y = -0.006x - 0.049$	0.965	0.014	0.891	1.4
BP	$y = -0.005x - 0.492$	0.853	0.012	0.322	2.05

The low correlation coefficient (R^2) values for adsorbents showed that adsorption of fluoride is not occurring exclusively onto one site per ion [170]. In reality, it is required that the predicted equilibrium adsorption capacity values from model, q_e (cal) should resemble with experimental, q_e (exp) values. But in this study the experimental and calculated values did not agree with each other for all the tested adsorbents. This suggests that the pseudo-first order equation didn't fit quite well with complete range of contact time and is thus relevant only for early stage of the process. Higher value of rate constant (k_1) in CLP and ALP signifies quicker adsorption rate of the fluoride. In this kinetic model, adsorption is controlled by diffusion and mass transfer of the fluoride ions to adsorption sites.

4.4.3 Pseudo-Second Order Kinetic Model

The adsorption behavior of fluoride onto GAC, sludge, shell, ULP, CLP and ALP for 5 mg/l F⁻ and BP for 10 mg/l F⁻ at 298 K and neutral pH is presented in Figure 4.18 using pseudo-second order kinetic model.

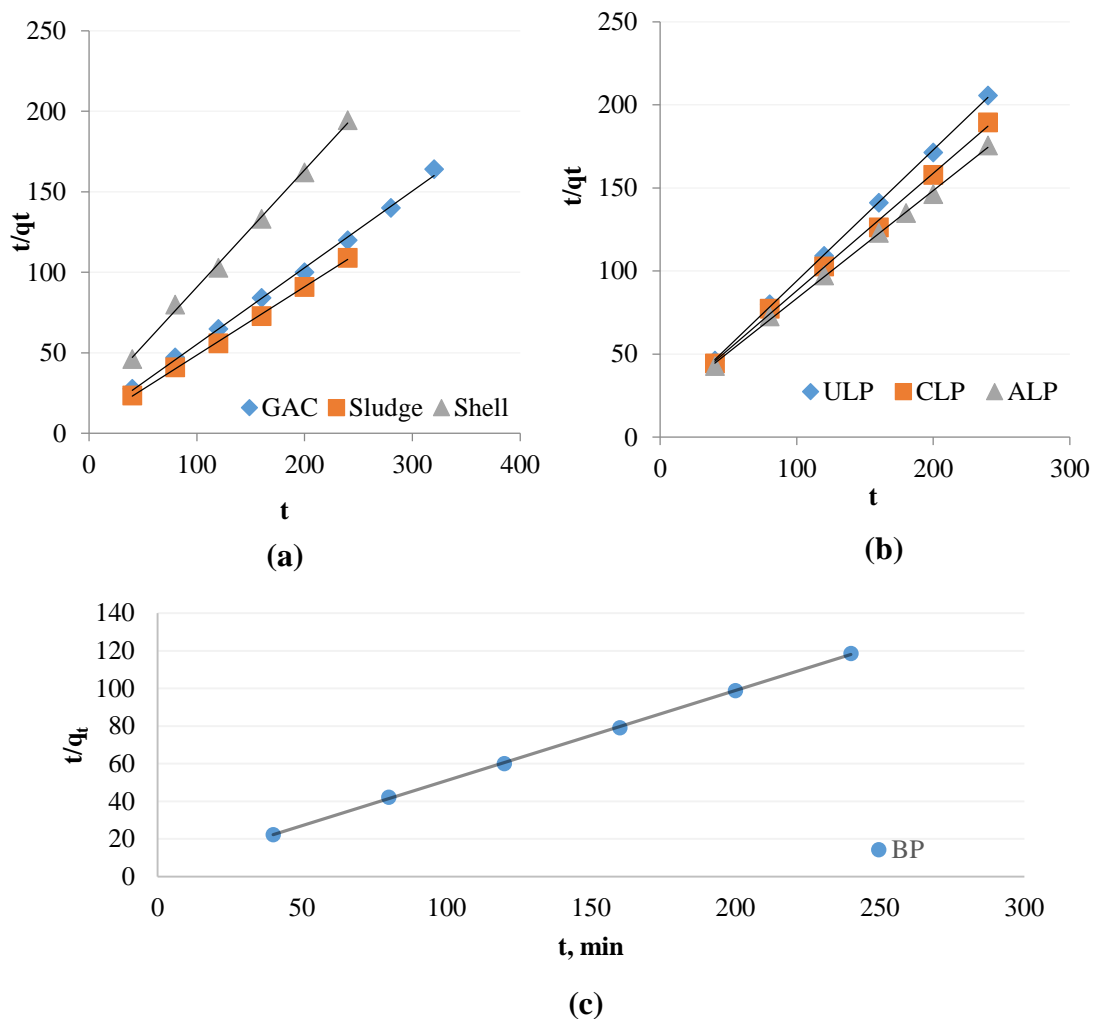


Figure 4.18 Pseudo second-order kinetic model for (a) GAC, Sludge and Shell at 5 mg/l F^- (b) ULP, CLP and ALP at 5 mg/l F^- (c) BP for 10 mg/l F^- at pH 7

Pseudo second-order kinetic approach gives better description of fluoride adsorption onto given adsorbents. For these type of reactions, the rate of adsorption is directly proportional to number of active sites on the adsorbent surface. With the help of above graphs the rate constant (k_2), amount of fluoride uptake at equilibrium (q_e) and initial adsorption rate (h) was calculated for all adsorbents and given in Table 4.12.

Table 4.12 Calculated parameters of Pseudo second order kinetic model for selected adsorbents

Adsorbents	Equations	(R ²)	q _e cal	q _e exp	k ₂	h= k ₂ q _e ²
GAC	y = 0.476x + 7.682	0.997	2.098	2.05	0.029	0.130
Sludge	y = 0.424x + 6.078	0.998	2.355	2.25	0.029	0.164
Shell	y = 0.728x + 17.93	0.998	1.373	1.26	0.029	0.055
ULP	y = 0.788x + 15.17	0.999	1.267	1.2	0.040	0.065
CLP	y = 0.707x + 17.39	0.997	1.414	1.3	0.028	0.057
ALP	y = 0.649x + 18.63	0.998	1.539	1.4	0.022	0.053
BP	y = 0.478x + 3.056	0.999	2.088	2.05	0.075	0.327

The correlation coefficient (R^2) values of linearized pseudo-second order equation seems higher because both the axes contain the variable t [171]. It was seen that $q_{e, \text{exp}}$ and $q_{e, \text{cal}}$ values from this model are very close to each other. The benefits of using this equation to estimate q_e values, is related to its small sensitivity to the random experimental errors. The rate constant (k_2) was found to increase with the increase in shaking speed, implying that equilibrium was attained relatively faster at higher agitation rate. This also suggests that diffusion is also important in the fluoride adsorption kinetics. If the adsorbents obey pseudo second order rate equation, then the overall rate of fluoride adsorption seems to be controlled by the chemical processes, through sharing of electrons between adsorbents and fluoride, or covalent forces, through electrons exchange between particles, and it may be rate-limiting step [172].

4.4.4 Elovich Equation

The linear plot of q_t vs $\ln t$ for GAC, sludge, shell, ULP, CLP and ALP for 5 mg/l F^- and BP for 10 mg/l F^- at different contact times was plotted to confirm the applicability of Elovich equation. The plots are shown in Figure 4.19.

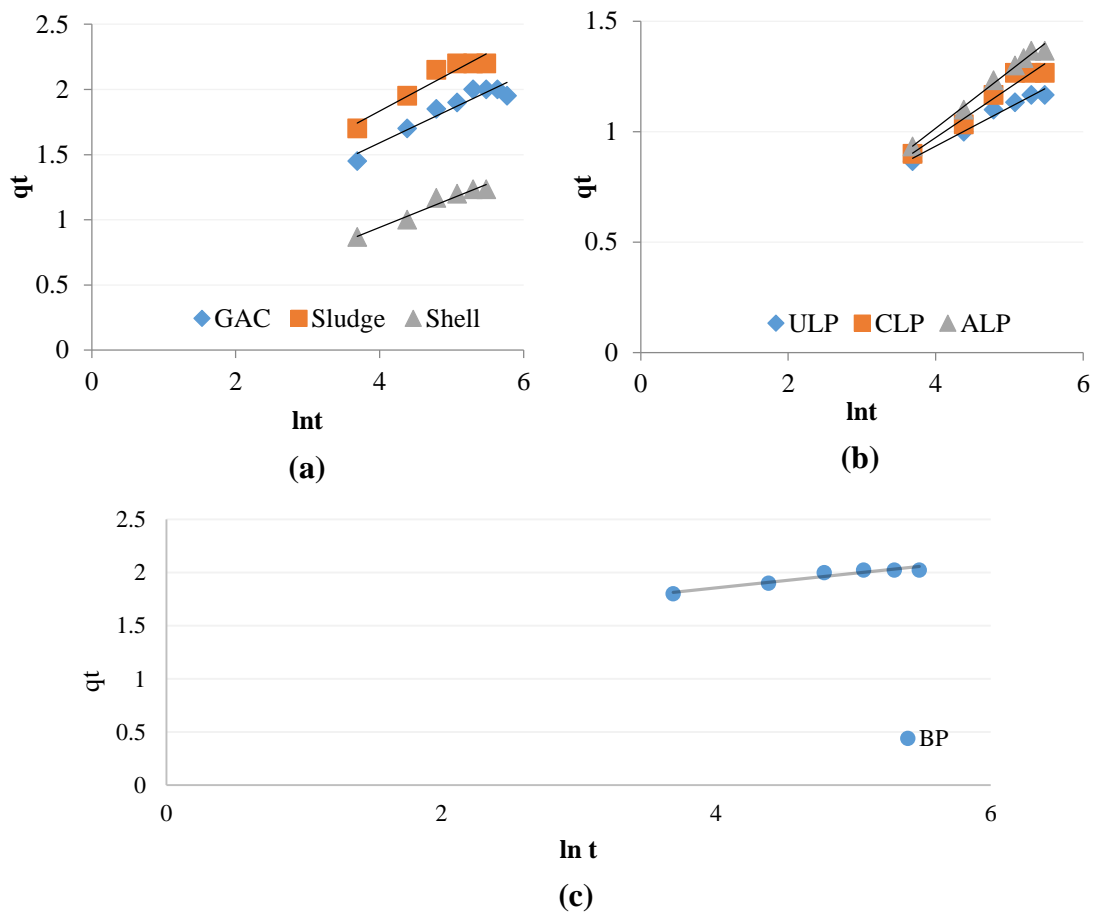


Figure 4.19 Elovich model for (a) GAC, Sludge and Shell at 5 mg/l F^- (b) ULP, CLP and ALP at 5 mg/l F^- (c) BP for 10 mg/l F^- at pH 7

As seen from Figure 4.19, the plots for all adsorbents gave linear relationship. The α and β values are obtained from intercept and slope of the graphs, as listed in Table 4.13.

Table 4.13 Calculated parameters of Elovich model for the selected adsorbents

Adsorbents	Equations	R^2	α	B
GAC	$y = 0.262x + 0.54$	0.910	2.053	3.809
Sludge	$y = 0.295x + 0.652$	0.920	2.683	3.382
Shell	$y = 0.221x + 0.056$	0.955	0.285	4.514
ULP	$y = 0.176x + 0.23$	0.974	0.650	5.681
CLP	$y = 0.225x + 0.068$	0.955	0.306	4.426
ALP	$y = 0.258x - 0.017$	0.988	0.241	3.871
BP	$y = 0.135x + 1.314$	0.9255	2248.8	7.3909

The kinetic curve of fluoride adsorption established a good fitting with Elovich model ($R^2 > 0.9$), and this indicates that the rate-controlling step is diffusion in nature [173]. While applying Elovich equation for modelling kinetic data, desorption rate is not taken into consideration. The value of $(1/\beta)$ signifies the number of the available binding sites and the $(1/\beta) \ln(\alpha\beta)$ value represents the amount of fluoride adsorbed when $\ln t$ is equal to zero. These characteristic parameters give an idea about the nature of the fluoride adsorption at the first step. The Elovich equation does not provide any information on the definite mechanisms for fluoride removal. However, it is widely used to describe adsorption phenomena on highly heterogeneous surface. Applicability of Elovich equation shows that fluoride adsorption onto the adsorbent surface is predominantly chemical in nature, which further supports the application of second order kinetics to adsorption of fluoride onto the given adsorbents.

4.5 Fluoride removal efficiencies of various low-cost adsorbents

The effectiveness of the selected adsorbents for the removal of 5 mg/l fluoride solution at optimum reaction conditions (Table 4.14) is shown in Figure 4.20.

Table 4.14 Optimum reaction conditions for adsorbents to treat 5 mg/l fluoridated water

Adsorbents	pH	Dose (g/l)	Agitation Speed (rpm)	Contact time (min)
Granular Activated Carbon	7	2	200	180
Sludge				160
Shell		3		200
Untreated Litchi Peel				160
Carbonized Litchi Peel				200
Acid treated Litchi Peel				160
Banana Peel		4		160

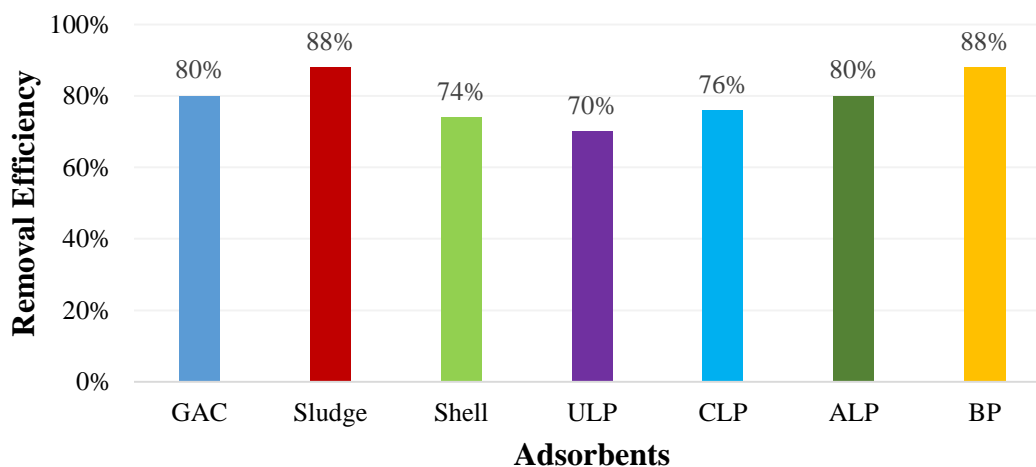


Figure 4.20 Order of effectiveness of adsorbents at their optimum conditions and initial fluoride concentration of 5 mg/l

As seen from Figure 4.20, sludge and BP rendered the maximum defluoridation efficiency of 88%, followed by GAC \simeq ALP (80%), CLP (76%), shell (74%) and ULP (70%) from 5 mg/l fluoridated solution. The positive charges on the hydroxylated surface of the Al, Ca, Mg, Si oxides in the sludge resulted in the adsorption and net catching reactions of fluoride. The rich organic functional groups (-OH, -NH₂, -COOH) present in BP played a major role in fluoride removal via two-step ligand exchange mechanism. The larger surface area of GAC favored the physisorption of F⁻ ions onto their porous structure and also the formation of C—F bond accounted for chemisorption process. The biosorption efficiency of litchi peel was greatly enhanced after acid treatment, possibly due to introduction of protonated functional groups onto adsorbent surface. The porosity is also supposed to be increased after the acid treatment which allows the binding of fluoride ions onto the porous structure. After the carbonization, the mesoporosity and macroporosity of CLP can increase through unblocking of pores initially occupied by the materials like cellulose and hemicellulose. The sea shell adsorbent could readily remove the fluoride ions in the form of insoluble CaF₂ by swapping out its calcium ions in favor of the fluoride ions.

The top three adsorbents which are worth using in the practical applications for treating fluoridated water are banana peel (BP), carbonized litchi peel (CLP) and sea shells. Klui Namwa is the most widely distributed ABB cultivar grown in Thailand and is available all year round. The BP adsorbent resembles fibrous nature and presence of carbonaceous materials favors the fluoride adsorption. Moreover, CLP is carbon rich

adsorbent with large number of acidic functional groups throughout its surface, and can electrostatically bind fluoride ions. The shell basically comprises of proteins in the outermost layer, followed by calcite layer and a smooth inner layer of platy calcium carbonate crystals. So, it can readily swaps out Ca atoms in favor of fluoride, locking them into solid form. These non-toxic and eco-friendly bio-materials exhibit high potential to effectively remove water contaminants like fluoride considering the wide availability of feedstock, low-cost and favorable physical/chemical surface properties.

Moreover, the comparison of these selected adsorbents with the various other adsorbents reported in literature are shown in Table 4.15.

Table 4.15 Comparison of F⁻ removal with other adsorbents (5 mg/l F⁻ solution at neutral pH)

Adsorbents	Dose (g/l)	Contact time (min)	Removal Efficiency	Ref.
Modified Bagasse	2	60	> 90%	[174]
Activated carbon: <i>Vitex negundo</i> barks	4	50	> 90%	[97]
<i>Tinospora cordifolia</i>	140	120	70%	[92]
Carbon: <i>Acacia Arabica</i> and <i>Acacia Farnesiana</i> fruit	4	40	> 85%	[175]
Nitric acid treated activated carbon: <i>Typha angustata</i>	4	40	> 85%	[176]
Sal (<i>Shorea robusta</i>) leaf powder	20 (0.3 mm)	60	63.6%	[177]
	20 (1 mm)		25.8%	
Granular Activated Carbon	2	180	80%	This Study
Sludge	2	180	88%	
Shell	3	160	74%	
Untreated Litchi Peel	3	200	70%	
Carbonized Litchi Peel	3	160	76%	
Acid Treated Litchi Peel	3	180	80%	
Banana Peel	4	160	88%	

Chapter 5

Conclusions and Recommendations

This chapter contains the formulated summary of the basic findings from this study and some discussions are made whether the predefined objectives are met. The recommendations for the follow-up studies are also included.

5.1 Conclusions

Lab scale investigations were carried out using low cost adsorbents such as activated sewage sludge, sea shell, litchi peel and banana peel for the fluoride removal, and their adsorption efficiencies was compared with that of GAC. Results indicate that these freely abundant local materials can be an economically viable option for the treating the low fluoride concentration water. Following conclusions are based on the results from this study supported by the information from literature.

The factors like surface area, pore volume and mechanical properties of adsorbents played a crucial role in fluoride removal process. As adsorption is a surface phenomenon, adsorbents having higher surface area and smaller particle size registered high defluoridation efficiencies. In case of litchi peel, the increased pore volume and surface area after modification allowed the binding of fluoride onto their porous structures. Besides, the adsorbents didn't crumble much during handling and use, which signifies their abrasion-resistance nature.

The infrared spectral analysis of agro-based adsorbents revealed that carbon bonded with hydrogen and oxygen atom is important for fluoride adsorption by lignocellulosic biomass. The hydrogen bonding and ligand exchange facilitated the binding of fluoride onto specific adsorption sites, and the mechanism of removal was primarily governed by chemical adsorption. Sewage sludge, on the other hand is a complex matrix comprising inorganic mineral structures and organic functional groups, which accounted for better fluoride removal efficiency. The observance of sharp peak on the sea shell confirmed the presence of pure aragonite (CaCO_3) structure, and this could readily swap out its Ca ions in favor of fluoride ions. Further, the fluoride layer over adsorbents surface after adsorption could be clearly visualized from SEM images.

The highest fluoride removal efficiency was observed at the pH values lower than the pH_{pzc} values for all adsorbents, and this allowed the electrostatic binding of fluoride to the corresponding groups present on the adsorbent surface. At neutral pH, GAC, sludge, shell, ULP, CLP, and ALP rendered 70%, 82%, 66%, 62%, 66% and 70% removal efficiency from 5 mg/l F^- solution, whereas BP showed up with 76% removal efficiency for 10 mg/l fluoridated solution. The high percentage of fluoride removal at neutral pH demonstrates the practical applicability of these adsorbents.

At the optimum reaction condition, sludge and BP showed the highest fluoride removal efficiency of 88% followed by $\text{GAC} \simeq \text{ALP} (80\%) > \text{CLP} (76\%) > \text{Shell} (74\%) > \text{ULP} (70\%)$ from 5 mg/l fluoridated solution. This shows that all the tested adsorbents could lower the fluoride concentration to regulated standard. The fluoride removal efficiency of the adsorbents increased with the increasing adsorbent dose, exposure time and speed of rotation, whereas the removal rate declined with the rise in initial fluoride concentration. The equilibrium was observed after 200 min for ULP and ALP, 180 min for GAC and sludge, and 160 min for shell, CLP and BP at the speed of 200 rpm. The rough fibrous surface texture with the smallest openings in ULP and ALP allowed the diffusion of fluoride ions. In case of BP, the fluoride removal efficiency dropped from 79% to 77% and from 75% to 68% with the increment of chloride and sulphate concentration from 50 to 250 mg/l. This shows that defluoridation rate decreased to some extent with the increase in sulphate concentration, but was independent of chloride ion concentration.

Both Langmuir and Freundlich isotherms fitted well to the experimental results and were statistically significant. This suggested a likelihood of mono and heterolayer formation onto adsorbents surface. The values of correlation coefficient for Freundlich isotherms were above 0.99 for all adsorbents, while for Langmuir isotherm the R^2 values were found to be in between 0.97 to 0.99. The R_L value in the present investigation was less than one, concluding that the fluoride adsorption is favorable. Likewise, value of slope ($1/n$) in Freundlich isotherm lied between 0 and 1 for all seven adsorbents and this indicated the increase in the bond energies with the increase in the surface density.

Based on the results of adsorption kinetics data analysis, pseudo second order kinetic model seems to be more compatible with obtained data from experiments, with less fluctuation in calculated and experimental uptake capacities (q_e). On the other hand,

although the plots of intraparticle diffusion rendered linear lines with good correlation coefficients, they fail to pass through origin for all the adsorbents, which suggested that the process is 'complex' with more than one mechanism limiting the rate of adsorption. Thus, the surface adsorption as well as intra-particle diffusion controlled the overall adsorption process at "liquid-solid" interfaces.

So, adsorption process is a promising option to other conventional methods for fluoride removal because of its simplicity in design, ease of operation, high efficiency, eco-friendly applications and economic feasibility. This type of green technology would not only address the effectiveness for treating fluoride contaminated water, but also bring an additional value to these agro-industrial waste enhancing the food-processing industry worldwide. This practice complements the final stages of production chain to give sustainable destination for the generated wastes. Additionally, once these adsorbents are used, they can be disposed without expensive regeneration because of their low-cost and ease of availability.

5.2 Recommendations for Future Work

Based on the obtained results and conclusions, the following recommendations are made:

- 1) The method development should include an experimental set-up with continuous-flow column studies, such that the system provides higher residence time and the mass balance is better accounted for.
- 2) A more detailed analysis is needed to improve our understanding of the adsorption and its complex mechanisms.
- 3) A pilot scale study is necessary to assess the applicability of these adsorbents in the exclusion of fluoride from real drinking water. Also, economic evaluation is required to assess the feasibility of process implementation in large scale applications.
- 4) In order to re-use the agro-based biomass several times, it is paramount to improve the textural characteristics of the adsorbents.

References

1. *Water Fluoridation Additives Fact Sheet*. [cited 2014 September 22, 2015]; Available from: <http://www.cdc.gov/fluoridation/factsheets/engineering/wfadditives.htm>.
2. Felsenfeld, A.J. and M.A. Roberts, *A report of fluorosis in the United States secondary to drinking well water*. *Jama*, 1991. **265**(4): p. 486-488.
3. Li, S., et al., *Eukaryotic resistance to fluoride toxicity mediated by a widespread family of fluoride export proteins*. *Proceedings of the National Academy of Sciences*, 2013. **110**(47): p. 19018-19023.
4. Cape, J.N., D. Fowler, and A. Davison, *Ecological effects of sulfur dioxide, fluorides, and minor air pollutants: recent trends and research needs*. *Environment International*, 2003. **29**(2): p. 201-211.
5. WHO *Fluoride in Drinking-water: Background document for development of WHO Guidelines for Drinking-water Quality*. 2004.
6. Edgar, A., L. Pizzolato, and J. Sheen, *Fluorine in igneous rocks and minerals with emphasis on ultrapotassic mafic and ultramafic magmas and their mantle source regions*. *Mineralogical Magazine*, 1996. **60**(399): p. 243-258.
7. Nagendra Rao, C. *Fluoride and environment—a review*. in *Proceedings of the Third International Conference on Environment and Health (eds Bunch MJ, Suresh VM and Kumaran TV)*, York University. 2003.
8. Tsuchiya, Y., *INORGANIC CHEMICALS INCLUDING RADIOACTIVE MATERIALS IN WATERBODIES*.
9. Harvesting, W., et al., *Tools & Resources*.
10. Whitford, G.M., *The metabolism and toxicity of fluoride*. 1996: Karger New York.
11. Biyani, P., *G.V. Black's Classification of Carious Lesions*, in *Dental Notebook*. 2013.
12. Thole, B., *Ground Water Contamination with Fluoride and Potential Fluoride Removal Technologies for East and Southern Africa*. *Perspectives in Water Pollution*. 2013.
13. *Dental Fluorosis*, in *FLUORIDEALERT.ORG*.
14. Resnick, D. and G. Niwayama, *Entheses and enthesopathy. Anatomical, pathological, and radiological correlation*. *Radiology*, 1983. **146**(1): p. 1-9.
15. Fawell, J.K. and K. Bailey, *Fluoride in drinking-water*. 2006: World Health Organization.
16. Roy, S. and G. Dass, *Fluoride contamination in drinking water—a review*. *J Resour Environ*, 2013. **3**: p. 53-58.
17. Dissanayake, C., *The fluoride problem in the ground water of Sri Lanka—environmental management and health*. *International Journal of Environmental Studies*, 1991. **38**(2-3): p. 137-155.
18. García, M.G. and L. Borgnino, *Fluoride in the Context of the Environment*. 2015.
19. Ayoob, S. and A.K. Gupta, *Fluoride in drinking water: a review on the status and stress effects*. *Critical Reviews in Environmental Science and Technology*, 2006. **36**(6): p. 433-487.

20. Foundation, F.R.R.D., *COUNTRIES WITH ENDEMIC FLUOROSIS DUE TO EXCESS FLUORIDE IN DRINKING WATER*, in *Fluorosis Research & Rural Development Foundation*, F.a. Fluorosis, Editor.
21. Lian-Fang, W. and H. Jian-Zhong, *Outline of control practice of endemic fluorosis in China*. Social science & medicine, 1995. **41**(8): p. 1191-1195.
22. Chaoke, L., J. Rongdi, and C. Shouren, *Epidemiological analysis of endemic fluorosis in China*. Journal of Environmental Science & Health Part C, 1997. **15**(2): p. 123-138.
23. Lin, N.-F., J. Tang, and J.-M. Bian, *Geochemical environment and health problems in China*. Environmental geochemistry and health, 2004. **26**(1): p. 81-88.
24. *Fluorosis-affected provinces, 2013*, in UNICEF. 2015.
25. Wen, D., et al., *Arsenic, fluoride and iodine in groundwater of China*. Journal of Geochemical Exploration, 2013. **135**: p. 1-21.
26. Isaac, A., et al., *Prevalence and manifestations of water-born fluorosis among schoolchildren in Kaiwara village of India: a preliminary study*. 2010.
27. Brindha, K. and L. Elango, *Fluoride in groundwater: causes, implications and mitigation measures*. Fluoride properties, applications and environmental management, 2011: p. 111-136.
28. Namkaew, M. and P. Wiwatanadate, *Association of fluoride in water for consumption and chronic pain of body parts in residents of San Kamphaeng district, Chiang Mai, Thailand*. Tropical Medicine & International Health, 2012. **17**(9): p. 1171-1176.
29. S Mongkolnchai-arunya, S.C., P Pukrittayakamee, W Visalseth, and P Suntornram. *Risk Factors of Dental Fluorosis in Thai Children*. in *4th International Workshop on Fluorosis Prevention and Defluoridation of Water* March 2-6, 2004. Colombo, Sri Lanka.
30. Takeda, T. and S. Takizawa, *Health Risks of Fluoride in the Chiang Mai Basin, Thailand*, in *Groundwater Management in Asian Cities*. 2008, Springer. p. 301-327.
31. Ghorai, S. and K. Pant, *Equilibrium, kinetics and breakthrough studies for adsorption of fluoride on activated alumina*. Separation and purification technology, 2005. **42**(3): p. 265-271.
32. Malhbtra, S., D. Kulkarni, and S.P. Pande, *Effectiveness of poly aluminum chloride (PAC) vis-a-vis alum in the removal of fluorides and heavy metals*. Journal of Environmental Science & Health Part A, 1997. **32**(9-10): p. 2563-2574.
33. Huang, C.J. and J.C. Liu, *Precipitate flotation of fluoride-containing wastewater from a semiconductor manufacturer*. Water Research, 1999. **33**(16): p. 3403-3412.
34. Shen, F., et al., *Electrochemical removal of fluoride ions from industrial wastewater*. Chemical Engineering Science, 2003. **58**(3-6): p. 987-993.
35. Hu, C.Y., et al., *Removal of fluoride from semiconductor wastewater by electrocoagulation-flotation*. Water Research, 2005. **39**(5): p. 895-901.
36. Lyengar, L., *22 Technologies for fluoride removal*.

37. Gumbo, F. and G. Mkongo. *Water defluoridation for rural fluoride affected communities in Tanzania*. in *First International Workshop on Fluorosis Prevention and Defluoridation of Water*, Int. Soc. Fluoride Res. 1995.
38. Suneetha, N., et al., *Defluoridation of water by a one step modification of the Nalgonda technique*. *Annals of Tropical Medicine and Public Health*, 2008. **1**(2): p. 56.
39. Ndiaye, P., et al., *Removal of fluoride from electronic industrial effluent by RO membrane separation*. *Desalination*, 2005. **173**(1): p. 25-32.
40. Richards, L.A., M. Vuachère, and A.I. Schäfer, *Impact of pH on the removal of fluoride, nitrate and boron by nanofiltration/reverse osmosis*. *Desalination*, 2010. **261**(3): p. 331-337.
41. Lhassani, A., et al., *Selective demineralization of water by nanofiltration Application to the defluorination of brackish water*. *Water Research*, 2001. **35**(13): p. 3260-3264.
42. Hu, K. and J.M. Dickson, *Nanofiltration membrane performance on fluoride removal from water*. *Journal of Membrane Science*, 2006. **279**(1-2): p. 529-538.
43. da Conceição, V.M., et al., *Removal of excess fluoride from groundwater using natural coagulant Moringa oleifera Lam and microfiltration*. *The Canadian Journal of Chemical Engineering*, 2015. **93**(1): p. 37-45.
44. dos Santos Bazanella, G.C., et al., *Fluoride Removal from Water Using Combined Moringa oleifera/Ultrafiltration Process*. *Water, Air, & Soil Pollution*, 2012. **223**(9): p. 6083-6093.
45. Min, B.R., A.L. Gill, and W.N. Gill, *A note on fluoride removal by reverse osmosis*. *Desalination*, 1984. **49**(1): p. 89-93.
46. Arda, M., et al., *Removal of fluoride from geothermal water by electrodialysis (ED)*. *Separation Science and Technology*, 2009. **44**(4): p. 841-853.
47. Kabay, N., et al., *Separation of fluoride from aqueous solution by electrodialysis: Effect of process parameters and other ionic species*. *Journal of Hazardous Materials*, 2008. **153**(1-2): p. 107-113.
48. Zeni, M., et al., *Study on fluoride reduction in artesian well—water from electrodialysis process*. *Desalination*, 2005. **185**(1-3): p. 241-244.
49. Hichour, M., et al., *Fluoride removal from waters by Donnan dialysis*. *Separation and Purification Technology*, 1999. **18**(1): p. 1-11.
50. Samadi, M.T., et al., *Removal of fluoride ions by ion exchange resin: kinetic and equilibrium studies*. *Environmental Engineering and Management Journal*, 2014. **13**(1): p. 205-214.
51. Mizuki, H., et al., *Note: Zr(IV)-Immobilized Resin Prepared by Surface Template Polymerization for Fluoride Ion Removal*. *Solvent Extraction and Ion Exchange*, 2011. **29**(1): p. 146-156.
52. UEZU, K., H. MIZUKI, and H. KAWAKITA, *SURFACE-TEMPLATED POLYMERS FOR REMOVAL OF FLUORIDE ION*.
53. Chaplin, M.F., *High performance liquid chromatography of biopolymers and biooligomers, part A: Principles, materials and techniques, volume 41A* By O. Mires, Elsevier Science Publishers, Amsterdam, 1988, pp. 375, price Dfl 285.00, \$150.00. ISBN 0-444-42951-4. *Journal of Chemical Technology & Biotechnology*, 1990. **49**(2): p. 199-200.

54. Farrah, H., J. Slavek, and W. Pickering, *Fluoride interactions with hydrous aluminum oxides and alumina*. Soil Research, 1987. **25**(1): p. 55-69.
55. Ghorai, S. and K.K. Pant, *Investigations on the column performance of fluoride adsorption by activated alumina in a fixed-bed*. Chemical Engineering Journal, 2004. **98**(1-2): p. 165-173.
56. Puri, B.K. and S. Balani, *Trace determination of fluoride using lanthanum hydroxide supported on alumina*. Journal of Environmental Science and Health, Part A, 2000. **35**(1): p. 109-121.
57. Adeno, F., et al., *Adsorptive removal of fluoride from water using nanoscale aluminium oxide hydroxide (AlOOH)*. Bulletin of the Chemical Society of Ethiopia, 2014. **28**(2): p. 215-227.
58. Tomar, G., A. Thareja, and S. Sarkar, *Enhanced fluoride removal by hydroxyapatite-modified activated alumina*. International Journal of Environmental Science and Technology, 2014: p. 1-10.
59. Bansiwala, A., et al., *Copper oxide incorporated mesoporous alumina for defluoridation of drinking water*. Microporous and Mesoporous Materials, 2010. **129**(1-2): p. 54-61.
60. Turner, B.D., P. Binning, and S. Stipp, *Fluoride removal by calcite: evidence for fluorite precipitation and surface adsorption*. Environmental science & technology, 2005. **39**(24): p. 9561-9568.
61. Islam, M. and R.K. Patel, *Evaluation of removal efficiency of fluoride from aqueous solution using quick lime*. Journal of Hazardous Materials, 2007. **143**(1-2): p. 303-310.
62. Larsen, M. and E. Pearce, *Defluoridation of drinking water by boiling with brushite and calcite*. Caries research, 2002. **36**(5): p. 341-346.
63. Tang, Y., et al., *Fluoride adsorption onto granular ferric hydroxide: Effects of ionic strength, pH, surface loading, and major co-existing anions*. Journal of Hazardous Materials, 2009. **171**(1-3): p. 774-779.
64. Liu, Q., H. Guo, and Y. Shan, *Adsorption of fluoride on synthetic siderite from aqueous solution*. Journal of Fluorine Chemistry, 2010. **131**(5): p. 635-641.
65. Vithanage, M., et al., *Modeling sorption of fluoride on to iron rich laterite*. Colloids and Surfaces A: Physicochemical and Engineering Aspects, 2012. **398**: p. 69-75.
66. Zhu, P., et al., *Adsorption of fluoride from aqueous solution by magnesia-amended silicon dioxide granules*. Journal of Chemical Technology & Biotechnology, 2009. **84**(10): p. 1449-1455.
67. Chang, C.-F., C.-Y. Chang, and T.-L. Hsu, *Removal of fluoride from aqueous solution with the superparamagnetic zirconia material*. Desalination, 2011. **279**(1-3): p. 375-382.
68. Li, Z., et al., *Removal of fluoride from water using titanium-based adsorbents*. Frontiers of Environmental Science & Engineering in China, 2010. **4**(4): p. 414-420.
69. Ansari, M., et al., *The defluoridation of drinking water using multi-walled carbon nanotubes*. Journal of Fluorine Chemistry, 2011. **132**(8): p. 516-520.
70. Bhargava, D., *Nomograph for Defluoridation of Water in Batch using Fish Bone Char*. Eli Dahi Sunsanee Rajchagool & Nipaphan Osiriphan, 2000: p. 73.

71. Kaseva, M., *Optimization of regenerated bone char for fluoride removal in drinking water: a case study in Tanzania*. J Water Health, 2006. **4**: p. 139-147.
72. Sivasamy, A., et al., *Studies on defluoridation of water by coal-based sorbents*. Journal of Chemical Technology and Biotechnology, 2001. **76**(7): p. 717-722.
73. Moges, G., F. Zewge, and M. Socher, *Preliminary investigations on the defluoridation of water using fired clay chips*. Journal of African Earth Sciences, 1996. **22**(4): p. 479-482.
74. Chidambaram, S., A. Ramanathan, and S. Vasudevan, *Fluoride removal studies in water using natural materials: technical note*. Water SA, 2004. **29**(3): p. 339-344.
75. Kumar, E., et al., *Defluoridation from aqueous solutions by nano-alumina: Characterization and sorption studies*. Journal of Hazardous Materials, 2011. **186**(2-3): p. 1042-1049.
76. Li, Y.-H., et al., *Adsorption of fluoride from water by amorphous alumina supported on carbon nanotubes*. Chemical Physics Letters, 2001. **350**(5-6): p. 412-416.
77. Wang, S.-G., et al., *Defluoridation performance and mechanism of nano-scale aluminum oxide hydroxide in aqueous solution*. Journal of Chemical Technology & Biotechnology, 2009. **84**(7): p. 1043-1050.
78. Oguz, E., *Equilibrium isotherms and kinetics studies for the sorption of fluoride on light weight concrete materials*. Colloids and Surfaces A: Physicochemical and Engineering Aspects, 2007. **295**(1-3): p. 258-263.
79. Yadav, A.K., et al., *Defluoridation of groundwater using brick powder as an adsorbent*. Journal of Hazardous Materials, 2006. **128**(2-3): p. 289-293.
80. Kagne, S., et al., *Hydrated cement: A promising adsorbent for the removal of fluoride from aqueous solution*. Journal of Hazardous Materials, 2008. **154**(1-3): p. 88-95.
81. Gao, S., J. Cui, and Z. Wei, *Study on the fluoride adsorption of various apatite materials in aqueous solution*. Journal of Fluorine Chemistry, 2009. **130**(11): p. 1035-1041.
82. Jayarathne, A., R. Weerasooriya, and R. Chandrajith, *A rapid method for the removal of fluoride in contaminated groundwater using natural crystalline apatite: a laboratory and field study*. Environmental Earth Sciences. **73**(12): p. 8369-8377.
83. Lv, L., et al., *Kinetic Studies on Fluoride Removal by Calcined Layered Double Hydroxides*. Industrial & Engineering Chemistry Research, 2006. **45**(25): p. 8623-8628.
84. Gupta, V.K., I. Ali, and V.K. Saini, *Defluoridation of wastewaters using waste carbon slurry*. Water Research, 2007. **41**(15): p. 3307-3316.
85. Jadhav A S, J.M.V., *Use of Maize Husk Fly Ash as an Adsorbent for Removal of Fluoride from Water*. International Journal of Recent Development in Engineering and Technology, 2014. **2**(2).
86. Kemer, B., et al., *Removal of fluoride ions from aqueous solution by waste mud*. Journal of Hazardous Materials, 2009. **168**(2-3): p. 888-894.
87. Malakootian, M., et al., *Fluoride removal using Regenerated Spent Bleaching Earth (RSBE) from groundwater: Case study on Kuhbonan water*. Desalination, 2011. **277**(1-3): p. 244-249.

88. Volesky, B., *Biosorption and me*. Water Research, 2007. **41**(18): p. 4017-4029.
89. Gadd, G.M., *Biosorption: critical review of scientific rationale, environmental importance and significance for pollution treatment*. Journal of Chemical Technology and Biotechnology, 2009. **84**(1): p. 13-28.
90. Yao, R., et al., *Defluoridation of water using neodymium-modified chitosan*. Journal of Hazardous Materials, 2009. **165**(1–3): p. 454-460.
91. Viswanathan, N., C. Sairam Sundaram, and S. Meenakshi, *Development of multifunctional chitosan beads for fluoride removal*. Journal of Hazardous Materials, 2009. **167**(1–3): p. 325-331.
92. Piyush, K.P., P. Madhurima, and S. Rekha, *Defluoridation of water by a biomass: Tinospora cordifolia*. Journal of Environmental Protection, 2012. **2012**.
93. Ramesh, K., *Adsorption of Methylene Blue Activated Carbon Prepared from Thermodyna*. Research Journal of Chemical, 2014. **4**(7): p. 36-42.
94. Patni, M. and A.M. Rambabu, *Low Cost Household Level Solution To Remove Fluoride From Drinking Water*.
95. Alagumuthu, G., V. Veeraputhiran, and R. Venkataraman, *Fluoride sorption using Cynodon dactylon based activated carbon*. Hemijiska industrija, 2011. **65**(1): p. 23-35.
96. Karthikeyan, G. and S.S. Ilango, *Fluoride sorption using Moringa Indica-based activated carbon*. Iranian Journal of Environmental Health Science & Engineering, 2007. **4**(1): p. 21-28.
97. Suneetha, M., B.S. Sundar, and K. Ravindhranath, *Removal of fluoride from polluted waters using active carbon derived from barks of Vitex negundo plant*. Journal of Analytical Science and Technology, 2015. **6**(1): p. 1-19.
98. Vardhan, C.V. and J. Karthikeyan. *Removal of fluoride from water using low-cost materials*. in *Fifteenth International Water Technology Conference, IWTC-15*. 2011.
99. AashMohammad, C.M., *REMOVAL OF FLUORIDE FROM SYNTHETIC WASTE WATER BY USING "BIO-ADSORBENTS"*. IJRET: International Journal of Research in Engineering and Technology, 2014.
100. Getachew, T., A. Hussien, and V. Rao, *Defluoridation of water by activated carbon prepared from banana (Musa paradisiaca) peel and coffee (Coffea arabica) husk*. International Journal of Environmental Science and Technology, 2015. **12**(6): p. 1857-1866.
101. Tomar, V., S. Prasad, and D. Kumar, *Adsorptive removal of fluoride from aqueous media using Citrus limonum (lemon) leaf*. Microchemical Journal, 2014. **112**: p. 97-103.
102. Alagumuthu, G. and M. Rajan, *Kinetic and equilibrium studies on fluoride removal by zirconium (IV): Impregnated groundnut shell carbon*. Hemijiska industrija, 2010. **64**(4): p. 295-304.
103. Zhu, H., et al. *Removal of fluorine from water by the aluminum modified peanut shell*. in *Information Science and Engineering (ICISE), 2010 2nd International Conference on*. 2010. IEEE.
104. Kumar, P.S. and K. Kirthika, *Equilibrium and kinetic study of adsorption of nickel from aqueous solution onto bael tree leaf powder*. Journal of Engineering Science and Technology, 2009. **4**(4): p. 351-363.

105. Krishna, R.H. and A. Swamy, *Physico-Chemical Key Parameters, Langmuir and Freundlich isotherm and Lagergren Rate Constant Studies on the removal of divalent nickel from the aqueous solutions onto powder of calcined brick*. Int. J. Eng. Res. Dev, 2012. **4**(1): p. 29-38.
106. Vijayaraghavan, K., et al., *Biosorption of nickel (II) ions onto Sargassum wightii: application of two-parameter and three-parameter isotherm models*. Journal of Hazardous Materials, 2006. **133**(1): p. 304-308.
107. Foo, K. and B. Hameed, *Insights into the modeling of adsorption isotherm systems*. Chemical Engineering Journal, 2010. **156**(1): p. 2-10.
108. Ho, Y., J. Porter, and G. McKay, *Equilibrium isotherm studies for the sorption of divalent metal ions onto peat: copper, nickel and lead single component systems*. Water, Air, and Soil Pollution, 2002. **141**(1-4): p. 1-33.
109. Goldberg, S., et al., *Equations and models describing adsorption processes in soils*. Chemical processes in soils, 2005: p. 489-517.
110. Rajkumar, S., et al., *Low-cost fluoride adsorbents prepared from a renewable biowaste: Syntheses, characterization and modeling studies*. Arabian Journal of Chemistry.
111. Amin, F., et al., *Biosorption of fluoride from aqueous solution by white—rot fungus Pleurotus eryngii ATCC 90888*. Environmental Nanotechnology, Monitoring & Management, 2015. **3**: p. 30-37.
112. Qiu, H., et al., *Critical review in adsorption kinetic models*. Journal of Zhejiang University Science A, 2009. **10**(5): p. 716-724.
113. Raven, K.P., A. Jain, and R.H. Loeppert, *Arsenite and arsenate adsorption on ferrihydrite: kinetics, equilibrium, and adsorption envelopes*. Environmental Science & Technology, 1998. **32**(3): p. 344-349.
114. Lazaridis, N. and D. Asouhidou, *Kinetics of sorptive removal of chromium (VI) from aqueous solutions by calcined Mg–Al–CO₃ hydrotalcite*. Water research, 2003. **37**(12): p. 2875-2882.
115. Guo, B., L. Hong, and H.-X. Jiang, *Macroporous Poly (calcium acrylate-divinylbenzene) Bead A Selective Orthophosphite Sorbent*. Industrial & engineering chemistry research, 2003. **42**(22): p. 5559-5567.
116. Ho, Y., J. Ng, and G. McKay, *Kinetics of pollutant sorption by biosorbents: review*. Separation & Purification Reviews, 2000. **29**(2): p. 189-232.
117. Habuda-Stanić, M.E.R.a.M., *Equilibrium and Kinetics Studies for the Adsorption of Fluoride onto Commercial Activated Carbons Using Fluoride Ion-Selective Electrode*. International Journal of ELECTROCHEMICAL SCIENCE, 2015. **10**: p. 8137 -8149.
118. M. Suneetha, B.S.S.a.K.R., *Studies on fluoride removal from polluted waters using active carbon derived from stems of Abutilon indicum plant* Journal of Chemical and Pharmaceutical Research, 2014. **6**: p. 574-592.
119. P. Satish, R.S., P. Naseema *Defluoridation of water using biosorbents: Kinetic and thermodynamic study*. International Journal of Research in Chemistry and Environment, January 2013. **3**(1): p. 125-135.
120. Yuh-Shan, H., *Citation review of Lagergren kinetic rate equation on adsorption reactions*. Scientometrics, 2004. **59**(1): p. 171-177.
121. MONDAL, N.K., et al., *Studies on Defluoridation of Water by Tea Ash: An Unconventional Biosorbent*. Chemical Science Transactions. **1**(2): p. 239-256.

122. Suman Mann, D.A.M., *Removal of Fluoride from Drinking Water Using Sawdust*. Int. Journal of Engineering Research and Applications, 2014. **4**(7): p. 116-123.
123. Chakrapani, C., et al., *Adsorption kinetics for the removal of fluoride from aqueous solution by activated carbon adsorbents derived from the peels of selected citrus fruits*. Journal of Chemistry, 2010. **7**(S1): p. S419-S427.
124. Rudzinski, W. and W. Plazinski, *Kinetics of solute adsorption at solid/solution interfaces: a theoretical development of the empirical pseudo-first and pseudo-second order kinetic rate equations, based on applying the statistical rate theory of interfacial transport*. The Journal of Physical Chemistry B, 2006. **110**(33): p. 16514-16525.
125. Ho, Y.-S. and G. McKay, *Pseudo-second order model for sorption processes*. Process biochemistry, 1999. **34**(5): p. 451-465.
126. El-Khaiary, M.I., G.F. Malash, and Y.-S. Ho, *On the use of linearized pseudo-second-order kinetic equations for modeling adsorption systems*. Desalination, 2010. **257**(1): p. 93-101.
127. Bhatnagar, A. and A. Minocha, *Assessment of the biosorption characteristics of lychee (Litchi chinensis) peel waste for the removal of Acid Blue 25 dye from water*. Environmental technology, 2010. **31**(1): p. 97-105.
128. Molina, A., et al. *Advancing banana and plantain R&D in Asia and the Pacific-Vol. 13. in Proceedings of the 3rd BAPNET Steering Committee meeting held in Guangzhou, China. 2004.*
129. Weber, T.W. and R.K. Chakravorti, *Pore and solid diffusion models for fixed-bed adsorbers*. AIChE Journal, 1974. **20**(2): p. 228-238.
130. Itodo, A., et al., *Intraparticle diffusion and intraparticulate diffusivities of herbicide on derived activated carbon*. Researcher, 2010. **2**(2): p. 74-86.
131. Castro, R.S., et al., *Banana peel applied to the solid phase extraction of copper and lead from river water: Preconcentration of metal ions with a fruit waste*. Industrial & Engineering Chemistry Research, 2011. **50**(6): p. 3446-3451.
132. Kruk, M. and M. Jaroniec, *Gas adsorption characterization of ordered organic-inorganic nanocomposite materials*. Chemistry of Materials, 2001. **13**(10): p. 3169-3183.
133. Pouloupoulos, V.J.I.a.S.G., *Adsorption, Ion Exchange and Catalysis : Design of Operations and Environmental Applications. 2006.*
134. Nicholas P. Cheremisinoff, P.N.C., *Hazardous Materials and Waste Management: A Guide for the Professional Hazards*, D. William Andrew, 2538 BE - Technology & Engineering, Editor. 1995. p. 277.
135. FAYLONA, M.G.P.G., *The ancient giant clam shells from Balabok Rockshelter, Philippines as potential recorders of environmental changes: a diagenesis assessment and sclerochronology study. 2010.*
136. Tan, T., D. Wong, and P. Lee, *Iridescence of a shell of mollusk Haliotis Glabra*. Optics Express, 2004. **12**(20): p. 4847-4854.
137. Almarri, M., X. Ma, and C. Song, *Role of surface oxygen-containing functional groups in liquid-phase adsorption of nitrogen compounds on carbon-based adsorbents*. Energy & Fuels, 2009. **23**(8): p. 3940-3947.

138. Oberoi, H.S., et al., *Ethanol production from orange peels: two-stage hydrolysis and fermentation studies using optimized parameters through experimental design*. Journal of agricultural and food chemistry, 2010. **58**(6): p. 3422-3429.
139. Harikumar, P.S.P., C. Jaseela, and T. Megha, *Defluoridation of water using biosorbents*. 2012.
140. Zazouli, M.A., et al., *ADSORPTION OF FLUORIDE FROM AQUEOUS SOLUTION BY MODIFIED AZOLLA FILICULOIDES*. Adsorption, 2014.
141. Gupta, N., et al., *Defluoridation of Groundwater using Low Cost Adsorbent like Bagasse Dust, Aluminium Treated Bagasse Flyash, Bone Powder and Shell Powder*. Bonfring International Journal of Industrial Engineering and Management Science, 2014. **4**(2): p. 72-75.
142. Kumar, S., A. Gupta, and J. Yadav, *Removal of fluoride by thermally activated carbon prepared from neem (Azadirachta indica) and kikar (Acacia arabica) leaves*. Journal of Environmental Biology, 2008. **29**(2): p. 227.
143. COMBUSTION–AN, B., *CTECHNICA*.
144. Tomar, V. and D. Kumar, *A critical study on efficiency of different materials for fluoride removal from aqueous media*. Chem. Cent. J, 2013. **7**(1): p. 1-15.
145. Sujana, M.G. and S. Anand, *Iron and aluminium based mixed hydroxides: a novel sorbent for fluoride removal from aqueous solutions*. Applied Surface Science, 2010. **256**(23): p. 6956-6962.
146. Tang, Y., et al., *Fluoride adsorption onto activated alumina: Modeling the effects of pH and some competing ions*. Colloids and Surfaces A: Physicochemical and Engineering Aspects, 2009. **337**(1–3): p. 33-38.
147. Bhatnagar, A., E. Kumar, and M. Sillanpää, *Fluoride removal from water by adsorption—a review*. Chemical Engineering Journal, 2011. **171**(3): p. 811-840.
148. Singh, J., P. Singh, and A. Singh, *Fluoride ions vs removal technologies: A study*. Arabian Journal of Chemistry.
149. Bradl, H.B., *Adsorption of heavy metal ions on soils and soils constituents*. Journal of Colloid and Interface Science, 2004. **277**(1): p. 1-18.
150. Ohimain, I., S. Bassey, and D. Bawo, *Uses of seas shells for civil construction works in coastal Bayelsa State, Nigeria: A waste management perspective*. Research Journal of Biological Sciences, 2009. **4**(9): p. 1025-1031.
151. Baker, M., et al., *Role of extracellular polymeric substances in the surface chemical reactivity of Hymenobacter aerophilus, a psychrotolerant bacterium*. Applied and environmental microbiology, 2010. **76**(1): p. 102-109.
152. Manna, S., et al., *Defluoridation of aqueous solution using alkali–steam treated water hyacinth and elephant grass*. Journal of the Taiwan Institute of Chemical Engineers, 2014.
153. Evans-Tokaryk, K., *Biogeochemical defluoridation*. 2011, University of Toronto.
154. Daifullah, A., S. Yakout, and S. Elreefy, *Adsorption of fluoride in aqueous solutions using KMnO₄-modified activated carbon derived from steam pyrolysis of rice straw*. Journal of Hazardous Materials, 2007. **147**(1): p. 633-643.
155. Wang, Y. and E.J. Reardon, *Activation and regeneration of a soil sorbent for defluoridation of drinking water*. Applied Geochemistry, 2001. **16**(5): p. 531-539.

156. Devi, R.R., et al., *Defluoridation of water using nano-magnesium oxide*. Journal of Experimental Nanoscience, 2014. **9**(5): p. 512-524.
157. Geethamani, C., et al., *Alkali-treated fly ash for the removal of fluoride from aqueous solutions*. Desalination and Water Treatment, 2014. **52**(19-21): p. 3466-3476.
158. El-Latif, M.A., A.M. Ibrahim, and M. El-Kady, *Adsorption equilibrium, kinetics and thermodynamics of methylene blue from aqueous solutions using biopolymer oak sawdust composite*. J. Am. Sci, 2010. **6**(6): p. 267-283.
159. Srimurali, M. and J. Karthikeyan. *Activated alumina: Defluoridation of water and household application. A study*. in *Proceedings of the 12th international water technology conference, Alexandria, IWTC*. 2008. Citeseer.
160. Srivastava, V.C., et al., *Adsorptive removal of phenol by bagasse fly ash and activated carbon: equilibrium, kinetics and thermodynamics*. Colloids and Surfaces A: Physicochemical and Engineering Aspects, 2006. **272**(1): p. 89-104.
161. Hossain, M., et al., *Removal of copper from water by adsorption onto banana peel as bioadsorbent*. Int. J. of Geomate, 2012. **2**(2): p. 227-234.
162. Yadav, A.K., et al., *Removal of fluoride from aqueous solution and groundwater by wheat straw, sawdust and activated bagasse carbon of sugarcane*. Ecological Engineering, 2013. **52**: p. 211-218.
163. Chen, N., et al., *Removal of fluoride from aqueous solution by adsorption onto Kanuma mud*. 2010.
164. Onyango, M.S., et al., *Adsorption equilibrium modeling and solution chemistry dependence of fluoride removal from water by trivalent-cation-exchanged zeolite F-9*. Journal of Colloid and Interface Science, 2004. **279**(2): p. 341-350.
165. Martin, M.J., et al., *Activated carbons developed from surplus sewage sludge for the removal of dyes from dilute aqueous solutions*. Chemical Engineering Journal, 2003. **94**(3): p. 231-239.
166. Ahalya, N., R. Kanamadi, and T. Ramachandra, *Biosorption of iron (III) from aqueous solutions using the husk of Cicer arietinum*. Indian Journal of Chemical Technology, 2006. **13**(2): p. 122.
167. Zhou, B., et al., *Preparation, characterization, and phenol adsorption of activated carbons from oxytetracycline bacterial residue*. Journal of the Air & Waste Management Association, 2012. **62**(12): p. 1394-1402.
168. Chen, N., et al., *Fluoride removal from water by granular ceramic adsorption*. Journal of colloid and interface science, 2010. **348**(2): p. 579-584.
169. Mohanty, K., et al., *Removal of chromium (VI) from dilute aqueous solutions by activated carbon developed from Terminalia arjuna nuts activated with zinc chloride*. Chemical Engineering Science, 2005. **60**(11): p. 3049-3059.
170. Nuhoglu, Y. and E. Malkoc, *Thermodynamic and kinetic studies for environmentally friendly Ni (II) biosorption using waste pomace of olive oil factory*. Bioresource Technology, 2009. **100**(8): p. 2375-2380.
171. Tseng, R.-L., F.-C. Wu, and R.-S. Juang, *Characteristics and applications of the Lagergren's first-order equation for adsorption kinetics*. Journal of the Taiwan Institute of Chemical Engineers, 2010. **41**(6): p. 661-669.
172. Ho, Y.-S. and G. McKay, *The kinetics of sorption of divalent metal ions onto sphagnum moss peat*. Water Research, 2000. **34**(3): p. 735-742.

173. Panday, K., G. Prasad, and V. Singh, *Mixed adsorbents for Cu (II) removal from aqueous solutions*. Environmental Technology, 1986. **7**(1-12): p. 547-554.
174. Ardekani, M.M.M., et al., *Journal of Environmental Treatment Techniques*. Journal of Environmental Treatment Techniques, 2013. **1**(1): p. 1-7.
175. Hanumantharao, Y., M. Kishore, and K. Ravindhranath, *Preparation and development of adsorbent carbon from Acacia farnesiana for defluoridation*. International Journal of Plant, Animal and Environmental Sciences, 2011. **1**(3): p. 209-223.
176. Hanumantharao, Y., M. Kishore, and K. Ravindhranath, *Characterization and defluoridation studies of active carbon derived from typha angustata plants*. J Analytical Sci Technol, 2012. **3**(2): p. 167-181.
177. Prerna Kumari, N.K., Gopal Pathak, *DEFLUORIDATION OF WATER BY A BIOMASS: SHOREA ROBUSTA*, in *International Conference on Recent Advances in Engineering Science and Management*. 2015: PHD Chamber of Commerce and Industry, NEW DELHI. p. 1-15.

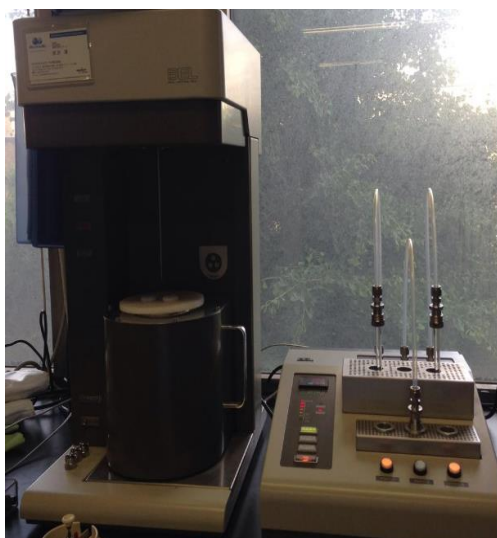
APPENEDICES

Appendix A

Procedure for the BET surface area measurement

The procedures for the sample preparation and measurement of BET surface area are listed under the following points:

- The sample tube was weighed after inserting the stopper, and was attached to the volumetric apparatus.
- Before performing N₂ gas adsorption-desorption at 77 K, prepared adsorbents were outgassed under vacuum at 300°C for 4 hours for removing the moisture content. The outgassing conditions must be established to yield reproducible BET plots, a constant weight of test powder with no detectable physical or chemical changes.
- The determination of dead volume was avoided by using reference and sample tubes connected by differential transducer.
- The Dewar vessel containing liquid nitrogen at 77.4 K was raised upto a definite point on the sample cell and the necessary volume of N₂ gas was admitted to give the lowest desired relative pressure.
- Finally, the volume adsorbed, V_a was measured. For multi-point measurements, measurement of V_a was repeated at successive P/P_o values. The plot was taken over 0.05-0.35 P/P_o range, as beyond these values, linearity of plot breaks down.
- The functioning of the apparatus was verified periodically by means of suitable reference materials of known surface area, such as α -alumina, having similar surface area to that of the test sample.



BELSORP-miniII for the measurement of surface area

Appendix B

Measurement of fluoride by UV-Visible Spectrophotometer

In the spectrophotometric method, a metal compound like iron, zirconium, thorium, lanthanum, aluminium, or cerium reacts with an indicator dye to build complex of small dissociation constant. This complex reacts with fluoride to give another new complex. SPADNS colorimetric method is based on the reaction of fluoride with zirconium dye to form a red colored complex. Fluoride discolors this red color of complex and thus the alteration in absorbance can be calculated using a spectrophotometer. The dye becomes progressively lighter on increasing the fluoride concentration. This method of fluoride measurement basically follows the given steps:

a) Preparation of the SPADNS solution

In distilled water, 958 mg of SPADNS (Trisodium 2- (parasulphenylazo) 1, 8 dihydroxy- 3, 6 naphthalenedisulphonate) was dissolved, which was further diluted to 500 ml.

b) Preparation of zirconyl-acid reagent

The reagent was prepared by dissolving 133 mg zirconyl chloride octahydrate in 25 ml DI water in 500 ml volumetric flask. Later on, 350 ml concentrated HCl was added, and the solution was diluted to 500 ml.

c) Preparation of the acid zirconyl-SPADNS reagent

Finally, equivalent volume of SPADNS solution and zirconyl acid reagent was mixed together.

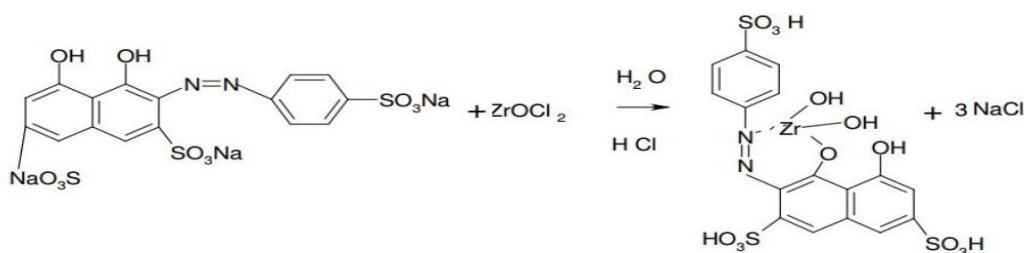


SPADNS Reagent

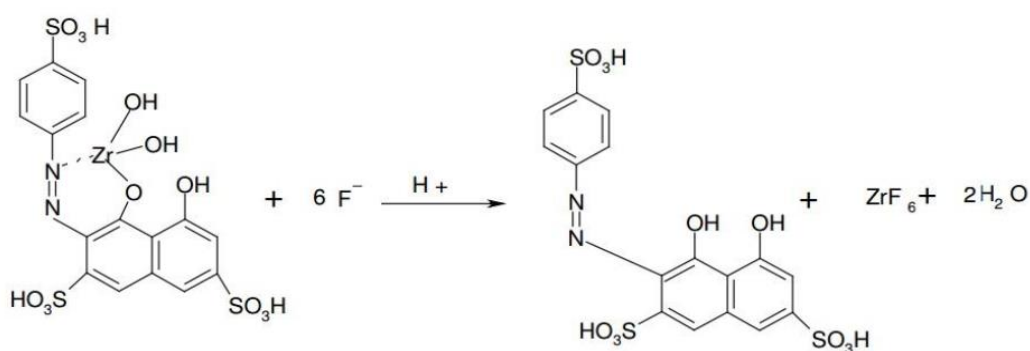


UV- Visible Spectrophotometer

Step 1: Formation of the SPADNS – ZrOCl₂ complex



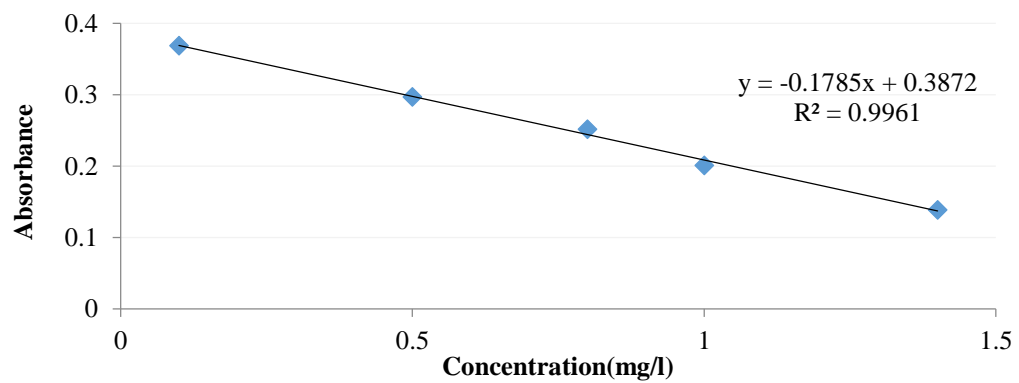
Step 2: Reaction of the complex with fluoride ions



Step 3: Preparation of Calibration Curve

The absorption of each solution was determined and the unknown samples were analyzed against the calibration curve prepared by standard solutions of fluoride. As the spectrophotometer can detect only up to 1.4 mg/l F⁻, dilution of unknown samples

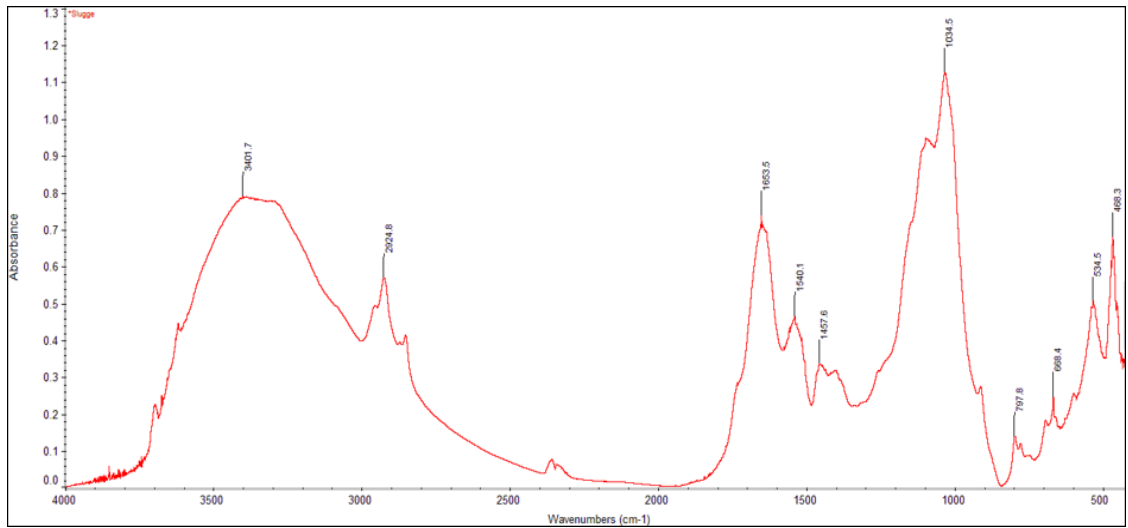
was performed and the results were accordingly evaluated using the appropriate dilution factor.



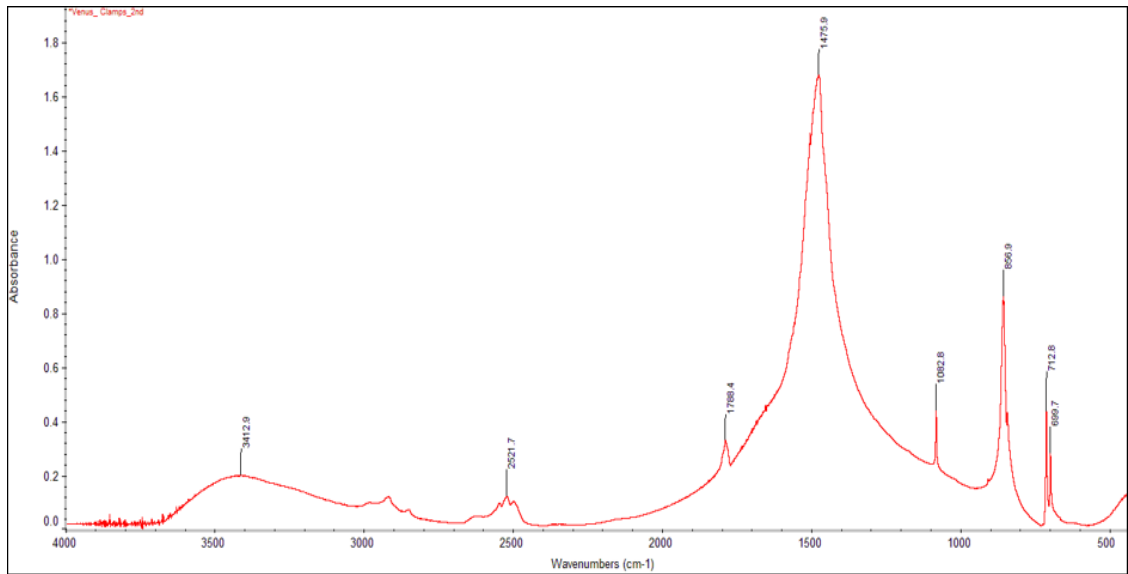
Calibration curve for measuring residual fluoride concentration

Appendix C

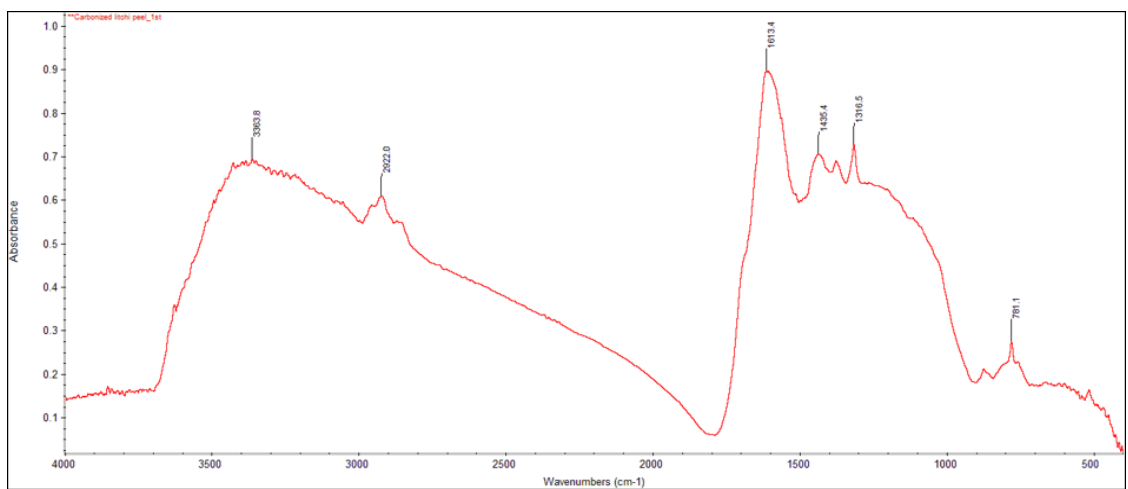
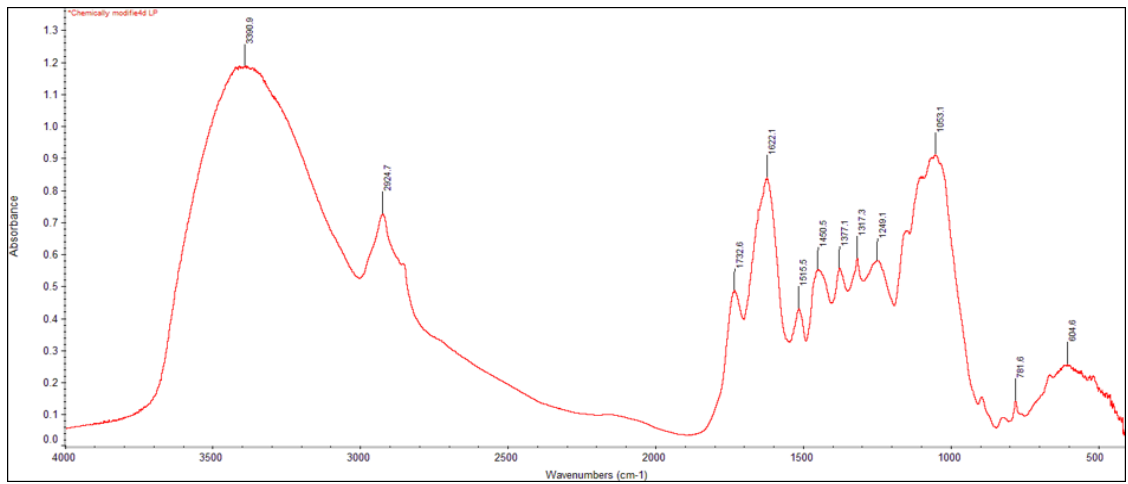
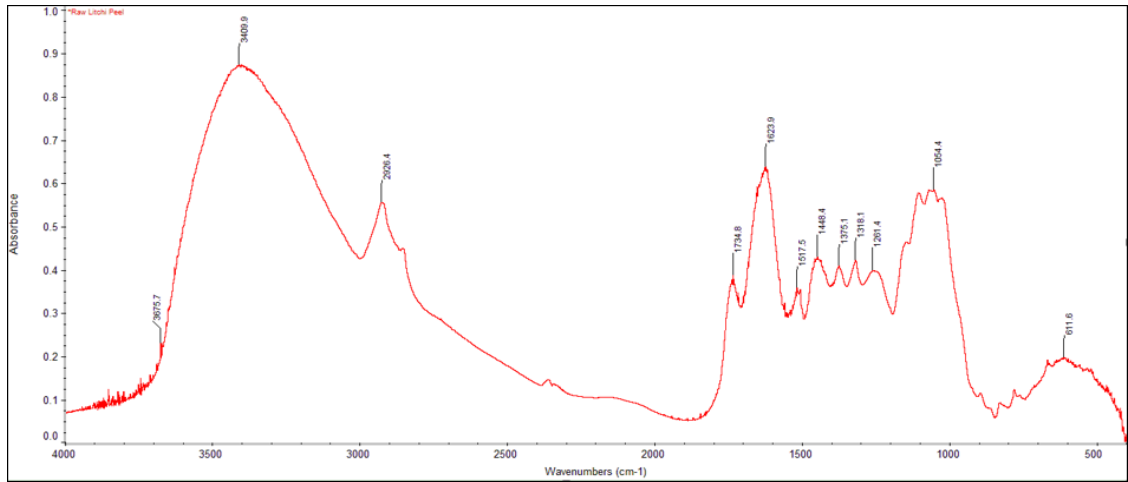
FTIR spectra of the selected adsorbents



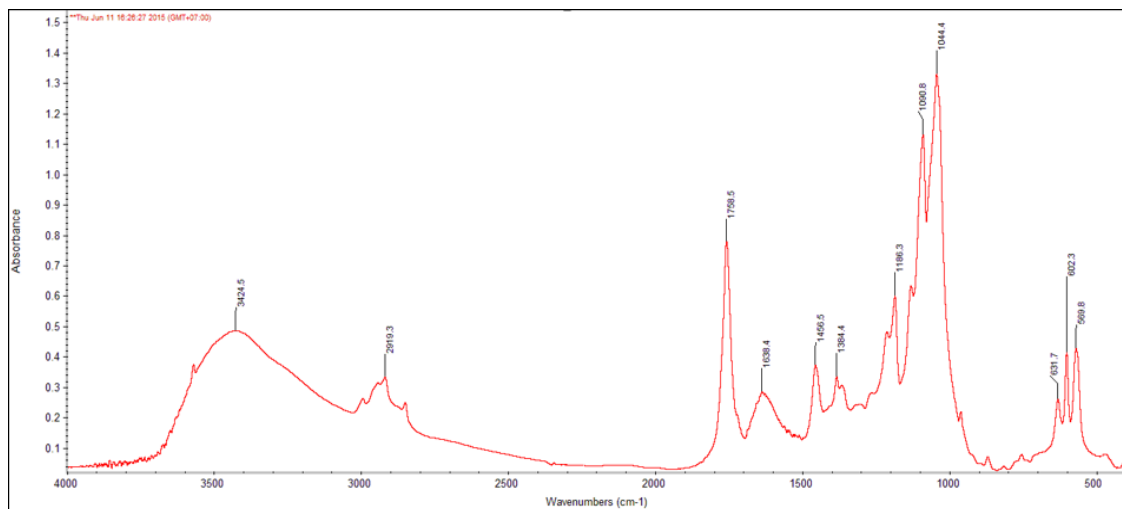
FTIR spectra of the sewage sludge powder



FTIR spectra of *Venus clams* shell powder



FTIR spectra of ULP, ALP and CLP powder



FTIR spectra of banana peel (BP) powder